Environmental Science & Technology

pubs.acs.org/est

Critical Review

Merits and Limitations of Radical vs. Nonradical Pathways in Persulfate-Based Advanced Oxidation Processes

Yiqi Yan, Zongsu Wei, Xiaoguang Duan, Mingce Long, Richard Spinney, Dionysios D. Dionysiou, Ruiyang Xiao,* and Pedro J. J. Alvarez*

Cite This: *Environ. Sci. Technol.* 2023, 57, 12153–12179

Read Online

ACCESS | Metrics & More | Article Recommendations

ABSTRACT: Urbanization and industrialization have exerted significant adverse effects on water quality, resulting in a growing need for reliable and eco-friendly treatment technologies. Persulfate (PS)-based advanced oxidation processes (AOPs) are emerging as viable technologies to treat challenging industrial wastewaters or remediate groundwater impacted by hazardous wastes. While the generated reactive species can degrade a variety of priority organic contaminants through radical and nonradical pathways, there is a lack of systematic and in-depth comparison of these pathways for practical implementation in different treatment scenarios. Our comparative analysis of reaction rate constants for radical *vs.* nonradical species indicates that radical-based AOPs may achieve high removal efficiency of organic contaminants with relatively short contact time. Nonradical AOPs feature advantages with minimal water matrix interference for complex wastewater treatments. Nonradical species (*e.g.*, singlet oxygen, high-valent metals, and surface activated PS) preferentially react with contaminants bearing electron-donating groups, allowing enhancement of degradation efficiency of known target contaminants. For byproduct formation, analytical limitations and computational chemistry applications are also considered. Finally, we propose a holistically estimated electrical energy per order of reaction (EE/O) parameter and show significantly higher energy requirements for the nonradical pathways. Overall, these critical comparisons help prioritize basic research on PS-based AOPs and inform the merits and limitations of system-specific applications.

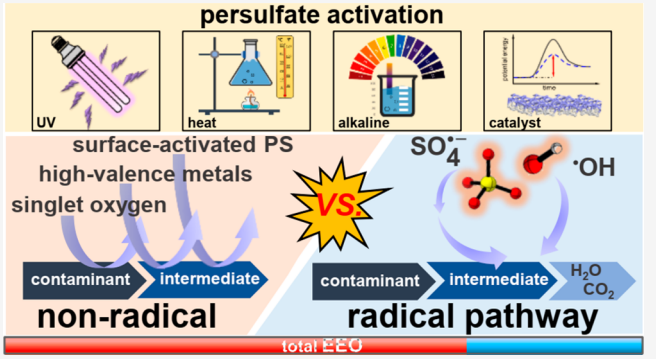

KEYWORDS: *persulfate activation, reactive species, energy consumption, nonradical pathway*

1. INTRODUCTION

There is growing interest in advanced treatment technologies that eliminate toxic chemicals and reduce the toxicity of wastewaters or impacted groundwater to acceptable limits. Among them, persulfate (PS)-based advanced oxidation processes (AOPs) have been extensively investigated for eliminating refractory organic contaminants in waters from bench to pilot scales.[1−3] PS typically refers to peroxymonosulfate (PMS, HSO_5^-) and peroxydisulfate (PDS, $S_2O_8^{2-}$). Although PMS by itself can degrade certain contaminants with electron-rich moieties (*e.g.*, sulfonamide antibiotics and *β*-lactam antibiotics),[4,5] it exhibits very low removal rates for other compounds if it is not activated.[6,7] Thus, for the efficient removal of contaminant mixtures, appropriate activation approaches are necessary to produce highly reactive species. Upon activation, removal of priority organic contaminants relies on the generation of reactive species through either radical or nonradical pathways. Therefore, understanding activation mechanisms and the merits and limitations of these two pathways is important for selecting and implementing an appropriate PS-based AOP for a given system.

Many fundamental questions should be considered for effective implementation of PS-based AOPs, including—What are the advantages and limitations for existing PS activation approaches? How should we evaluate the PS utilization and decontamination efficiency? How do functional groups on target compounds (TCs) influence the reactivities for both PS activation pathways? What differences exist in the byproduct distribution between these two pathways? How can we enhance cost efficacy for different PS activation pathways?

Previous literature reviews have critically considered opportunities and roadblocks associated with PS-based

Received: July 1, 2023
Revised: July 14, 2023
Accepted: July 17, 2023
Published: August 3, 2023

Table 1. Summary of Radical/Nonradical Species and Activation Methods for PS-Based Oxidation[a]

reactive species		activation methods	
radical species ($SO_4^{\bullet-}$, $^{\bullet}OH$)	catalyst-free	✓ ultraviolet ✓ heat ✓ ultrasound irradiation ✓ electricity	external energy
		✓ alkali	chemical
	catalyst-based	✓ metal cations (*e.g.*, Ag^+, Co^{2+}, Mn^{2+}, Fe^{2+}, Ce^{3+}) ✓ metal oxides (*e.g.*, Fe_3O_4, CuO, MnO, Co_3O_4) ✓ zero-valent metal (*e.g.*, Fe^0, Cu^0, Al^0, Mn^0) ✓ metal composites (*e.g.*, Co/TiO_2, $MnO_2/ZnFe_2O_4$)	metal-based
		✓ pristine carbonaceous materials (*e.g.*, CNTs, graphene, nanodiamond) ✓ heteroatoms/metal-doped carbon (*e.g.*, N/S-doped, Co/Ni-doped)	carbon-based
non-radical species ($^1O_2$, high valent metals, surface activated PS, HOCl)	catalyst-free	✓ inorganic anions (*e.g.*, Cl^-, Br^-, I^-) ✓ organic compounds (*e.g.*, phenols and quinones)	chemical
	catalyst-based	✓ metal cations (*e.g.*, Fe^{2+}, Cu^{2+}) ✓ metal oxides (*e.g.*, MnO_2, CuO, Cu_2O) ✓ zero-valent metals (*e.g.*, Fe^0, Cu^0) ✓ metal composites (*e.g.*, Au/TiO_2, Pt/Al_2O_3, Rh/Al_2O_3)	metal-based
		✓ pristine carbonaceous materials (*e.g.*, CNTs, graphene, nanodiamond, biochar) ✓ heteroatoms/metal-doped carbon (*e.g.*, N-doped, S-doped, Pd-doped)	carbon-based

[a]The blue shadowed part is the radical species induced degradation, while the gray shadowed part is the nonradical species.

AOPs,[8] and have addressed several of these questions with a focus on catalytic materials and mechanisms associated primarily with the nonradical pathway.[9−12] However, critical comparisons of the merits and limitations of nonradical vs. radical systems are lacking, and limited attention has been given to how the water matrix affects the relative performance of these pathways.

This review provides a holistic comparison of radical and nonradical pathways of PS-based AOPs. We first summarize the advantages and limitations of the different PS activation approaches. Then we systematically compare radical and nonradical pathways in depth from seven perspectives, namely, degradation kinetics and mechanisms, water matrix interference, selectivity, temperature, pH, formation of halogenated byproducts, and electrical energy requirements. We compile k values of relevant oxidizing species (*i.e.*, $SO_4^{\bullet-}$, $^{\bullet}OH$, and $^1O_2$) reacting with various organic contaminants, and consider the influence of functional groups of contaminants on the degradation kinetics. Accordingly, we compare the k values of the foregoing oxidants with organic compounds containing electron donating groups (EDGs) and electron withdrawing groups (EWGs). We highlight the water matrix interference in radical-induced pathways with the emphasis on the possible transformation to secondary/tertiary radicals, and mechanistically clarify different observations about the influence of temperature and pH on degradation kinetics. We also evaluate energy requirements for radical and nonradical mediated AOPs through electrical efficiency per log order of reaction (EE/O), a "gold standard"[13] for operating cost assessment. Finally, we recommend research priorities to advance PS-based AOPs from the bench scale to practical applications.

2. PS ACTIVATION APPROACHES

PS activation approaches can be divided into two categories: catalyst-free and catalyst-based (Table 1). The former represents the mainstream, which leverages external energy (*e.g.*, ultraviolet irradiation, heat, ultrasound, and electricity)[14−17] and chemicals (*e.g.*, alkaline, quinones, halides).[18−20] The homolytic fission of O−O bond of PS is achieved through the input of external energy, but this approach faces high energy requirements, high equipment costs, and poor equipment durability.[21] While chemical activation processes avoid these drawbacks, they are constrained by chemical cost and logistics, corrosion of reactors, and formation of carcinogenic byproducts.[22,23] Besides, chemical activation exhibits relatively low contaminant removal efficiency due to formation of less reactive species.[24]

Catalyst-based activation approaches (using metallic or carbonaceous catalysts) are being increasingly adopted in PS-AOPs.[25] Metallic catalysts can be divided into metal cations (*e.g.*, Fe^{2+}, Cu^{2+}, Ag^+),[26] metal oxides (*e.g.*, Fe_3O_4, CuO, MnO),[27,28] zero-valent metals (*e.g.*, Fe^0, Cu^0),[29] and metal composites (*e.g.*, Co/TiO_2, Au/TiO_2)[30,31] (Table 1). Despite their high reusability and low energy consumption, metal ion (*e.g.*, Fe^{2+}, Cu^{2+}) speciation in homogeneous systems is highly pH-dependent and may form precipitates that are difficult to recycle, ultimately requiring subsequent disposal.[32] Further, some metal catalysts such as Cu^{2+} and Mn^{2+} may not be appropriate for practical applications due to their residues potentially exceeding water quality standards.[33] In contrast, heterogeneous catalysts can be easily separated from treated waters for reuse and exhibit good stability under industrial operating conditions.[34] Particularly, cobalt oxide has been frequently used to activate PS, and it is one of the most efficient activators. However, Co^{2+} leaching from its condensed phases poses a great concern, as Co^{2+} is considerably toxic and potentially carcinogenic.[35] Thus, research has shifted toward the use of other catalysts.

Many studies used pristine carbonaceous materials (*e.g.*, carbon nanotubes, graphene, nanodiamond) due to their low toxicity, high stability, and high surface area (Table 1).[36] However, their catalytic performance is usually poor compared to metal-based catalysts since they have undetermined active centers and inherently complex structures.[37] Thus, to enhance the performance of pristine carbonaceous materials, various approaches that modify their structural and surface properties have been developed. Among these, chemical modification (*i.e.*, incorporation of foreign atoms into carbon structure) is the most prevailing approach.[38] Introducing heteroatoms to pristine carbonaceous materials produces a layered and porous structure with larger surface areas and abundant reactive sites.[39] This modification promotes electron mobility, thus

https://doi.org/10.1021/acs.est.3c05153
Environ. Sci. Technol. 2023, 57, 12153−12179

producing more reactive species and ultimately enhancing catalytic performance.[40] In addition to poor performance, the utilization of carbonaceous catalysts may also face an intractable problem that the catalysts themselves can react with the reactive species they produced. For example, graphene can be deteriorated by hydroxyl radicals (•OH), rendering a "holey graphene" morphology.[41] Note that, based on the definition of catalyst (*i.e.*, "a substance that increases the rate of a chemical reaction without itself undergoing any permanent chemical change"[42]), many materials that participate as reactants (*e.g.*, Fe^0 and Cu^0) should not be considered as catalysts. These materials should be termed activators. However, most current PS activation studies do not explicitly distinguish between the catalysts and activators.

Although many efforts have been directed toward designing new catalysts that harbor more active sites, reaction kinetics and selectivity of the generated reactive species are also a critical consideration to enhance the degradation efficiency of specific contaminants. Therefore, we consider here PS-based AOPs from the perspective of reactive species rather than catalysts phase (*i.e.*, homogeneous vs. heterogeneous).

One can classify the reactive species generated *via* PS activation as radical and nonradical species (Table 1).[10] Radical induced oxidation of a contaminant is mainly attributed to sulfate and hydroxyl radicals ($SO_4^{\bullet-}$and •OH) formed through PS activation. Superoxide radical $O_2^{\bullet-}$ may also participate, but its role is elusive. Only limited research has confirmed the contribution of $O_2^{\bullet-}$ for the direct degradation of contaminants.[43] This could be attributed to relatively low reactivity of $O_2^{\bullet-}$ with organic contaminants.[44,45] Other studies showed that $O_2^{\bullet-}$ serves as a precursor to other reactive species such as •OH.[46,47] The nonradical oxidation pathway involves reactive species such as singlet oxygen $^1O_2$, high-valent metals, and surface-activated PS (or surface-active PS complex). Note that there are two low-lying-state oxygen species, $^1\Delta_gO_2$ and $^1\Sigma_g^+O_2$. $^1\Sigma_g^+O_2$ is highly reactive with a short lifetime (~10^{-12} s), and it efficiently deactivates to $^1\Delta_gO_2$ with a lifetime of 10^{-3}–10^{-6} s through electronic-to-vibrational energy transfer. In this review, $^1O_2$ refers to $^1\Delta_gO_2$ due to its environmental relevance.[48] While most reviews on PS-based AOPs focus on various activation methods and their applications, a comprehensive and systematic comparison of radical and nonradical pathways is scarce.

Based on catalytic materials (*i.e.*, carbonaceous and metallic catalysts), a variety of mechanisms have been proposed for the degradation of contaminants by nonradical species. For carbonaceous materials, three oxidation pathways are recognized, namely, electron-transfer, surface-activated PS, and formation of $^1O_2$ (Figure 1).[11] In Pathway I (electron transfer), catalysts serve as an electron "bridge" to facilitate charge transport from contaminant to PS.[49,50] In Pathway II (surface-activated PS), PS adsorbs to the surface of carbonaceous catalysts, ultimately forming metastable activated PS complex with higher redox potential for removal of contaminants.[51,52] In Pathway III (formation of $^1O_2$), PS can be oxidized to generate $SO_5^{\bullet-}/O_2^{\bullet-}$ (a), which further transforms to $^1O_2$ and subsequently reacts with the contaminants (eqs 1–5);[53,54] the other source of $^1O_2$ is the dioxirane structure (b), which is generated from C═O groups in carbon-based catalysts during PS activation (eqs 6 and 7).[55]

$$HSO_5^- \rightarrow SO_5^{\bullet-} + H^+ + e^- \quad (1)$$

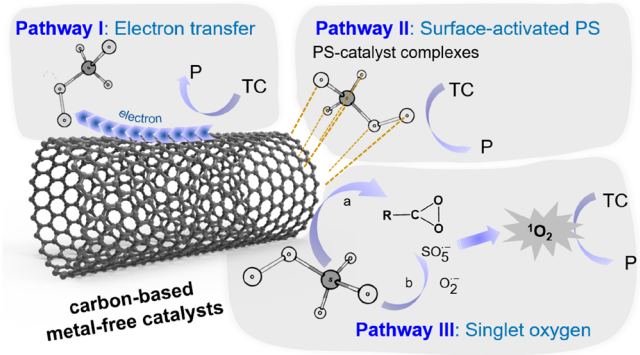

Figure 1. Different nonradical PS activation pathways for the carbon-based metal-free catalysts. TC and P stand for target compounds and their degradation products, respectively. (a) Epoxy structure is formed *via* the oxidation of C═O groups in carbonaceous catalysts by PS. (b) PS and electron-poor C atom on catalysts act as electron donor and acceptor, respectively. The electron transfer from PS to C atom allows formation of $SO_5^{\bullet-}$.[314] For $O_2^{\bullet-}$, it was reported to form by the base-catalyzed hydrolysis of PS.[18] For metallic catalysts, apart from the above-mentioned pathways,[56−58] high-valent metals are also used to remove contaminants.[59,60]

$$4SO_5^{\bullet-} + 2H_2O \rightarrow 4HSO_4^- + 3^1O_2 \quad (2)$$

$$S_2O_8^{2-} + 2H_2O \rightarrow HO_2^{\bullet-} + 2SO_4^{2-} + 3H^+ \quad (3)$$

$$S_2O_8^{2-} + HO_2^{\bullet-} \rightarrow SO_4^{2-} + SO_4^{\bullet-} + H^+ + O_2^{\bullet-} \quad (4)$$

$$2O_2^{\bullet-} + 2H_2O \rightarrow {}^1O_2 + H_2O_2 + 2OH^- \quad (5)$$

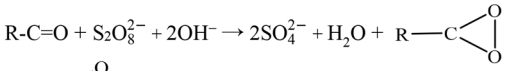

(6)

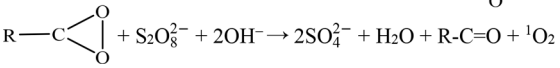

(7)

Overall, improved PS activation would lead to a higher AOP efficiency. However, cost-effective application of PS-based AOPs requires not only developing materials with better catalytic performance but also a systematic perspective to select the appropriate pathway (radical, nonradical, or their combination) to degrade specific contaminants in a given matrix. Therefore, a systematic comparison of these two pathways, including their merits and limitations, is included in the next section.

3. COMPARISON OF RADICAL AND NONRADICAL OXIDATION PROCESSES

Radical and nonradical oxidation in PS-based AOPs have received growing attention in the environmental sciences and chemistry literature, as evidenced by the exponentially increasing number of publications with a doubling time of 2.3 years (Figure 2a).[61,62] A brief overview of key milestones in the development of PS-based AOPs is included in this figure (Figure 2c). Previous reviews addressed six aspects of this process, including degradation of a range of contaminants,[63,64] PS activation mechanisms,[65,66] comparison with other AOPs,[13,67] identification of reaction pathways,[9,68] determination of reactive species,[69,70] and quantum chemistry calculations[71,72] (Figure 2b). Unlike previous reviews, we offer a critical comparison of radical and nonradical oxidation pathways regarding degradation kinetics, water matrix

https://doi.org/10.1021/acs.est.3c05153
Environ. Sci. Technol. 2023, 57, 12153−12179

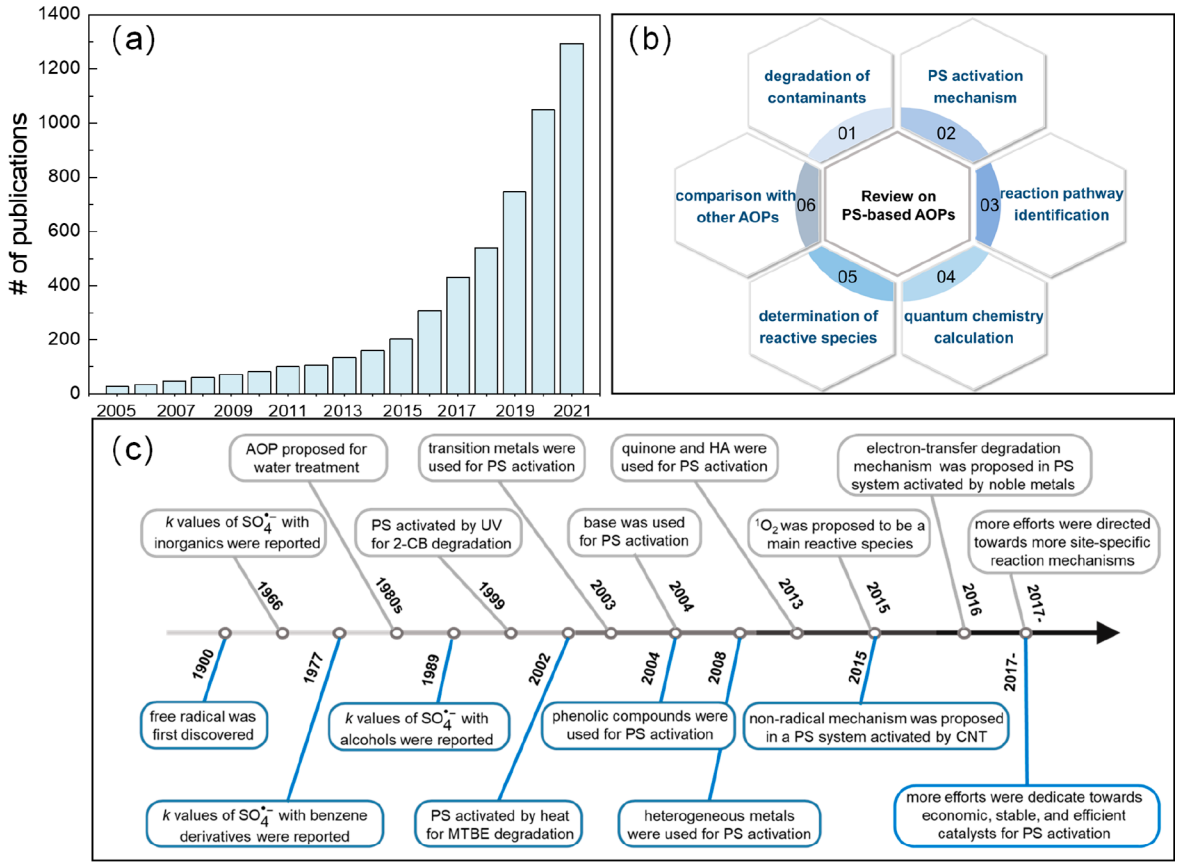

Figure 2. Peer-reviewed publications with the topic of PS activation: (a) Increasing number of publications over years with doubling time of 2.26 years (retrieved from Web of Science as of June 2022). (b) Topical foci of past literature reviews on PS-based AOPs. (The literature for 6 topics were mentioned and cited in the main text.) (c) The milestones over the progress of PS-based AOPs.[163,231,315−323]

interference, selectivity toward contaminants, temperature, pH, byproduct formation, and energy requirements. This section aims to provide a strong empirical basis for choosing an appropriate approach to degrade a specific class of contaminants.

3.1. Degradation Kinetics and Mechanisms. *3.1.1. Degradation Kinetics.* Degradation of contaminants is typically evaluated by degradation efficiency (% removal) at a given time and pseudo-first-order rate constants (k', min^{-1}). Mounting evidence demonstrates that reaction kinetics of radicals with various organic contaminants are faster than with nonradical species. For instance, the degradation of imidacloprid (IMI) was much faster with radical versus the nonradical-dominated PS reactions (*i.e.*, 87% versus 24% removal within 3 h).[73] Similarly, the k' value for bisphenol A (BPA) degradation was 6.3 times faster with $SO_4^{\bullet-}$ radicals than that with $^1O_2$.[74,75] However, neither degradation efficiency nor k' intrinsically reflect the nature of bimolecular reactions, as they vary with reaction time, reactor geometry, and initial concentration of target contaminants and reactive species, hindering comparisons. For example, different studies investigated acetaminophen (ACT) degradation by $SO_4^{\bullet-}$. The k' value was 0.033 min^{-1} in the presence of 0.28 mM ACT and 0.2 mM PS,[76] versus 0.199 min^{-1} with 1.4 mM ACT and 28.2 mM PS.[77] Thus, the difference in k' values for this same reaction varied by 6-fold, highlighting the importance of reaction conditions and matrix effects for k' determination.

The second-order rate constant (k, M^{-1} s^{-1}) circumvents this issue because it intrinsically reflects bimolecular reaction kinetics.[78] There are a large number of studies on the kinetics of radical ($SO_4^{\bullet-}$, $^{\bullet}OH$) and nonradical species (typically, $^1O_2$) reacting with compounds. Previous studies collected k values of these oxidants with different classes of organic compounds, including alcohols, acids, and aromatics,[8] and highlighted the selectivity of different reactive species. Generally, $SO_4^{\bullet-}$ exhibits less propensity to be scavenged by nontarget contaminants than $^{\bullet}OH$, but more propensity than nonradical species. To augment this effort, we compiled k values of different reactive species with specific organic contaminants for a higher resolution of the different reactivities. The reported k values of $SO_4^{\bullet-}$ and $^{\bullet}OH$ with various contaminants vary from 10^5 to 10^9 M^{-1} s^{-1},[79,80] while the k values of $^1O_2$ range from 10^3 to 10^7 M^{-1} s^{-1}[81] (Table 2). Differences in redox potentials may be one of the reasons for the discrepancy of k values. As shown in Table 3, the measured redox potential of $^1O_2$ is 0.81 V vs. NHE)[82] is significantly lower than that of $SO_4^{\bullet-}$ and $^{\bullet}OH$ (*i.e.*, 2.5−3.1 V vs. NHE, 1.8−2.7 V vs. NHE, respectively).[83] The higher redox potential indicates that radicals are thermodynamically more favorable to oxidizing relatively reduced organic compounds. Note that the redox potential is an important thermodynamic property. But kinetics and thermodynamic properties are not *a priori* correlated (with the possible exception of electron transfer reactions[84]).

Considering the effect of compound functional groups on kinetics, we further classified these contaminants into five categories, including amine (n = 5), carbonyl (n = 7), hydroxyl (n = 10), benzene ring (n = 21), and halogen groups (n = 10) (Figure 3). Note that we used the benzene ring rather than

https://doi.org/10.1021/acs.est.3c05153
Environ. Sci. Technol. 2023, 57, 12153−12179

Table 2. Comparison of Oxidants (*i.e.*, $SO_4^{\bullet-}$, $^{\bullet}OH$, and $^1O_2$) in Terms of Their k (M^{-1} s^{-1}) Values for Reactions with Organic Contaminants

	k (M^{-1} s^{-1})		
Contaminant	$SO_4^{\bullet-}$	$^{\bullet}OH$	$^1O_2$[a]
1,3-dichlorobenzene	1.1×10^{9}[230]	2.2×10^{9}[108]	$<10^4$
1-propanol	5.9×10^{7}[231]	2.8×10^{9}[108]	5.7×10^4
2,4,6-trichlorophenol	4.2×10^{9}[232]	6.3×10^{9}[233]	1.7×10^7
2,4-dichlorophenol	7.4×10^{9}[234]	3.3×10^{10}[235]	7.0×10^5
4-chlorophenol	8.7×10^{9}[234]	2.8×10^{10}[235]	6.0×10^6
4-chlorobenzoicaid	3.6×10^{8}[236]	5.0×10^{9}[236]	1.4×10^{7}[236]
4-nitrophenol	6.6×10^{8}[237]	3.8×10^{9}[238]	2.6×10^5
acetaminophen	1.3×10^{9}[85]	7.1×10^{9}[86]	3.4×10^5
acetophenone	1.8×10^{9}[239]	5.4×10^{9}[240]	2.7×10^{4}[241]
amoxicillin	2.9×10^{9}[242]	7.9×10^{9}[243]	1.4×10^5
anisole	4.9×10^{9}[244]	5.4×10^{9}[244]	2.0×10^{5}[245]
atrazine	2.6×10^{9}[236]	3.0×10^{9}[236]	4.0×10^{4}[236]
benzene	6.7×10^{8}[242]	7.8×10^{9}[108]	1.8×10^7
benzoic acid	1.2×10^{9}[242]	4.3×10^{9}[243]	$<10^6$
benzophenone	4.0×10^{9}[239]	8.7×10^{9}[246]	4.0×10^{3}[247]
bisphenol A	1.6×10^{9}[10]	6.9×10^{9}[248]	3.0×10^5
bromobenzene	1.8×10^{9}[249]	4.8×10^{9}[235]	1.9×10^{3}[231]
chlorobenzene	1.5×10^{9}[249]	5.6×10^{9}[250]	2.3×10^4
chloramphenicol	9.1×10^{8}[236]	1.8×10^{9}[236]	1.5×10^{6}[236]
cyclohexane	5.9×10^{5}[251]	6.1×10^{9}[80]	5.9×10^4
diclofenac	6.7×10^{9}[252]	7.5×10^{9}[253]	1.3×10^7
ethanol	5.6×10^{7}[254]	1.9×10^{9}[255]	7.1×10^4
fluorobenzene	9.8×10^{8}[256]	5.7×10^{9}[256]	2.3×10^4
furfuryl alcohol	1.3×10^{10}[69]	1.5×10^{10}[69]	1.2×10^8
imidacloprid	2.3×10^{9}[236]	7.5×10^{9}[236]	5.5×10^{6}[236]
L-histidine	2.5×10^{9}[69]	7.1×10^{9}[69]	3.2×10^{7}[69]
methanol	1.1×10^{7}[69]	9.7×10^{8}[69]	3.9×10^{3}[69]
nitrobenzene	$<10^{6}$[163]	3.9×10^{9}[257]	5.0×10^3
norfloxacin	9.0×10^{9}[258]	8.0×10^{9}[259]	1.8×10^6
phenol	8.8×10^{9}[260]	6.6×10^{9}[108]	2.6×10^6
pyridine	2.2×10^{8}[261]	3.0×10^{9}[108]	7.1×10^4
primidone	5.3×10^{8}[236]	6.7×10^{9}[236]	5.7×10^{5}[236]
sulfamethoxazole	1.2×10^{10}[262]	5.5×10^{9}[253]	2.0×10^4
sulfamethoxypyridazine	5.0×10^{10}[69]	6.2×10^{9}[69]	1.8×10^{6}[69]
sulfisoxazole	7.1×10^{10}[69]	7.4×10^{9}[69]	6.5×10^{7}[69]
thiacloprid	4.5×10^{9}[236]	4.8×10^{9}[236]	5.3×10^{5}[236]
tetrahydrofuran	2.4×10^{8}[263]	4.0×10^{9}[264]	4.8×10^4
tert-butanol	8.4×10^{5}[231]	6.0×10^{8}[108]	1.8×10^3
trimethoprim	7.7×10^{9}[236]	8.9×10^{9}[236]	6.2×10^{5}[236]

[a]The k values for $^1O_2$ reacting with contaminants are all from Wilkinson et al., 1995,[81] unless specified.

aromatics, as aromatics cover a wider range of compounds. We then compared the k values for these species with the contaminants containing the same functional group. As illustrated in Figure 3, regardless of functional groups, the k values with radicals (gray and purple bars) are significantly higher than those with $^1O_2$ (blue bars). Taking acetaminophen (ACT) as an example, the k values with $SO_4^{\bullet-}$ and $^{\bullet}OH$ were 1.3×10^9 and 7.1×10^9 M^{-1} s^{-1},[85,86] respectively, which was 4 orders of magnitude higher than that of $^1O_2$ (3.4×10^5 M^{-1} s^{-1}).[87] Note that many k values for the reactions of $^1O_2$ and contaminants were measured in organic solutions (*e.g.*, bromobenzene and chlorobenzene) rather than in aqueous phase, hindering comparability.[88] The solution matrix strongly influences the lifetime (τ) of $^1O_2$ (*e.g.*, 0.9 ms in CCl_4 *vs.* 2 μs in H_2O), and the short τ results in the low effective concentration in aqueous solution to oxidize the organic compounds.[89]

For wastewater treatment, total organic carbon (TOC) is one of the most important nonspecific water quality parameters inferring the complex matrix of organic substances from anthropogenic and natural sources.[90] In general, mineralization rates of organic contaminants assessed by residual TOC measurements are higher for treatment with radicals than with $^1O_2$.[11] Note that several studies used a decrease of TOC as an indicator for $^1O_2$ generation.[91] However, Lee *et al.* disputed this approach, postulating that $^1O_2$ is not powerful enough to mineralize many organic contaminants.[8]

Nonradical species include not only $^1O_2$, but also high-valent metals and surface-activated PS. Although several studies demonstrated their participation in the treatment process, few studies have reported k values for these nonradical species with organic contaminants[92] (which could be confounded because no method has yet been developed to produce these

https://doi.org/10.1021/acs.est.3c05153
Environ. Sci. Technol. 2023, 57, 12153−12179

Table 3. Comparison of Redox Potential (V, vs. normal hydrogen electrode), lifetime (s), pK_a, Diffusion Coefficient ($cm^2\ s^{-1}$), Absorption Maximum (nm), and Enthalpy of Formation (kcal mol^{-1}) for Radical and Nonradical Species[a]

reactive species	redox potential	lifetime	pK_a	diffusion coefficient[b]	absorption maximum	enthalpy of formation[d]
$SO_4^{\bullet-}$	$E^\circ(SO_4^{\bullet-}/SO_4^{2-})$ = 2.5-3.1 [83]	(3-4) × 10^{-5} [83]	< 0 [194]	1.49 × 10^{-5}	450 [265]	-145 [109]
$^\bullet OH$	$E^\circ(^\bullet OH/OH^-)$ = 1.8-2.7 [83]	1.0× 10^{-9} [108]	11.9 [108]	2.30 × 10^{-5}, [108]	225 [108]	8.93 [266]
$Cl^\bullet$	$E^\circ(Cl^\bullet/Cl^-)$ = 2.2-2.6 [267]	N.A.	N.A.	2.42 × 10^{-5}	320 [265]	28.9[e]
$Cl_2^{\bullet-}$	$E^\circ(Cl_2^{\bullet-}/2Cl^-)$ = 2.1-2.3 [267]	N.A.	N.A.	1.70 × 10^{-5}	340 [265]	-61.4
$HOCl^{\bullet-}$	$E^\circ(HOCl^{\bullet-}/Cl^-)$=1.9 [267]	N.A.	-4.7[a]	1.54 × 10^{-5}	211[c]	-66.4
$Br^\bullet$	$E^\circ(Br^\bullet/Br^-)$ = 2.0 [268]	N.A.	N.A.	1.74 × 10^{-5}	156[c]	37.3[e]
$Br_2^{\bullet-}$	$E^\circ(Br_2^{\bullet-}/2Br^-)$ = 1.7 [268]	N.A.	N.A.	1.61 × 10^{-5}	360 [265]	-55.9
$CO_3^{\bullet-}$	$E^\circ(CO_3^{\bullet-}/CO_3^{2-})$ =1.6 [269]	5.0 × 10^{-4} [145]	< 0 [270]	1.97 × 10^{-5}	600 [265]	-112 [e]
$ClO^\bullet$	$E^\circ(ClO^\bullet/ClO^-)$ = 1.4-1.8 [267]	N.A.	N.A.	2.34 × 10^{-5}	165[d]	24.6
$^1O_2$	$E^\circ(^1O_2/O_2^{\bullet-})$ = 0.81 [271]	2.0 × 10^{-6} [89]	N.A.	2.61 × 10^{-5}	N.A.	22.5 [48]
HOCl	$E^\circ(HOCl/Cl^-)$ =1.5 [272]	≈ 2600 [273]	7.5 [274]	2.01 × 10^{-5}	242 [275]	-17.8 [276]
Fe^{IV}	$E^\circ(Fe^{IV}/Fe^{III})$ =1.8-2.0 [104]	N.A.	N.A.	N.A.	N.A.	N.A.
Co^{III}	$E^\circ(Co^{III}/Co^{II})$ =1.8-1.9 [104]	N.A.	N.A.	N.A.	N.A.	N.A.
Cu^{III}	$E^\circ(Cu^{III}/Cu^{II})$ =1.6-2.3 [104]	N.A.	N.A.	N.A.	N.A.	N.A.

[a]Radicals are within blue shadowed areas, while nonradical species are in gray shadow. Note that except $SO_4^{\bullet-}$ and $^\bullet OH$, other radicals are the possible secondary/tertiary radicals between halide/carbonate anions with $SO_4^{\bullet-}$/$^\bullet OH$. (a) The pK_a of $HOCl^{\bullet-}$ was calculated by the means of DFT at M052X/6-31+G** and PCMP/M052X/6-311++G** level of theory. (b) The diffusion coefficients were calculated by the means of DFT at B3LYP/6-311++G (3df, 3pd) level of theory, unless specified. (c) The absorption maxima were calculated by the means of DFT at TD/B3LYP/6-311++G** level of theory. (d) The enthalpies of formation at 298 K in gas phase were calculated with the G4 composite method using the Gaussian 09, unless otherwise specified. (e) The data were collected from NIST. N.A.: Not available.

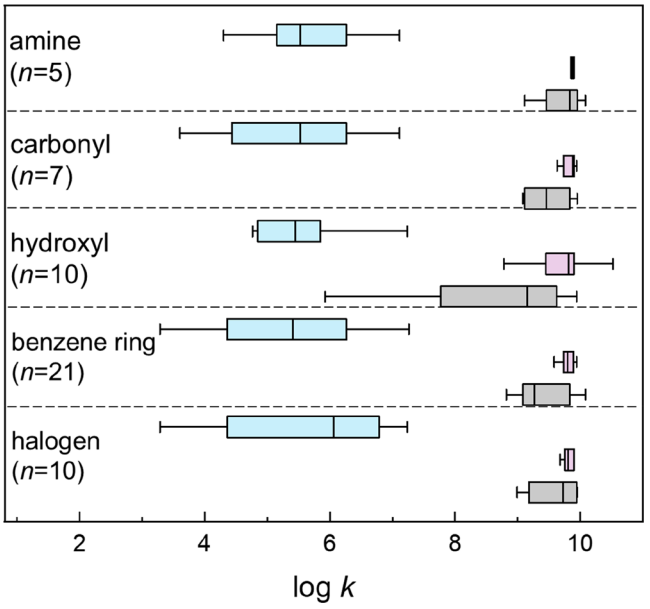

Figure 3. Comparison of k values for the reactions of selected organic compounds with $^1O_2$ (blue bar), $^\bullet OH$ (purple bar), and $SO_4^{\bullet-}$ (gray bar). The selected compounds were classified into 5 functional groups, namely, amine, carbonyl, hydroxyl, benzene ring, and halogen group. (Compounds with carboxyl group were incorporated into carbonyl group, and compounds with carboxamide group were incorporated into amine group. The left and right side of each box represent the lower and upper quartiles, respectively. The left and right bars represent the minimum and maximum values. Vertical line in the middle of the box denotes the median value.

nonradical species under steady-state or without other coexisting species).[93] Overall there is a critical need to develop efficient determination methods for k values of nonradical species and advance our understanding of these relatively unexplored reaction kinetics. Note that steady-state concentrations of these reactive species should be considered for a more holistic comparison of radical versus nonradical pathway kinetics. However, concentrations of reactive species vary greatly in different systems and are strongly dependent on reaction conditions (*e.g.*, initial concentration of precursors, water matrix, and pH).

3.1.2. Reaction Mechanisms. Radicals and nonradical species exhibit different reaction pathways in reacting with contaminants. In radical systems, $SO_4^{\bullet-}$ and $^\bullet OH$ degrade many organic compounds primarily by similar mechanisms: (1) hydrogen atom abstraction (HAA); (2) single electron transfer (SET); and (3) radical addition formation (RAF).[94,95] However, there is a slight difference between these two types of species. For example, for aliphatic carboxylic compounds, the first step of $SO_4^{\bullet-}$ reacting with them is via electron abstraction from an oxygen atom in carboxylic group to $SO_4^{\bullet-}$ itself.[96] In contrast, $^\bullet OH$ preferentially abstracts a hydrogen atom from the α position in the aliphatic chain.[97]

In nonradical systems, deciphering the reaction pathways presents many challenges, and the only nonradical species that is relatively well understood might be $^1O_2$.[98] As a highly selective electrophile, electrophilic addition was indicated as the typical reaction pathway for $^1O_2$ reacting with unsaturated compounds (Figure 4).[98,99] For an isolated double bond, it reacts with $^1O_2$ via cycloaddition forming 1,2-cycloperoxides (Figure 4a), while for a double bond connected to a polar hydrogen-bearing group, 1,3-addition is typically the reaction pathway forming allylic hydroperoxides (Figure 4b). Conjugated dienes react with $^1O_2$ via Diels−Alder reactions, forming endoperoxide (Figure 4c). For phenols and naphthols, 1,4-addition can be the main reaction mechanism, forming a hydroperoxide (Figure 4d).

$^1O_2$ can also combine with sulfur atoms in sulfides. This reaction can be envisioned as donation of the sulfur's lone electron pair into the empty π orbitals of $^1O_2$, forming peroxysulfoxide.[100,101] This product is unstable and can undergo a series of reactions, including homolytic cleavage of the peroxy bond and substitution reactions with nucleophiles. Compared with radicals, $^1O_2$ is less thermodynamically favorable to oxidize reduced organic compounds via electron transfer. However, there are several exceptions. Some investigations studied the reaction of phenolic compounds with EDGs and $^1O_2$, and observed that the compounds lose

https://doi.org/10.1021/acs.est.3c05153
Environ. Sci. Technol. 2023, 57, 12153−12179

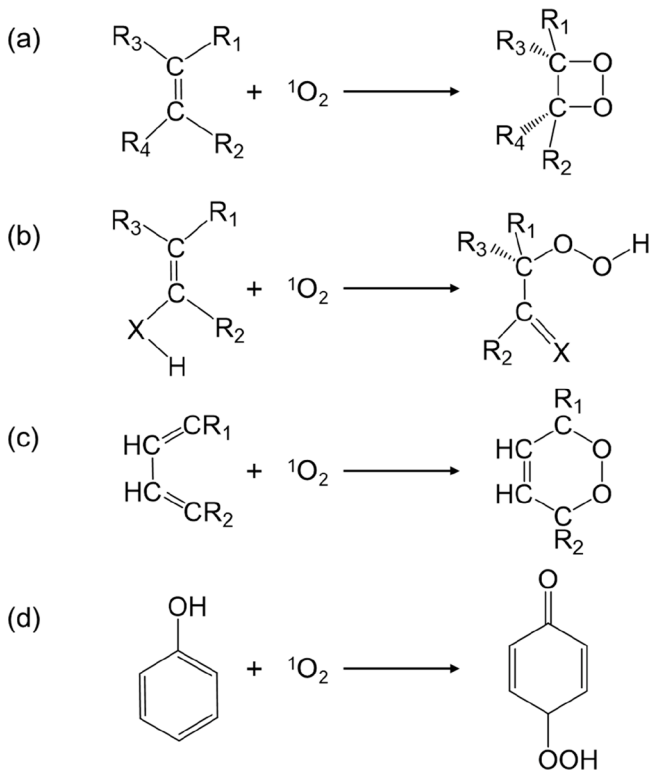

Figure 4. Typical reactions of $^1O_2$ addition to unsaturated compounds. (a) Addition to olefins; (b) addition to olefin derivatives with hydrogen-bearing groups: X refers to CR_2/NR/O; (c) Diels–Alder reaction to conjugated dienes; and (d) addition to phenol and naphthol derivatives.

one electron forming radical cations, and $^1O_2$ gains one electron forming $O_2^{\bullet-}$.[102] In addition, $^1O_2$ can react with compounds containing nitrogen atoms via electron transfer, and this pathway can be assessed by Fukui functions of f^- and f^0.[103,104] For example, the highest f^- value of sulfamethoxazole (SMX) is located on amino N atom, indicating that this atom is the most vulnerable to lose electron and be attacked by electrophilic $^1O_2$.[105]

The different reactivities between radicals and $^1O_2$ may be partially attributed to the combined effect of their lifetimes and redox potentials (Table 3). Compared to $^1O_2$ (2 μs in H_2O and 0.81 V vs. NHE),[89] with similar diffusion coefficients (Table 3), the lifetime and redox potential of $SO_4^{\bullet-}$ are significantly higher (30–40 μs in H_2O and 2.5–3.1 V vs. NHE),[106] allowing faster mass transfer of $SO_4^{\bullet-}$. For $^\bullet$OH, the lifetime is shorter (approximately ns in H_2O) than $SO_4^{\bullet-}$,[107] which can be explained by its enthalpy of formation. As shown in Table 3, the enthalpy of formation of $^\bullet$OH (8.93 kcal mol^{-1})[108] is significantly higher than that of $SO_4^{\bullet-}$ (−145 kcal mol^{-1}),[109] indicating that $^\bullet$OH is more reactive and has a greater tendency to participate in chemical reactions. In water treatment, there is only one pathway to quench $^\bullet$OH (*i.e.*, reactions with a water matrix). In contrast, in addition to scavenging by water matrix, $^1O_2$ can be physically quenched, undergoing energy transfer back to ground state $^3O_2$ and radiative emission (*i.e.*, phosphorescence).[110−112]

For high-valent metals, three pathways have been recognized, namely electron transfer, HAA and oxygen atom transfer (OAT).[113] For electron transfer, high-valent metals typically exhibit relatively high redox potentials (Table 3),[104] indicating that they are thermodynamically favorable to react with contaminants containing EDGs. For example, Fe(IV) with redox potential of 1.80 V can react with BPA and acetamidophenol, while it shows low reactivity toward organic compounds containing EWGs (*e.g.*, benzoic acid and nitrobenzene).[114] For HAA, high-valent metals can abstract a hydrogen atom from contaminants, yielding intermediate radicals. They further react with other substrates or undergo self-recombination.[92] For OAT, high-valent metals can react with sulfoxides (*e.g.*, methyl-phenyl sulfoxide and dimethyl sulfoxide) and produce corresponding sulfones.[115] These sulfones are not formed in radical-induced pathways.[116] Therefore, sulfoxides can be used as a chemical probe to identify the degradation pathway initiated by high-valent metals.[117,118]

PMS direct oxidation of contaminants is also an important nonradical pathway, particularly for contaminants with electron-donating groups (EDGs) when PMS is not activated. The degradation can be induced by two electrons, one electron, and $^1O_2$.[119−121] For two-electron oxidation (the most common pathway), PMS is more apt to be attacked by nucleophiles, followed by oxygen atom transfer:

$$HSO_5^- + TC \rightarrow HSO_4^- + TC{-}O \quad (8)$$

This oxidation pathway was reported for antibiotics containing sulfur atoms (*e.g.*, β-lactam and sulfonamides antibiotics).[4,5] In addition to organic contaminants, the nonpolar PMS can also react with several inorganic ions via two-electron transfer, including X^-, CN^-, N_3^-, and HCO_3^-.[8] Therefore, when elucidating these effects of anions, caution must be exercised, as they can scavenge reactive species and deplete PMS. For one-electron oxidation, PMS can react with contaminants forming organic radical cations (eq 9).[122] This is due to the fact that PMS has a redox potential of 1.82 V, which is comparable to that of many oxidants (*e.g.*, HOCl of 1.48 V, H_2O_2 of 1.80 V and $KMnO_4$ of 1.68 V).[2]

$$HSO_5^- + TC \rightarrow SO_4^{2-} + OH^- + TC^{\bullet+} \quad (9)$$

The resulting $TC^{\bullet+}$ is not stable and can undergo further oxidation or back reduction (BR) to TC. Reduction from $TC^{\bullet+}$ to TC can be triggered by dissolved organic matter (DOM), coexisting contaminants, and $O_2^{\bullet-}$.[123−125] In addition, many studies claimed that PMS can undergo self-decomposition, especially at slightly alkaline pH forming $^1O_2$ (eqs 10 and 11) that subsequently degrades some contaminants.[126]

$$HSO_5^- \rightarrow SO_5^{\bullet-} + H^+ + e^- \quad (10)$$

$$SO_5^{\bullet-} + SO_5^{\bullet-} \rightarrow S_2O_8^{2-} + {}^1O_2 \quad (11)$$

However, degradation of target contaminants via $^1O_2$ from the self-decomposition of PMS is limited, as PMS decomposes slowly in water.[127]

3.2. Water Matrix. In natural waters, inorganic ions and natural organic matter (NOM) are commonly present and can greatly influence PS-based AOPs.[128] Compared to nonradical species, radicals are more sensitive to effects of the water matrix. In this review, we also consider DOM, a class of water-soluble NOM, since not all NOMs (*e.g.*, humins and humic acid at low pH) are soluble in water.[129] We also include the influence of effluent organic matter (EfOM), consisting of NOM, soluble microbial products (SMPs), and trace organic chemicals.[130,131]

https://doi.org/10.1021/acs.est.3c05153
Environ. Sci. Technol. 2023, 57, 12153−12179

For radical systems, coexisting substances in natural waters can either inhibit or promote the degradation efficiency of contaminants. As inhibitors, inorganic anions may quench radicals and compete with target contaminants for radicals, resulting in decreased removal efficiency.[132] For example, the degradation efficiency of 1,1,1-tricholroethane (TCA) degradation by ultrasound-activated PS decreased from 89% to 35%, as the concentrations of anions (Cl^-, HCO_3^-, CO_3^{2-}) increased from 0.001 to 0.1 M, indicating that these anions hindered degradation kinetics.[133] A series of reactions have been proposed for $SO_4^{\bullet-}$ and $^\bullet OH$ with these anions to support the inhibition effect they observed:

$$SO_4^{\bullet-} + Cl^- \rightarrow Cl^\bullet + SO_4^{2-} \quad (12)$$

$$SO_4^{\bullet-} + HCO_3^- \rightarrow SO_4^{2-} + H^+ + CO_3^{\bullet-} \quad (13)$$

$$SO_4^{\bullet-} + CO_3^{2-} \rightarrow SO_4^{2-} + CO_3^{\bullet-} \quad (14)$$

$$^\bullet OH + Cl^- \rightarrow HOCl^{\bullet-} \quad (15)$$

$$^\bullet OH + CO_3^{2-} \rightarrow CO_3^{\bullet-} + OH^- \quad (16)$$

$$^\bullet OH + HCO_3^- \rightarrow CO_3^{\bullet-} + H_2O \quad (17)$$

Figure 5a presents possible transformation pathways of these secondary radicals, based on their physicochemical properties (Table 3). Taking reactive chlorine species as an example, a proportion of $Cl^\bullet$ may be coupled to terminate the chain reaction and generate Cl_2 (eq 18). The remaining $Cl^\bullet$ may react with excess Cl^- to produce $Cl_2^{\bullet-}$ (eq 19), which may also recombine with another $Cl_2^{\bullet-}$, yielding Cl_2 and chloride (eq 20). Subsequently, the newly generated Cl_2 may hydrolyze, forming HOCl (eq 21). Under UV irradiation, a fraction of HOCl can dissociate to form $^\bullet OH$ and $Cl^\bullet$ (eq 22) and in turn react with excess HOCl producing $ClO^\bullet$ (eq 23 and 24).[134] Further, $ClO^\bullet$ can be scavenged by CO_3^{2-}; however, this reaction can be neglected due to the low k value of 600 $M^{-1}\,s^{-1}$ (eq 25).[135] $HOCl^{\bullet-}$ from eq 15, can be rapidly converted to form $Cl^\bullet$ through protonation, with k of 2.1 × $10^{10}\,M^{-1}\,s^{-1}$ at pH below 7.2 (eq 26). Conversely, when pH is above 7.2, $HOCl^{\bullet-}$ is the dominant species and it can further dissociate back to $^\bullet OH$ and Cl^- with k of 6.1 × $10^9\,M^{-1}\,s^{-1}$ (eq 27).[136] Due to the reversible reaction of Cl^- and $^\bullet OH$, the effect of Cl^- is complex, and Cl^- might be both an inhibitor or promoter in $^\bullet OH$ based-AOPs for wastewater treatment. For the $CO_3^{\bullet-}$, it can self-terminate to yield CO_2 (eq 28). In addition, a fraction of $CO_3^{\bullet-}$ may react with DOM, forming CO_3^{2-} and $DOM^{\bullet+}$ (eq 29).[137]

$$Cl^\bullet + Cl^\bullet \rightarrow Cl_2 \quad (18)$$

$$Cl^\bullet + Cl^- \rightarrow Cl_2^{\bullet-} \quad (19)$$

$$Cl_2^{\bullet-} + Cl_2^{\bullet-} \rightarrow Cl_2 + 2Cl^- \quad (20)$$

$$Cl_2(aq) + H_2O \rightarrow HOCl + H^+ + Cl^- \quad (21)$$

$$HOCl + h\nu \rightarrow {}^\bullet OH + Cl^\bullet \quad (22)$$

$$HOCl + Cl^\bullet \rightarrow ClO^\bullet + H^+ + Cl^- \quad (23)$$

$$HOCl + {}^\bullet OH \rightarrow ClO^\bullet + H_2O \quad (24)$$

$$ClO^\bullet + CO_3^{2-} \rightarrow CO_3^{\bullet-} + ClO^- \quad (25)$$

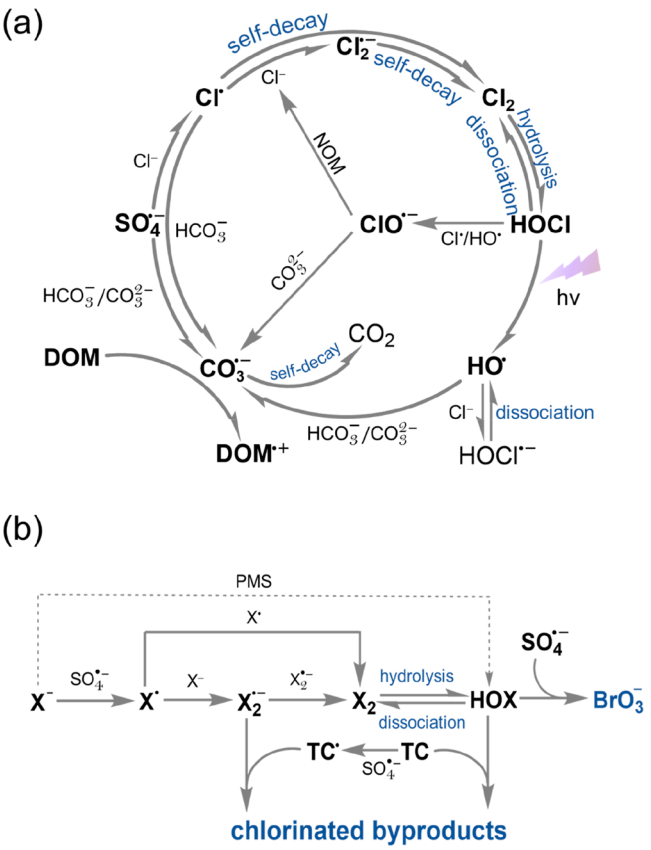

Figure 5. Transformation of coexisting inorganic anions in radical system. (a) Primary and secondary reactions for $SO_4^{\bullet-}$ and $^\bullet OH$ with coexisting inorganic anions (*i.e.*, Cl^-, HCO_3^-, and CO_3^{2-}). (b) Generation of halogenation byproducts between halides and $SO_4^{\bullet-}$. X and TC refer to halide ions (*i.e.*, Cl^- or Br^-) and target compounds, respectively. The dotted arrow shows formation of hypohalous acid (HOX) from the oxidation of halides by PS; this pathway is not frequently reported.[211]

$$HOCl^{\bullet-} + H^+ \rightarrow Cl^\bullet + H_2O \quad (26)$$

$$HOCl^{\bullet-} \rightarrow {}^\bullet OH + Cl^- \quad (27)$$

$$CO_3^{\bullet-} + CO_3^{\bullet-} \rightarrow CO_2 + CO_4^{2-} \quad (28)$$

$$CO_3^{\bullet-} + DOM \rightarrow CO_3^{2-} + DOM^{\bullet+} \quad (29)$$

In addition to anions, NOM and EfOM can also suppress the degradation of TC. During piroxicam (PIR) degradation in a Fe^{2+}/PS system, the removal of PIR decreased from 69% in ultrapure water to 26% in the presence of 10 mg L^{-1} of humic acid (HA). This inhibition was attributed to the interaction between HA and $SO_4^{\bullet-}$.[138] To quantify the suppressive effect of NOM on $SO_4^{\bullet-}$-induced degradation, the k value of $SO_4^{\bullet-}$ with HA was determined using an indirect kinetic competition method.[139] This k value was reported to be 6.6 × 10^3 L mg-$C^{1-}\,s^{-1}$ (mg-C refers to mg carbon). In addition to HA, the reactivity of $SO_4^{\bullet-}$ with four typical types of NOM was also measured, including Elliott Soil fulvic acid (ESFA), Suwannee River fulvic acid (SRFA), Suwannee River aquatic natural organic matter (SRNOM), and Nordic Lake aquatic natural organic matter (NLNOM). The k values obtained by laser flash photolysis (LFP) were between 1.53 × 10^3 and 3.50 × 10^3 L mg-$C^{1-}\,s^{-1}$.[140] These kinetic data corroborate that NOM can quench radicals, resulting in decreased degradation

https://doi.org/10.1021/acs.est.3c05153
Environ. Sci. Technol. 2023, 57, 12153−12179

kinetics. Hence, for practical remediation of PS-based AOPs, radicals consumed by the water matrix should be carefully considered when the PS dosage is determined. The contribution (f) of the water matrix to scavenging radicals can be calculated as

$$f = \frac{k_s[S]}{k_s[S] + k_{TC}[TC]} \times 100\% \quad (30)$$

where k_s and k_{TC} are second-order rate constants of radicals with scavengers and target compounds, respectively. To evaluate the inhibition effects of the water matrix, the concentrations of coexisting substances and their k values with radicals should be considered. For example, even when Br^- is present at very low concentrations (0.5 mg L^{-1}), its k value with $^{\bullet}OH$ is 1.1×10^{10} M^{-1} s^{-1}, thus Br^-readily scavenges $^{\bullet}OH$ with an f value of 24%.[141]

Interestingly, many studies reported a positive (*i.e.*, promotive) effect of anions on the degradation of contaminants in PS-based AOPs. For example, the inorganic ions Br^-, CO_3^{2-}, and PO_4^{3-} enhanced phenol (PhOH) oxidation during treatment by heat-activated PS.[142] Apparently, Br^- scavenges $SO_4^{\bullet-}$ producing $Br^{\bullet}$, further reacting with Br^- and OH^- to form bromine radicals (*e.g.*, $Br_2^{\bullet-}$ and $BrOH^{\bullet-}$):

$$SO_4^{\bullet-} + Br^- \rightarrow Br^{\bullet} + SO_4^{2-} \quad (31)$$

$$Br^{\bullet} + Br^- \rightarrow Br_2^{\bullet-} \quad (32)$$

$$HO^- + Br^{\bullet} \rightarrow BrOH^{\bullet-} \quad (33)$$

The bromine reactive species produced can selectively react with PhOH, thus, increasing the overall degradation rate. However, this study did not explain the selectivity of bromine reactive species, which we postulate act as electrophiles with a strong tendency to react with electron-rich compounds via electron transfer. The positive effect of CO_3^{2-} and PO_4^{3-} can be attributed to the protonation of anions, which increases the solution pH:

$$\text{carbonate ion} + H_2O \rightarrow HCO_3^- + HO^- \quad (34)$$

$$PO_4^{3-} + H_2O \rightarrow HPO_4^{2-} + HO^- \quad (35)$$

Then, under basic conditions, PS can be activated to increase the yield of radicals for contaminant degradation.[18] Furthermore, when solution pH is higher than 10, PhOH exists in anionic form (*i.e.*, phenoxide), which is more reactive (1−7 orders of magnitude higher) with radical species.[143,144] Overall, distinguishing the contribution of alkaline activation and reactivity of phenoxide to PhOH degradation still remains a hurdle without buffering the working solution. Alternatively, another explanation for the positive effect of CO_3^{2-} could be that it can react with $SO_4^{\bullet-}$ generating $CO_3^{\bullet-}$:

$$CO_3^{2-} + SO_4^{\bullet-} \rightarrow CO_3^{\bullet-} + SO_4^{2-} \quad (36)$$

The formed $CO_3^{\bullet-}$ may oxidize PhOH, a compound with electron rich moiety via single electron transfer pathway.[145]

The effect of the water matrix on degradation of contaminants in nonradical systems also depends on the concentration of co-occurring substances. When the concentration of these substances is relatively low, nonradical species have the advantage of being less affected by water matrix. For example, $^1O_2$ was the main reactive oxygen species (ROS) when Fe-doped g-C_3N_4 was used to activate PS for BPA removal. In this work, a negligible effect was observed on BPA degradation efficiency upon increasing the concentration of anions (*e.g.*, Cl^-, NO_3^-, and SO_4^{2-}) from 0 to 5 mM.[146] Note that this phenomenon can also be used to preliminarily assess reaction mechanisms. (If perturbation is observed, it is a radical-induced reaction; otherwise, it is a nonradical mechanism.) However, high concentrations of co-occurring substances (especially inorganic anions) can enhance contaminant degradation by enabling PS activation to generate nonradical species.[11,147] For example, PMS alone exhibited almost no reactivity with 2,4-dichlorophenol (2,4-DCP). However, in the presence of 50 mM Cl^-, 2,4-DCP was completely removed within 60 min, and the main ROS in the in the Cl^-/PMS system was deduced to be HOCl.[148]

$$Cl^- + HSO_5^- \rightarrow SO_4^{2-} + HOCl \quad (37)$$

In addition to Cl^-, a number of recent studies proposed that other anions (*e.g.*, HCO_3^-, PO_4^{3-}, and BO_2^-) can active PS to generate nonradical species for contaminant degradation.[147,149] For example, HCO_3^- reacts with PS forming peroxymonocarbonate (HCO_4^-), which was proposed to be an efficient oxidant.[150]

$$HCO_3^- + S_2O_8^{2-} + 2OH^- \rightarrow HCO_4^- + 2SO_4^{2-} + H_2O \quad (38)$$

Moreover, several studies indicated that as a base nucleophile (Nu), pyrophosphate ($P_2O_7^{4-}$) was expected to react with PMS forming intermediates ($NuOH^+$) by breaking the peroxide bond.[151] Subsequently, $NuOH^+$ reacts with PMS, generating $^1O_2$ for the degradation of contaminants.

$$Nu + HSO_5^- \rightarrow NuOH^+ + SO_4^{2-} \quad (39)$$

$$NuOH^+ + HSO_5^- \rightarrow Nu + {}^1O_2 + HSO_4^- + H^+ \quad (40)$$

3.3. Selectivity. In broad terms, selectivity refers to when one reaction is overwhelmingly more favorable than others.[152] Here, selectivity refers to radical/nonradical species in PS-based AOPs preferentially reacting with compounds bearing specific functional groups and not others, rather than to reactive species with a high anti-interference capacity in a complex matrix (*e.g.*, with inorganic anions and NOM).

In nonradical systems, benzene compounds with electron-donating groups (EDGs) such as hydroxyl, amino, alkoxy, and phenyl-ester, are more prone to react with nonradical species than compounds with electron-withdrawing groups (EWGs). A few recent studies proposed the ionization potential (*IP*) is an important parameter to assess the capacity of electron donating/withdrawing effects. Compounds with EDGs tends to have a low *IP* value, while EWGs will result in a high *IP* value.[153] In addition, many studies proposed that there is a threshold *IP* value (9.0 eV) determining the feasibility of reaction in N-graphene/PMS systems.[154,155] Below 9.0 eV, degradation of contaminants by nonradical species can be achieved, whereas low reactivity (*i.e.*, slow kinetics or no reaction at all) was observed for compounds with *IP* greater than this value.[10,155] Although this threshold may not be applicable for other systems, the trend of easier degradation with lower *IP* still holds true for nonradical species.[70,156] Note the selectivity investigation of nonradical species is often limited to $^1O_2$, but this review extends to surface activated PS and high-valent metals.

$^1O_2$ exhibited low reactivity with benzoic acid (BA) with a high *IP* value of 9.47 eV, whereas PhOH and BPA with a lower

https://doi.org/10.1021/acs.est.3c05153
Environ. Sci. Technol. 2023, 57, 12153−12179

Table 4. Reaction Rate Constant k for the Reactions of $SO_4^{\bullet-}$/$^{\bullet}OH$ with the Six Compounds Mentioned in Nonradical Induced Degradation[a]

compounds	IP	functional group and Σσ	k (M^{-1} s^{-1})	
			$SO_4^{\bullet-}$	$^{\bullet}OH$
phenol	8.49	—OH, strong EDG, − 0.37	8.8×10^9	6.6×10^9
tetracycline	6.94	—OH, strong EDG, N.A.	2.2×10^9	4.6×10^9
bisphenol A	7.44	—OH, strong EDG, N.A.	1.6×10^9	6.9×10^9
2,4-dichlorophenol	8.38	—Cl, weak EWG, 0.23[b]	7.4×10^9	3.3×10^9
benzoic acid	9.47	—COOH, moderate EWG, 0.44	1.2×10^9	4.3×10^9
terephthalic acid	9.90	—COOH, moderate EWG, 0.88[c]	1.7×10^8	4.0×10^9

[a]IP refers to ionization potential with the unit of eV. EDG and EWG stands for electron donating and withdrawing groups, respectively, and Σσ is the summation of the Hammett substituent constants for a TC. N.A.: Not available. [b]$\Sigma\sigma = \sigma(OH) + \sigma(Cl)_m + \sigma(Cl)_p = -0.37 + 0.373 + 0.227 = 0.23$. m and p refer to meta and para position, respectively. [c]$\Sigma\sigma = 2 \times \sigma(COOH) = 2 \times 0.44 = 0.88$.

IP of 8.49 and 7.44 eV, respectively, were readily degraded by $^1O_2$.[157] Surface-activated PS can effectively degrade phenolic compounds with *IP* below 9.0, while compounds bearing EWGs (*e.g.*, BA, 9.47 eV and nitrobenzene, 10.2 eV) were resistant to degradation.[158] Similarly for high-valent metals, compounds with EDGs have lower *IP* values (*e.g.*, tetracycline hydrochloride (TCHC) of 6.94 eV and BPA of 7.44 eV), resulting in high degradation efficiency of 89% and 100%, respectively.[159] In contrast, terephthalic acid (TPA, 9.90 eV)[160] and 2,4-DCP (8.38 eV) containing EWGs with higher *IP* values were less likely to be degraded within 1 h.[156] Note that the *IP* values of TCHC and 2,4-DCP in Table 4 were calculated by density functional theory (DFT) at M062X/6-31G* level of theory.[161]

In radical systems, numerous studies have shown that radicals indiscriminately react with target compounds containing either EDGs or EWGs.[10,77] For comparison with nonradical systems, we considered the above-mentioned compounds (*i.e.*, PhOH, TCHC, BPA, 2,4-DCP, BA, and TPA). We tabulated the k values of these compounds containing EDGs and EWGs (Table 4). Their Hammett substituent constants (σ), an empirical parameter for the prediction of equilibrium and rate constants of benzene derivatives, are also listed. The σ values of EDGs are positive and the σ values of EWGs are negative. As shown in Table 4, although the σ values of compounds are significantly different, their k values are all on the order of 10^9 M^{-1} s^{-1}, approximating diffusion-controlled processes.

Note that the nonselectivity of radicals should be considered in a relative context. Otherwise, this perception may be debatable, as $SO_4^{\bullet-}$ exhibits a wide range in reactivity toward contaminants bearing EDGs or EWGs.[153,162] For example, considering k values for reactions of $SO_4^{\bullet-}$ with substituted benzenes (determined by pulse radiolysis at pH 7), the k value of anisole (with alkoxy EDG) was reported to be 4.9×10^9 M^{-1} s^{-1}, which is significantly higher than that of *p*-nitrobenzoate (with carboxyl and nitro EWGs) ($k \leq 10^6$ M^{-1} s^{-1}).[163]

3.4. Temperature and pH. In principle, the temperature, pH, and ionic strength (*IS*) are three important parameters in determining the reaction kinetics and mechanisms in complex water matrices. In the following section, we discussed the effects of temperature and pH on degradation processes of contaminants via radical and nonradical pathways. However, *IS* is not explicitly discussed in this section, as most studies focused on its effects on performance of catalysts (*e.g.*, zeta potential and adsorption profile), rather than different pathways.[164,165] In addition, *IS* affects the generation of reactive species, which was already discussed in detail in section 3.2.

3.4.1. Temperature. Temperature is a key environmental factor that affects the degradation processes of contaminants in PS-based AOPs. In radical systems, within a certain temperature range (*e.g.*, from 40 to 60 °C[166] and from 40 to 80 °C[167]), higher temperature is more likely to break the peroxide (O−O) bond of PS and hence, generate more radical species, ultimately enhancing removal efficiency of target contaminants. This trend was documented in many studies.[168,169] However, it is not applicable to the high-temperature ranges (*e.g.*, 75 °C[170] and 60 °C[171]). Extremely high temperature may lead to radical-self-quenching or reacting with PS (not radical-induced degradation of contaminants) due to high concentration of radicals.[172] For example, perfluorooctanoic acid (PFOA) degradation by $SO_4^{\bullet-}$ under high pressure was slower at 150 °C than at 80 °C, because high $SO_4^{\bullet-}$ levels triggered radical self-quenching reactions.[173] Note that previous reviews mainly focused on the temperature effects on radical yields. However, little consideration has been given to the effects of temperature on byproduct distribution, catalytic performance, and catalyst synthesis for PS-based AOPs, which are addressed below.

Several individual studies investigated the effects of temperature on contaminant transformation pathways and byproduct distribution in PS-based AOPs.[174,175] Decarboxylation and hydroxylation may coexist for BA transformation in $SO_4^{\bullet-}$-induced degradation. At 22 °C, hydroxylation was the prominent degradation pathway, but with the temperature increased to 70 °C, the proportion of decarboxylation significantly increased.[176] Regarding distribution of byproducts, formation of brominated and iodinated dihaloacetamides (DHAcAms) during PS oxidation in the presence of Br^- and I^- was investigated. The iodinated-disinfection byproducts (I-DBPs) were the predominant products with temperatures lower than 35 °C, whereas brominated-disinfection byproducts (Br-DBPs) became increasingly dominant at temperatures above 35 °C.[177]

Temperature also affects the performance of catalysts in radical and nonradical systems.[37,178] For example, using hexagonally ordered mesoporous carbon,[179] complete removal of 2,4-DCP required 2 h at 25 °C versus 0.6 h at 45 °C. In addition to the fact that higher temperature accelerates decomposition of PS, higher temperature could promote adsorption between the catalyst and PS, ultimately enhancing the performance of the mesoporous carbon catalyst. Note that we did not find other studies reporting the effect of the reaction temperature on catalytic performance; rather, most studies investigated the effect of the temperature on synthesiz-

https://doi.org/10.1021/acs.est.3c05153
Environ. Sci. Technol. 2023, 57, 12153−12179

ing catalysts. For example, a positive effect of higher annealing temperature (500−1100 °C) was found for preparing nanodiamonds (ND),[180] which was reflected on enhanced PhOH degradation efficiency due to the optimization of surface oxygen functionalities and reconstruction of carbon configuration. In contrast, another study used modified metal−organic framework (MOF) to activate PS for orange G (OG) degradation.[181] Fourteen types of MIL-Fe (Materials of Institut Lavoisier) under different temperatures (100−200 °C) were prepared, and it was found that the optimum temperature was 150 °C. At this temperature, this MIL-Fe catalyst has the largest surface area and highest content of coordinatively unsaturated Fe^{2+} sites.[181] Overall, the effect of the temperature on the catalytic performance likely depends on the type of catalyst and associated mechanisms.

Very few studies on temperature effects are available for nonradical systems,[73] since an increase in temperature is accompanied by the generation of radicals via heat activation of PS. In order to acquire complete understanding on the influence of temperature in nonradical systems, more reductionist efforts are needed to clarify the coexisting radical interference.

3.4.2. pH. In radical systems, many studies reported that both $SO_4^{\bullet-}$ and $^{\bullet}OH$ are the principal species responsible for the destruction of contaminants, and their efficiency may be influenced by pH conditions.[182,183] However, there is no consensus about how the pH affects PS-based AOPs. A few studies indicate that PS can be acid-catalyzed to generate more $SO_4^{\bullet-}$ at low pH (eqs 41 and 42), thus increasing treatment efficiency.[184,185]

$$S_2O_8^{2-} + H^+ \rightarrow HS_2O_8^- \quad (41)$$

$$HS_2O_8^- + e^- \rightarrow SO_4^{\bullet-} + SO_4^{2-} + H^+ \quad (42)$$

Although eq 41 and 42 were proposed by many researchers, the stoichiometric relationship between $S_2O_8^{2-}$ and $SO_4^{\bullet-}$ has not been elucidated. Here, we just adopted this acid-catalyzed explanation to account for the decrease of pH for a higher degradation efficiency of contaminant. For example, *p*-chloroaniline (PCA) degradation significantly increased from 25% to 100% when the pH was decreased from 11 to 3.[186] A similar trend was observed for the removal of ofloxacin using PMS as a precursor, but this trend was attributed to the superior performance of the catalyst (*i.e.*, FeCu-*g*-C_3N_4) under acidic conditions, rather than to higher $SO_4^{\bullet-}$concentration.[187] In sharp contrast, other studies observed increased degradation efficiency with increasing pH.[188,189] They attributed the trend to two factors. First, base activates PS,[18] generating more $SO_4^{\bullet-}$:

$$2S_2O_8^{2-} + 2H_2O \rightarrow 3SO_4^{2-} + SO_4^{\bullet-} + O_2^{\bullet-} + 4H^+ \quad (43)$$

Second, the generated $SO_4^{\bullet-}$ can be quickly (6.5×10^9 M^{-1} s^{-1}) transformed to the more oxidative $^{\bullet}OH$ in alkaline solutions:[83]

$$SO_4^{\bullet-} + OH^- \rightarrow SO_4^{2-} + {}^{\bullet}OH \quad (44)$$

For instance, as the pH increased from 1.3 to 13.9 during PhOH degradation in a heat-activated PS process, the *k*' values exhibited a 320-fold increase from 0.003 h^{-1} to 0.963 h^{-1}.[190] Note that some studies observed neither of the above trends, and some reported a bell-shaped effect of pH on degradation efficiency.[191,192] Taking BPA degradation in a heat/PS system as an example, the *k*' value was 0.129 min^{-1} at pH 3, it increased to 0.143 min^{-1} at pH 6.5, and then decreased to 0.079 min^{-1} at pH 11.[193] The effect of the pH on radical speciation was not discussed in this study. However, as shown in Table 3, the pK_a value of $SO_4^{\bullet-}$ is less than 0, indicating that $SO_4^{\bullet-}$ is the only form under any pH condition.[194] For $^{\bullet}OH$, the pK_a value was reported to be 11.9, indicating that $O^{\bullet-}$ is only a dominant species under extreme alkaline conditions (pH > 12).[108]

The influence of pH in nonradical systems is even more debatable. Many researchers suggested that the degradation kinetics increased with an increase of pH. For example, the *k*' value of PhOH degradation increased from 1.4 to 6.6 min^{-1} as pH increased from 4.5 to 8.0 in a carbon based-catalyst/PS system. This study claimed that basic condition accelerated electron transfer from PhOH to PS.[195] However, others observed an obvious loss of degradation efficiency with an increase in pH. With Fe(III)− and nitrogen−carbon (Fe−N−C) catalysts for 2,4-DCP degradation, the degradation rate gradually decreased as the pH increased from 3.5 to 9.0. This observation can be attributed to the surface of Fe−N−C becoming more negatively charged at high pH, resulting in increased repulsion between the surface of Fe−N−C and the anionic PS.[196] Some studies proposed that there was also a bell-shaped trend of pH in nonradical systems. Using Mn doped CuO with Cu: Mn ratio of 6:1 for removing ofloxacin (OFX),[197] The *k*' value was 8.13×10^{-3} min^{-1} at pH 4, and it increased to 0.196 min^{-1} at pH 8, but eventually decreased to 0.095 min^{-1} at pH 10. This trend was attributed to a combination of adsorption capacity toward OFX of Mn doped CuO and concentration of surface activated PS. Interestingly, some studies suggested that the variability of pH did not affect the degradation kinetics of contaminants. With sludge-derived biochar for PS activation and SMX as target compound, the unchanged degradation kinetics of SMX at pH ranging from 3.0 to 9.0 were observed. Although the mechanism for this result was not discussed, this process was proposed to be applied for antibiotic degradation in real wastewater treatment with a wide pH range from 5.0 to 9.0.[198]

Overall, the impact of pH on a specific degradation process is a result of various factors (some may be covariables), including the redox potentials of radicals/nonradical species,[191] PS states,[18] protonation states of target contaminants,[199] reactive sites, and catalytic performance.[200] However, many current studies reached a conclusion without excluding other potential confounding effects, making it almost impossible to discern the contribution from each factor. These contrary observations and confounded conclusions are the major hindrance to fully understanding the complex impact of pH.

3.5. Formation of Halogenated Byproducts. Many manufacturing sectors, such as agro-food, petroleum, and leather industries, are likely to produce wastewaters with high concentrations of halides (*e.g.*, F^-, Cl^-, and Br^-),[201,202] and generation of toxic halogenated byproducts is a concern for scaling up PS-based AOPs. In general, radicals exhibit higher reactivity with halides than nonradical species. Thus, the radical pathway is more likely to produce halogenated byproducts (*e.g.*, chlorophenols, bromate) than nonradical species.

$SO_4^{\bullet-}$ participates in a series of side reactions with Cl^- (Figure 5b). For example, $SO_4^{\bullet-}$ reacts with Cl^- yielding $Cl^{\bullet}$ with a *k* value of 2.7×10^8 M^{-1} s^{-1} (eq 12). Then, the resulting $Cl^{\bullet}$ reacts with Cl^- forming $Cl_2^{\bullet-}$ (eq 19). Additionally, $Cl_2^{\bullet-}$

https://doi.org/10.1021/acs.est.3c05153
Environ. Sci. Technol. 2023, 57, 12153−12179

can react with an intermediate organic radical ($R^{\bullet}$ in eq 45) from the reaction between $SO_4^{\bullet-}$ and TC. The excess reactive chlorine radicals (*i.e.*, $Cl_2^{\bullet-}$ and $Cl^{\bullet}$) may recombine to yield Cl_2 (eqs 18 and 20), and then Cl_2 hydrolyses to form HOCl (eq 21). In addition, they reported that Cl^- can reduce PMS through an electron transfer pathway, producing Cl_2 and HOCl (eqs 46 and 47). The newly generated available chlorine species (*i.e.*, HOCl) can also directly react with TC (eq 48). Note that eq 45 and eq 48 give rise to chlorinated byproducts.

$$R^{\bullet} + Cl_2^{\bullet-} \rightarrow R{-}Cl + Cl^- \quad (45)$$

$$Cl^- + HSO_5^- \rightarrow SO_4^{\bullet-} + HOCl \quad (46)$$

$$2Cl^- + HSO_5^- + H^+ \rightarrow SO_4^{2-} + Cl_2 + H_2O \quad (47)$$

$$TC{-}H + HOCl \rightarrow TC{-}Cl + H_2O \quad (48)$$

Using gas chromatography−mass spectrometry (GC-MS), several chlorinated byproducts, such as 2,4,6-trichlorophenol (TCP) and 1,1,3,3-tetrachloropropanone (TeCP) have been identified during the 2,4-DCP degradation in a Co^{2+}/PMS system.[174] In contrast, in a nonradical system for the 2,4-DCP degradation using CuO to activate PS under mild conditions, $SO_4^{\bullet-}$ was not detected. In this system, chloro-hydroquinone and chloro-benzoquinone were transiently detected initially, but unlike the radical based system above, they were rapidly degraded into carboxylates rather than transformed to hazardous chlorophenols (*i.e.*, TCP and TeCP).[203]

Transformation processes of Br^- in cobalt-mediated PS activation (Figure 5b) have been invesitigated.[204] In principle, $SO_4^{\bullet-}$ can react with Br^- to form $Br^{\bullet}$ with a k value of 3.5×10^9 M^{-1} s^{-1} (eq 31). Then, $Br^{\bullet}$ reacts immediately with Br^- yielding $Br_2^{\bullet-}$, Br_2, and HBrO through a series of reactions (eqs 32 and 49−52). Eventually, HBrO is oxidized by $SO_4^{\bullet-}$ forming BrO_3^- (eq 53), which is classified as human carcinogen.

$$Br_2^{\bullet-} + Br^{\bullet} \rightarrow Br_2 + Br^- \quad (49)$$

$$Br_2^{\bullet-} + Br_2^{\bullet-} \rightarrow Br_2 + 2Br^- \quad (50)$$

$$Br^{\bullet} + Br^{\bullet} \rightarrow Br_2 \quad (51)$$

$$Br_2 + H_2O \rightarrow HBrO + H^+ + Br^- \quad (52)$$

$$HBrO \xrightarrow{SO_4^{\bullet-}} \text{intermediates} \rightarrow BrO_3^- \quad (53)$$

However, in a nonradical system, $^1O_2$ was proposed to be a major species responsible for chlorophenol (CP) degradation, and no carcinogenic BrO_3^- was detected. This result highlights an advantage of nonradical systems, which are less prone to generate toxic byproducts.[56]

Note that there may be other toxic halogenated byproducts formed in radical systems that are not detected due to analytical limitations. For example, GC-MS is an effective method to detect volatile and semivolatile byproducts, but its response to many polar and large compounds is extremely low, especially for polybrominated byproducts.[205,206] Such byproducts are usually analyzed by liquid chromatography−mass spectrometry (LC-MS). In addition, samples in aqueous phase require pretreatment before analysis; thus, it is difficult to provide online monitoring in engineering practice.[207] Some novel techniques have been implemented for the byproduct analysis. For example, GC × GC-MS using two chromatographic columns with different separation mechanisms to enhance the separability of polybrominated byproducts has shown to greatly improve peak quality.[208]

Computational chemistry due to its low-cost and high efficiency, is increasingly used to identify potential intermediates,[209] but its use has not been reported in context of PS-based AOPs. Nevertheless, this approach holds great potential for byproduct identification based on promising results for other systems. For example, considering the degradation of estriol by chlorination in a pilot-scale water distribution system,[210] the frontier electron density (FED) theory was used to identify the structures of intermediate products, and DFT calculations were used to identify the degradation pathways. This study calculated FED^2_{HOMO} on the atoms in estriol by means of DFT at the B3LYP/6-311++G** level of theory. Results indicated that the C8 position has the highest FED^2_{HOMO} (1.55), revealing that the detachment of hydroxyl groups occurs very easily. Similarly, to compare the reactivity and byproduct distribution of polycyclic aromatic hydrocarbons (PAHs) during chlorination, a dozen geometrical electrostatic and chemical descriptors of PAHs were calculated at mPW1PW91/MIDIX+ level of theory.[205] The results showed that the reactivities of parent PAHs were reasonably related to their quantum chemical hardness, and acenaphthene was determined to be the major precursor of Cl-PAHs. These studies demonstrated that computational chemistry can be a promising tool to determine certain physicochemical properties of DBPs and unravel reaction mechanisms in PS-based AOPs.

In addition to reduce in halogenated byproducts formation, toxicity of contaminants also decreases after nonradical treatment.[50] Based on predictions of Ecological Structure Activity Relationships (ECOSAR), the toxicity of products was evaluated during the degradation of 17α-ethinylestradiol (EE2) by PMS in the presence of Br^-. The results showed that the ring-opening products possess toxicity at a level lower than that of the parent compound EE2. The decreased toxicity was attributed to the higher hydrophilicity of products than EE2.[211]

3.6. Evaluation of Electrical Energy Requirements.

When considering a new technology for application into water engineering, there are many pragmatic factors (*e.g.*, process safety, maintenance, reliability, scale up, and operation cost) that should be considered. Energy requirement is no doubt a key application-oriented challenge, and it can be measured in terms of electrical energy per log order (EE/O) or electrical energy per mass (EE/M).[212] In the context of PS-based AOPs, EE/O is more widely used, as the concentration of contaminant in this treatment scenario is relatively low and degradation kinetics follows a pseudo-first-order (EE/M for zero-order reaction kinetics). The EE/O is defined as the electrical energy (kWh) required to degrade a contaminant by 1 order of magnitude in 1 m^3 water to be treated:[213]

$$EE/O = \frac{1000 \times P \times t}{60 \times V \times \log(C_0/C_f)} \quad (54)$$

where P is the power of electrical energy (kW), t is the contact time, V is the volume of treated water (L), and C_0 and C_f are the initial and final concentrations of contaminant. Comparing to EE/O, total price is not an appropriate economic end point to reflect energy requirement, as it changes rapidly with the de/inflation, undermining comparability among cases.

In fact, the concept of EE/O has evolved. When it was first introduced, it was limited to the electricity used during the destruction of contaminant (*e.g.*, UV-based AOPs, electron-

https://doi.org/10.1021/acs.est.3c05153
Environ. Sci. Technol. 2023, 57, 12153−12179

beam and gamma-ray irradiation), as these processes are electric-energy-intensive, thus electrical energy for the destruction of contaminant represents a major fraction of the operative costs.[212] For example, H_2O_2 consumption may be an important component to the operating cost, contributing from 20% to 70% of the total.[214] Thus, the demand for oxidants (H_2O_2 in their case) has been proposed to be incorporated into the EE/O by regarding H_2O_2 as "stored electrical energy".[215] UV/H_2O_2 operating costs stem largely from H_2O_2 consumption, and the UV contribution accounts generally for less than 10% of the total cost. For ozone-based systems, the O_3 dose can also be converted to electrical energy requirement for the determination of EE/O values.[216] A recent study (UV/PS system) considered PS as electrical energy, and introduced a conversion factor (ratio of the unit price of PS to the price of electricity) to convert PS doses to energy unit.[217] This trend indicates that chemical demand should be taken account for a more holistic EE/O calculation.[218,219]

Accordingly, we included the EE/O values associated with producing PS (EE/O_{PS}) by similarly introducing a conversion factor that is equal to the ratio of the unit price of PS to the unit price of electricity. Then, EE/O_{PS} is calculated as

$$EE/O_{PS} = \frac{f \times C_{PS}}{\log(C_0/C_f)} \quad (55)$$

where f is a factor that converts the amount of PS used into energy consumption, and C_{PS} is the concentration of PS. In addition, we include energy requirements of catalysts by the cost of their elements, as catalysts are equally important for generating reactive species. Assuming a binary (A and B) catalyst, its EE/O value (EE/O_{catal}) was calculated as

$$EE/O_{catal} = \frac{f \times dose_A}{\log(C_0/C_f)} + \frac{f \times dose_B}{\log(C_0/C_f)} \quad (56)$$

Thus, total EE/O value (EE/O_{total}) can be expressed as

$$EE/O_{total} = EE/O + EE/O_{PS} + EE/O_{catal} \quad (57)$$

Accurate estimation of electrical energy for catalysts is difficult, as some of the catalysts can be recycled and reused. For example, a carbon-based catalyst (magnetic rape straw biochar) retained high catalytic performance after 8 cycles for the degradation of tetracycline hydrochloride.[220] Similarly, a metal-based catalyst ($FeMoO_4$) exhibited more than 85% removal efficiency in the 10th cycle.[221] However, for simplicity, we did not consider the recyclability and reusability of catalysts for the electrical energy estimation.

In radical systems, we collected published EE/O_{total} values of UV/PS, heat/PS, US/PS, and electron beam/PS processes from the peer-reviewed literature (Table 5, n = 61). We also calculated EE/O_{total} values for catalyst/PS in both radical and nonradical systems via eqs 54−57 (Table 6). For nonradical systems, we chose carbon nanotubes (CNTs) as a representative catalyst in this review, rather than other metallic catalysts or heteroatom-doped carbon. This is due to the facts that commercial CNTs are commonly used in PS-based AOPs, and their electrical energy requirements are easily available.[222,223] Note that for many catalysts, both radical and nonradical pathways may coexist. For these complex systems, the EEO values of a specific pathway may be overestimated, as the EEO value is the sum of radical plus nonradical pathway contributions. However, we did not differentiate them and assumed that one pathway dominated the degradation of contaminants, as shown or presumed by the reviewed literature.

Table 5. Reported EE/O_{total} Values (kWh·m^{-3} order^{-1}) for Degradation of Contaminants by Radical Species through Activation of PS

activation method	contaminant	EE/O_{total}
UV	cylindrospermopsin[277]	3.80 × 10^{-4}
UV	microcystin-LR[278]	0.19, 0.65
UV	ciprofloxacin[224]	0.65−1.93
UV	ciprofloxacin[279]	24.8, 10.9
UV	sulfadiazine[280]	1.72
UV	amoxicillin[279]	9.46
UV	iodoacetic acid[281]	0.04−0.39
UV	tetracycline[282]	408
UV	brilliant green[283]	5.40, 6.80
UV	chloramphenicol[284]	16.8
UV	ethyl paraben[285]	61.0, 144
UV	clofibric acid[286]	0.73
UV	atrazine[287]	0.187, 0.348
UV	benzophenone-3[218]	0.21
UV	ibuprofen[288]	1.42
UV	thiamphenicol[289]	36.6
US	ibuprofen[290]	264, 314
US	sodium dodecyl sulfate[291]	980
US	dissolved organic carbon[292]	51−66
UV/TiO_2	sulfadiazine[280]	138
UV/TiO_2	metronidazole[293]	22.1
UV/TiO_2	microcystin-LR[278]	0.03, 0.07
HC/UV/ZnO/$ZnFe_2O_4$[a]	carbamazepine[294]	127
UV/GAC-TiO_2[b]	sulfadiazine[280]	34.5
UV/TiO_2	ibuprofen [288]	0.029−0.243
UV/TiO_2	herbicide[295]	482
UV/TiO_2	sulfadiazine[280]	30.7
US/Fe_3O_4@AC[c]	acid red 73[296]	3.33−13.3
heat	theophylline[297]	47.4−558
electrochemical	tetracycline[298]	11.5
electrochemical	basic violet 16 dye[299]	0.26, 1.48
electron beam	gallic acid[300]	0.07
electron beam	citric acid[301]	0.199
electron beam	total organic carbon[301]	0.674
electron beam	phenol[302]	0.256

[a]HC/UV/ZnO/$ZnFe_2O_4$: Hydrodynamic cavitation (HC) assisted UV/PS with composite ZnO and $ZnFe_2O_4$ particles.[294] [b]GAC-TiO_2: A complex catalyst synthesized by granular activated carbon (GAC) and TiO_2.[280] [c]Fe_3O_4@AC: Nano Fe_3O_4 particles loaded on activated carbon

Figure 6 compares EE/O_{total} values for contaminant degradation by radical (n = 76) and nonradical species (n = 30) from PS activation. Apparently, EE/O_{total} values for individual degradation processes vary by several orders of magnitude. For radical systems, EE/O_{total} values range from 3.8 × 10^{-4} to 980 kWh·m^{-3} order^{-1}, while for nonradical systems EE/O_{total} values range from 2.91 to 2.94 × 10^6 kWh·m^{-3} order^{-1}. Despite cases of high variability, we observed pronounced differences between the two pathways. The average value in the radical system is 66.2 kWh·m^{-3} order^{-1}, which is notably lower than that in nonradical system (2.34 × 10^5 kWh·m^{-3} order^{-1}). For example, the EE/O_{total} value in a radical system was reported to be 1.024 kWh·m^{-3} order^{-1}, corresponding to the use of UV to activate PDS and generate

https://doi.org/10.1021/acs.est.3c05153
Environ. Sci. Technol. 2023, 57, 12153−12179

Table 6. Calculated EE/O_{total} Values (kWh·m^{-3} $order^{-1}$) for Degradation of TCs by Radical and Nonradical Species through Activation of PS[e]

TC, reference	PS formula and energy consumption	catalyst and energy consumption	dose	vol	power	time	k'	EE/O_{total}
ofloxacin[303]	$Na_2S_2O_8$, 13.5	CuO[a], 30.0	0.5 g L^{-1} CuO, 1 mM PS	0.1	4.82×10^{-3}	1.0	4.3×10^{-2}	43.0[b]
tetrabromobisphenol A[304]	$KHSO_5$, 7.64	$CuFe_2O_4$[c], 47.6	0.1 g L^{-1} $CuFe_2O_4$ 0.1 mM PS	0.1	8.40×10^{-4}	0.5	7.1×10^{-2}	9.08
			0.1 g L^{-1} $CuFe_2O_4$ 0.2 mM PS		8.51×10^{-4}		0.12	5.44
			0.1 g L^{-1} $CuFe_2O_4$ 0.3 mM PS		8.63×10^{-4}		0.19	3.36
acid orange 7[305]	$KHSO_5$, 7.64	CuO[a], 30.0	0.05 g L^{-1} CuO, 5 mM PS	0.25	2.59×10^{-3}	0.25	4.0×10^{-3}	398
			0.2 g L^{-1} CuO, 5 mM PS		5.95×10^{-3}		0.52	7.04
			0.1 g L^{-1} CuO, 2 mM PS		2.86×10^{-3}		0.94	1.87
			0.1 g L^{-1} CuO, 5 mM PS		3.73×10^{-3}		0.21	10.9
			0.1 g L^{-1} CuO, 10 mM PS		5.18×10^{-3}		0.17	18.7
			0.1 g L^{-1} CuO, 20 mM PS		8.08×10^{-3}		5.9×10^{-2}	84.0
dichlorophenoxyacetate[306]	$KHSO_5$, 7.64	Fe_2O_3[c], 1.36×10^2	0.5 g L^{-1} HNPs, 3 mM PS	0.2	2.23×10^{-2}	1.0	2.7×10^{-2}	159
acid orange 7[307]	$Na_2S_2O_8$, 13.5	GAC, 10.5	1.0 g L^{-1} GAC, 5.7 mM PS	0.25	7.22×10^{-3}	5.0	6.6×10^{-3}	33.6
2,4-dichlorophenol[223]	$Na_2S_2O_8$, 13.5	CNTs, 1.46×10^3	0.1 g L^{-1} CNTs, 0.05 mM PS	0.2	2.93×10^{-2}	0.5	0.137	82.1[b]
furfuryl alcohol[308]	$KHSO_5$, 7.64	CNTs, 3.24×10^6	0.1 g L^{-1} CNTs, 1 mM PS	0.04	12.9	1.0	0.38	3.31×10^4
2,4-dichlorophenol[55]	$Na_2S_2O_8$, 13.5	CNTs, 1.46×10^3	0.05 g L^{-1} CNTs, 0.031 mM PS	0.2	1.5×10^{-2}	0.5	0.11	52.6
			0.15 g L^{-1} CNTs, 0.031 mM PS		4.4×10^{-2}		0.21	79.8
2-bromophenol[225]	$K_2S_2O_8$, 17.7	CNTs, 1.46×10^4	50 mg L^{-1} CNTs 200 μM PS	0.25	0.182	0.67	0.16	261
			50 mg L^{-1} CNTs 400 μM PS		0.183		0.18	233
			50 mgL^{-1} CNTs 500 μM PS		0.183		0.19	221
			50 mg L^{-1} CNTs 600 μM PS		0.183		0.18	233
			100 mg L^{-1} CNTs 500 μM PS		0.365		0.42	199
			150 mg L^{-1} CNTs 500 μM PS		0.548		0.72	175
4-nitrophenol[309]	$KHSO_5$, 7.64	CNTs, 1.46×10^3	0.1 g L^{-1} CNTs 0.5 mM PS	0.05	7.4×10^{-3}	1.0	0.44	12.8
4-hydroxybenzoic acid[309]							0.73	7.77
4-chlorophenol[309]							1.02	5.57
4-methylphenol[309]							1.63	3.48
4-aminophenol[309]							1.96	2.91
2,4-dichlorophenol[310]	$Na_2S_2O_8$, 13.5	CNF, 2.74×10^4	0.25 g L^{-1} CNF 0.06 mM PS	0.2	1.37	1.0	9.21×10^{-2}	2.86×10^3
phenol[158]	$KHSO_5$, 7.64	CNTs, 1.46×10^3	0.1 g L^{-1} CNTs 1 mM PS	0.2	1.5×10^{-2}	1.0	1.90×10^{-2}	303
sulfamethoxazole[311]	$KHSO_5$, 7.64	rGO, 2.67×10^5	0.5 g L^{-1} rGO, 0.8 mM PS	0.06	8.00	5.0	7.16×10^{-3}	1.43×10^5
sulfamethoxazole[311]	$KHSO_5$, 7.64	N-rGO[d], 2.67×10^5	0.5 g L^{-1} N-rGO, 0.8 mM PS	0.06	8.00	5.0	1.01×10^{-2}	1.01×10^5
bisphenol A[312]	$KHSO_5$, 7.64	g-C_3N_4, 6.71×10^5	0.1 g L^{-1} g-C_3N_4, 2 mM PS	0.2	13.4	0.03	3.10	2.77×10^4
hydroquinone[222]	$K_2S_2O_8$, 17.7	CNTs, 3.37×10^6	0.1 g L^{-1} CNTs 1 mM PS	0.1	33.7	1.0	0.511	2.53×10^4
phenol[222]							2.68×10^{-2}	4.83×10^5
4-chlorophenol[222]							3.20×10^{-2}	4.04×10^5
4-methoxy-phenol[222]							0.122	1.06×10^5
2,4-dichlorophenol[222]							6.5×10^{-2}	1.96×10^5
acetaminophen[222]							9.56×10^{-2}	1.35×10^5
bisphenol A[222]							3.83×10^{-2}	3.38×10^5
4-nitrophenol[222]							4.40×10^{-3}	2.94×10^6
methylparaben[222]							6.20×10^{-3}	2.09×10^6
bisphenol A[313]	$KHSO_5$, 7.64	CuO, 1.47×10^2	0.1 g L^{-1} CuO, 0.5 mM PS	0.1	1.5×10^{-3}	1.0	3.00×10^{-3}	196

https://doi.org/10.1021/acs.est.3c05153
Environ. Sci. Technol. 2023, 57, 12153−12179

Table 6. continued

[a]CuO was synthesized by $Cu(NO_3)_2{\cdot}3H_2O$ (*i.e.*, the molar ratio is 1:1). The reported price of $Cu(NO_3)_2{\cdot}3H_2O$ was 2.55\$ kg^{-1} and its energy consumptions was 30.0 \$ kg^{-1}. [b]Taking tetrabromobisphenol A and 2,4-dichlorophenol as an example for radical and nonradical species, respectively. In radical system, Li et al. synthesized CuO by $Cu(NO_3)_2{\cdot}3H_2O$ for PS activation. Based on their information, the costs of PS and $Cu(NO_3)_2{\cdot}3H_2O$ were 1.15 and 2.55 \$ kg^{-1}, respectively. The energy consumptions were calculated to be 13.5 and 30.0 kWh kg^{-1}, respectively. (*i.e.*, PS: 1.15 \$ kg^{-1} ÷ 0.085 \$ kWh^{-1} = 13.5 kWh kg^{-1}; $Cu(NO_3)_2{\cdot}3H_2O$: 2.55 \$ kg^{-1} ÷ 0.085 \$ kWh^{-1} = 30.0 kWh kg^{-1}). They added 2.38×10^{-5} kg PS and 1.5×10^{-4} kg $Cu(NO_3)_2{\cdot}3H_2O$. (*i.e.*, PS: 238×10^{-3} kg $mol^{-1} \times 1 \times 10^{-3}$ M × 0.1 L = 2.38×10^{-5} kg; $Cu(NO_3)_2{\cdot}3H_2O$: 0.5×10^{-3} kg $L^{-1} \times 0.1$ L ÷ (80×10^{-3} kg mol^{-1}) × 236×10^{-3} kg mol^{-1} = 1.5×10^{-4} kg). The total electric power consumption of PS and CuO were calculated as 4.82×10^{-3} kWh. (*i.e.*, 2.38×10^{-5} kg ×13.5 kWh kg^{-1} + 1.5×10^{-4} kg× 30.0 kWh kg^{-1} = 4.82×10^{-3} kWh). Finally, the EE/O_{total} was calculated as 43.0 kWh·m^{-3} $order^{-1}$ via eqs 54−57. In nonradical systems, Cheng et al. used CNTs to activate PS. Based on their information, the costs of PS and CNTs are 1.15 and 1.24×10^2 \$ kg^{-1}, respectively. The energy consumptions were calculated as 13.5 and 1.46×10^3 kWh kg^{-1}, respectively. (*i.e.*, PS: 1.15 \$ kg^{-1} ÷ 0.085 \$ kWh^{-1} = 13.5 kWh kg^{-1}; CNTs: 1.24×10^2 \$ kg^{-1} ÷ 0.085 \$ kWh^{-1} = 1.46×10^3 kWh kg^{-1}). They added 2.38×10^{-6} kg PS and 2.0×10^{-5} kg CNTs. (*i.e.*, PDS: 238×10^{-3} kg $mol^{-1} \times 0.05 \times 10^{-3}$ M × 0.2 L = 2.38×10^{-6} kg; CNTs: 0.1×10^{-3} kg $L^{-1} \times 0.2$ L = 2.0×10^{-5} kg). The total electric power consumption of PS and CNTs were calculated as 2.93×10^{-2} kWh. (*i.e.*, 2.38×10^{-6} kg ×13.5 kWh kg^{-1} + 2.0×10^{-5} kg × 1.46×10^3 kWh kg^{-1} = 2.93×10^{-2} kWh). Finally, the EE/O_{total} was calculated as 82.1 kWh·m^{-3} $order^{-1}$ *via* eqs 54−57. $CuFe_2O_4$ was synthesized by $Cu(NO_3)_2{\cdot}3H_2O$ and $Fe(NO_3)_3{\cdot}9H_2O$ (*i.e.*, the molar ratio is 1:1:2). Their reported prices were 2.55 and 1.5 \$ kg^{-1}, respectively. Their energy consumptions were 30 and 17.6 kWh kg^{-1}, respectively. [c]Fe_2O_3 was synthesized by $FeCl_3{\cdot}3H_2O$ and urea. Their prices were 11 and 0.55 \$ kg^{-1}, respectively. Their energy consumptions were 129.4 and 6.47 kWh kg^{-1}, respectively. HNPs is refer to hematite nanoparticles. [d]Nitrogen-doped reduced graphene oxide (N-rGO) was synthesized by reduced graphene oxide (rGO) and urea. Their prices were 2.23×10^4 and 0.8 \$ kg^{-1}, respectively. Their energy consumptions were 2.67×10^5 and 9.41 kWh kg^{-1}, respectively. [e]The EE/O was calculated on the basis of MWH 2005. The collected cases cover a wide range of TC. The cost of PS and catalyst are in the unit of \$ kg^{-1}. The energy consumption is in the unit of kWh kg^{-1} and was calculated as the ratio of the unit price of chemical to the price of electricity (*i.e.*, 0.085\$ kWh^{-1}. Taking $Na_2S_2O_8$ as an example, the energy consumption of it was calculated: 1.15 \$ kg^{-1} ÷ 0.085 \$ kWh^{-1} = 13.5 kWh kg^{-1}). Volume and electric power are in the unit of litter and kWh, respectively. First-order rate constant for TC degradation (k') is in the unit of min^{-1}. (The blue shadowed part is for radical species induced degradation, while the grey shadowed part is for non-radical species induced degradation.)

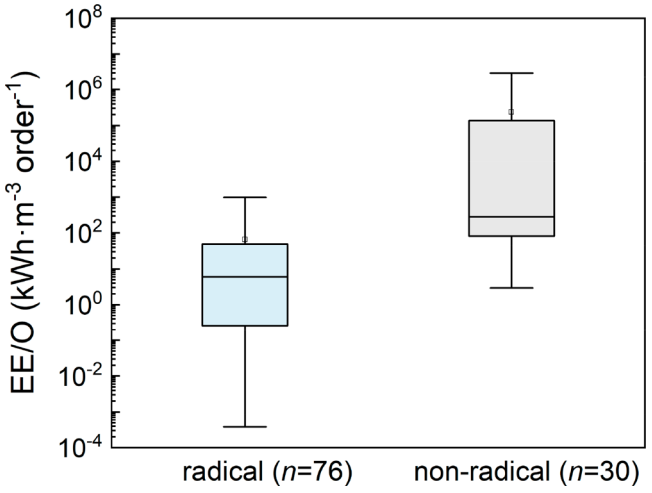

Figure 6. Comparison of EE/O_{total} values for degradation of contaminants by radical (blue bar) and nonradical species (gray bar) through PS activation. The bottom and top of each box represent the lower and upper quartiles, respectively. The bottom and top bars represent the minimum and maximum values, respectively. The horizontal line and open square denote median and mean of the data set, respectively.

$SO_4^{\bullet-}$ for ciprofloxacin (CIP) degradation. In the presence of 0.96 g L^{-1} PDS, CIP at the initial concentration of 10 mg L^{-1} was completely eliminated within 30 min, and the k' value was determined to be 0.2 min^{-1}.[224] In nonradical system, CNT was used to activate PS for bromophenol degradation, and the EE/O_{total} values ranged from 175 to 233 kWh·m^{-3} $order^{-1}$ with an increase of CNTs dosage from 50 to 150 mg L^{-1}. The electrical energy of CNTs was collected from the manufacturer reported in this study (1.24×10^3 \$ kg^{-1} ÷ 0.085 \$ kWh^{-1} = 1.46×10^4 kWh kg^{-1}).[225] Note that we only considered the energy requirements for catalysts, and the direct energy consumption for the synthesis process of catalysts was not accounted for, as it is difficult to obtain such information. Even with the energy requirements for catalyst synthesis, our inference that the EE/O value for nonradical systems is higher than that for radical systems holds, because including energy requirements for catalyst synthesis into EE/O_{total} would simply increase the EE/O value in nonradical systems.

Differences in EE/O_{total} values can be attributed to a variety of factors, such as direct electricity consumption (*e.g.*, oven, hydrothermal reactor), electrical energy requirements for producing PS and the catalyst, contaminant degradation kinetics, and byproduct accumulation (using less energy than complete mineralization). The higher EE/O_{total} in nonradical systems than radical systems (Figure 6) can be mainly attributed to the higher electrical energy consumption and the lower degradation kinetics for PS/catalyst systems. These results challenge the common wisdom that total energy requirements are mainly associated with high electricity consumption, and highlight that designing durable, high-performance catalysts that can be synthesized in an energy-efficient manner is needed to decrease the overall EE/O. Note that a new degradation pathway of direct oxidative transfer process (DOTP) was recently reported,[226] which enabled efficient treatment at a very low dosage of oxidants. Interestingly, the energy consumption of this nonradical pathway was significantly lower than that of radical-based AOPs, as PS dosage in DOTP was 50 times lower than radical pathway. In addition, the cost of catalyst in nonradical system was relatively low (\$2 kg^{-1}). However, there are two distinct differences between our calculations and theirs. First, we did not consider a 50-fold excess of the PS dosage, resulting in a significant decrease in PS consumption. Second, our assumed catalyst cost was significantly higher (*e.g.*, \$124 kg^{-1} for CNTs).

In AOPs, coexisting substances typically act as radical scavengers, resulting in an increased PS consumption. Additionally, when UV is used to activate PS, DOM can be a strong UV absorber, competing with PS for incoming photons, ultimately resulting in an extra consumption of electricity energy. For example, the addition of 0.4 mg L^{-1}

https://doi.org/10.1021/acs.est.3c05153
Environ. Sci. Technol. 2023, 57, 12153−12179

NOM and 1 mg L^{-1} NO_3^- increased the EE/O value for nitrosodimethylamine (NDMA) degradation in a UV/H_2O_2 system from 0.4 to 1.2 kWh·m^{-3} $order^{-1}$. These coexisting substances not only scavenge the formed $^{\bullet}OH$, but also reduced the fraction of photons that can reach H_2O_2.[227] However, the majority of the reported EE/O values were calculated in pure water, rather than in a real water matrix, and this critical issue is frequently overlooked in bench-scale studies. These EE/O_{total} values, reflecting the cost of this technique, are only suitable for bench-scale experiments. For pilot-scale and full applications, energy loss during transmission, labor cost, and cost of equipment maintenance should also be fully taken into consideration. But these costs change rapidly with de/inflation and other market forces, thus were not covered.

4. IMPLICATIONS AND OUTLOOK

PS-based AOPs have attracted significant research interest, and most studies have focused on the development of new activation strategies and efficient catalysts. However, selection and optimization of an appropriate PS-based AOP for a given system remains challenging, partly due to insufficient predictive understanding of radical *vs.* nonradical activation pathways in the context of important system-specific factors such as containment degradation kinetics and mechanisms, oxidant utilization efficiency, water matrix interferences, selectivity, byproducts formation, and energy requirements (Table 7). This critical literature review offers the following pertinent insight: (1) Degradation kinetics with radicals are typically faster and yield higher mineralization extent than those based on $^1O_2$, a common nonradical oxidative species. For practical implementation, radical-based approaches may achieve high removal efficiency of contaminants with relatively short contact time; (2) Radicals are generally more susceptible to react with interfering compounds in the water matrix, although some inorganic anions may directly activate PS to generate more nonradical species and increase degradation efficiency. Thus, for a complex water matrix, nonradical systems offer advantages for minimizing water matrix interference, ultimately sustaining high contaminant degradation efficiency; (3) Radicals indiscriminately react with contaminants with either EWGs or EDGs. In contrast, nonradical species preferentially react with EDGs because most of these species favor the electron-transfer pathway. Thus, one could optimize degradation efficiency by considering the functional groups (EWGs or EDGs) of known contaminants; (4) While contaminant removal rates tend to increase with temperature, a bell-shaped response has been reported when high temperatures accelerate radical-self-quenching or reactions with PS to generate less reactive species that hinder efficiency; (5) Radical pathways are more likely to produce toxic halogenated byproducts. Thus, if the water matrix is conducive to forming such byproducts, nonradical systems are preferred; and (6) overall (holistically estimated) EE/O values for nonradical systems are generally higher than for radical systems, due to slower degradation kinetics and higher energy requirements for catalyst fabrication used in nonradical systems. But this should not forestall research and development of superior catalysts, since the energy requirement is not the only metric needed to evaluate catalysts. Sustained long-term performance (*e.g.*, solar-driven catalytic systems) and unintended life cycle impacts should also be taken into consideration.

Table 7. Comparison of Degradation of Contaminants by Radical and Nonradical Species Generated *via* Activation of PS, in Terms of Six Aspects: Reaction Kinetics, Temperature, pH, Interference of Water Matrix, Selectivity to Contaminants, Formation of Byproducts, and Electrical Energy Consumption[a]

	radicals	nonradical species
reaction kinetics and mechanism	a. relatively fast reaction kinetics	a. reaction kinetics for $^1O_2$, relatively slow; for other nonradical species, lack of investigations
	b. reaction mechanism HAA, SET and RAF pathways	b. reaction mechanism for $^1O_2$, electrophilic addition, electron transfer and combination with sulfur atom in sulfides; for high-valent metals, electron transfer, HAA and OTA pathways
temperature and pH	a. temperature high temperature fast degradation kinetics; extremely high temperature accelerates radical side reactions, reducing kinetics	a. temperature lack of investigations
	b. pH (no consensus), previous studies observed a variety of contradictory trends (*i.e.*, increasing, decreasing, or constant) for the degradation kinetics of different compounds with an increase of pH	b. pH (no consensus), in acidic pH, persulfate generated more $SO_4^{\bullet-}$ increasing degradation; in basic pH, the generated $SO_4^{\bullet-}$ are transformed to $^{\bullet}OH$, increasing degradation
water matrix	sensitive	tolerant
selectivity	no	sensitive to contaminants with EDGs
byproducts	highly halogenated byproducts	very few (even no) byproducts
total electrical energy consumption	low	high

[a]EDG stands for electron donating groups.

https://doi.org/10.1021/acs.est.3c05153
Environ. Sci. Technol. 2023, 57, 12153−12179

Despite the considerable progress in PS-based AOPs, there are still significant hurdles that should be surmounted through research. (1) Many studies reported that radical and nonradical reactions may occur simultaneously in certain PS systems, and thus it is difficult to differentiate these pathways and estimate their contributions to the overall degradation process. However, accurate differentiation of pathways underscores an optimization opportunity for pathway tunability and control through catalyst and process design. (2) We encourage the exploration of more economic, stable, and efficient catalysts for the generation of reactive species. One promising way is the decoration of pristine carbonaceous material through defect engineering and elemental doping. These precisely functionalized catalysts enable us to overcome the limitation of metal leaching and maximize the exposure of active sites to accelerate PS activation. In addition, due to the potential synergistic effect of modified heteroatoms, the catalytic oxidation and reusability have been dramatically enhanced comparing to the pristine carbons.[228] (3) More systematic and comprehensive studies of nonradical pathways are still needed to clarify the interaction between PS and catalyst surfaces, identify the activation mechanism, as well as the associated features in catalytic degradation of contaminant. In this regard, combination of experimental approaches and theoretical simulations may be of great assistance in advancing mechanistic understanding of PS activation in nonradical systems. (4) Many studies indicated that compounds with lower *IP* values can be preferentially degraded by nonradical species. Such structure−reactivity relationships are needed to bridge the significant gap between limited experimental data and the increasing number of anthropogenic contaminants, to help select appropriate AOPs. (5) Understandings of the physicochemical properties of contaminants before treatment is a must, as it allows for selective reactions toward specific contaminants with less interfering with the background water matrix. (6) While the oxidation capacity of nonradical species is generally lower than that of radicals, the redox potential of nonradical species may be tunable via modification of the structure/composition of catalysts, which is an understudied area.[229] Therefore, despite significant challenges, there are many timely research opportunities to advance PS-based AOPs to widespread practical applications.

AUTHOR INFORMATION

Corresponding Authors

Ruiyang Xiao − *Institute of Environmental Engineering, School of Metallurgy and Environment, Central South University, Changsha 410083, China; Chinese National Engineering Research Center for Control & Treatment of Heavy Metal Pollution, Changsha 410083, China;* orcid.org/0000-0001-9516-2202; Phone: +86-731-88830875; Email: xiao.53@csu.edu.cn

Pedro J. J. Alvarez − *Department of Civil and Environmental Engineering, Rice University, Houston 77005, United States;* orcid.org/0000-0002-6725-7199; Phone: +01-713-3485903; Email: alvarez@rice.edu

Authors

Yiqi Yan − *Institute of Environmental Engineering, School of Metallurgy and Environment, Central South University, Changsha 410083, China; Chinese National Engineering Research Center for Control & Treatment of Heavy Metal Pollution, Changsha 410083, China*

Zongsu Wei − *Centre for Water Technology (WATEC) & Department of Engineering, Aarhus University, DK-8200 Aarhus N, Denmark;* orcid.org/0000-0001-8747-2251

Xiaoguang Duan − *School of Chemical Engineering and Advanced Materials, The University of Adelaide, Adelaide SA5005, Australia;* orcid.org/0000-0001-9635-5807

Mingce Long − *School of Environmental Science and Engineering, Key Laboratory of Thin Film and Microfabrication Technology (Ministry of Education), Shanghai Jiao Tong University, Shanghai 200240, China;* orcid.org/0000-0002-5168-8330

Richard Spinney − *Department of Chemistry and Biochemistry, The Ohio State University, Columbus, Ohio 43210, United States;* orcid.org/0000-0002-8074-3386

Dionysios D. Dionysiou − *Environmental Engineering and Science Program, Department of Chemical and Environmental Engineering, University of Cincinnati, Cincinnati, Ohio 45221, United States;* orcid.org/0000-0002-6974-9197

Complete contact information is available at: https://pubs.acs.org/10.1021/acs.est.3c05153

Notes

The authors declare no competing financial interest.

ACKNOWLEDGMENTS

Funding from National Natural Science Foundation of China (Nos. 21976212 and 52121004) are gratefully acknowledged. Partial funding for PJA was provided by the NSF ERC on Nanotechnology-Enabled Water Treatment (EEC-1449500). We gratefully acknowledge Zhi Jiang and Quanzhen Liu for their valuable comments on this manuscript.

NOMENCLATURE AND ABBREVIATIONS

Chemicals

$^1O_2$	singlet oxygen
ACT	acetaminophen
ACs	aromatic contaminants
BA	benzoic acid
BPA	bisphenol A
CA	clofibric acid
CNTs	carbon nanotubes
CP	chlorophenol
CIP	ciprofloxacin
DBPs	disinfection byproducts
DCP	2,4-dichlorophenol
DOM	dissolved organic matter
DHAcAms	dihaloacetamides
e^-_{aq}	hydrated electron
EfOM	effluent organic matter
ESFA	Elliott soil fulvic acid
GAC	granular activated carbon
HA	humic acid
HCO_4^-	peroxymonocarbonate
HOX	hypohalous acid
HNPs	hematite nanoparticles
IMI	imidacloprid
MOF	metal−organic framework
NP	4-nitrophenol
NB	nitrobenzene
NOM	natural organic matter
ND	nanodiamonds

https://doi.org/10.1021/acs.est.3c05153
Environ. Sci. Technol. 2023, 57, 12153−12179

NLNOM	Nordic Lake NOM
Nu	nucleophile
NDMA	nitrosodimethylamine
N-rGO	nitrogen-doped reduced graphene oxide
OFX	ofloxacin
OG	orange G
PCA	*p*-chloroaniline
PDS	peroxydisulfate
PAHs	polycyclic aromatic hydrocarbons
$P_2O_7^{4-}$	pyrophosphate
PIR	piroxicam
abbr.	note
PFOA	perfluorooctanoic acid
PhOH	phenol
PMS	peroxymonosulfate
PS	persulfate
rGO	reduced graphene oxide
ROS	reactive oxygen species
SRNOM	Suwannee River NOM
SRFA	Suwannee River fulvic acid
SMPs	soluble microbial products
SMX	sulfamethoxazole
TC	target compound
TCA	1,1,1-tricholroethane
TCHC	tetracycline hydrochloride
TCP	2,4,6-trichlorophenol
TeCP	tetrachloropropanone
TOC	total organic carbon
TPA	terephthalic acid

Others

AOPs	advanced oxidation processes
DOTP	direct oxidative transfer process
EDGs	electron donating groups
EE/O	electrical energy per log order
EWG	electron withdrawing group
FED	frontier electron density
IP	ionization potential
IS	ionic strength
LFP	laser flash photolysis
LC-MS	liquid chromatography−mass spectrometry
HAA	hydrogen atom abstraction
HC	hydrodynamic cavitation
GC-MS	gas chromatography mass spectrometry
ΔG°	Gibbs free energy change
k	second-order rate constant
K_a	dissociation constant
k'	pseudo-first-order rate constant
NHE	normal hydrogen electrode
OAT	oxygen atom transfer
RAF	radical addition formation
SET	single electron transfer
US	ultrasound
UV	ultraviolet

REFERENCES

(1) Zhang, B.-T.; Zhang, Y.; Teng, Y.; Fan, M. Sulfate Radical and Its Application in Decontamination Technologies. *Crit. Rev. Environ. Sci. Technol.* **2015**, *45* (16), 1756−1800.

(2) Wang, J.; Wang, S. Activation of persulfate (PS) and peroxymonosulfate (PMS) and application for the degradation of emerging contaminants. *Chem. Eng. J.* **2018**, *334*, 1502−1517.

(3) Gao, L.; Minakata, D.; Wei, Z.; Spinney, R.; Dionysiou, D. D.; Tang, C.-J.; Chai, L.; Xiao, R. Mechanistic study on the role of soluble microbial products in sulfate radical-mediated degradation of pharmaceuticals. *Environ. Sci. Technol.* **2019**, *53* (1), 342−353.

(4) Chen, J.; Fang, C.; Xia, W.; Huang, T.; Huang, C.-H. Selective Transformation of *β*-Lactam Antibiotics by Peroxymonosulfate: Reaction Kinetics and Nonradical Mechanism. *Environ. Sci. Technol.* **2018**, *52* (3), 1461−1470.

(5) Ji, Y.; Lu, J.; Wang, L.; Jiang, M.; Yang, Y.; Yang, P.; Zhou, L.; Ferronato, C.; Chovelon, J. M. Non-activated peroxymonosulfate oxidation of sulfonamide antibiotics in water: Kinetics, mechanisms, and implications for water treatment. *Water Res.* **2018**, *147*, 82−90.

(6) Zhou, P.; Zhang, J.; Zhang, Y.; Zhang, G.; Li, W.; Wei, C.; Liang, J.; Liu, Y.; Shu, S. Degradation of 2,4-dichlorophenol by activating persulfate and peroxomonosulfate using micron or nanoscale zero-valent copper. *J. Hazard. Mater.* **2018**, *344*, 1209−1219.

(7) Qi, C.; Liu, X.; Lin, C.; Zhang, H.; Li, X.; Ma, J. Activation of peroxymonosulfate by microwave irradiation for degradation of organic contaminants. *Chem. Eng. J.* **2017**, *315*, 201−209.

(8) Lee, J.; von Gunten, U.; Kim, J. H. Persulfate-based advanced oxidation: critical assessment of opportunities and roadblocks. *Environ. Sci. Technol.* **2020**, *54* (6), 3064−3081.

(9) Peng, W.; Dong, Y.; Fu, Y.; Wang, L.; Li, Q.; Liu, Y.; Fan, Q.; Wang, Z. Non-radical reactions in persulfate-based homogeneous degradation processes: A review. *Chem. Eng. J.* **2021**, *421*, 127818.

(10) Kohantorabi, M.; Moussavi, G.; Giannakis, S. A review of the innovations in metal- and carbon-based catalysts explored for heterogeneous peroxymonosulfate (PMS) activation, with focus on radical vs. non-radical degradation pathways of organic contaminants. *Chem. Eng. J.* **2021**, *411*, 127957.

(11) Ding, Y.; Wang, X.; Fu, L.; Peng, X.; Pan, C.; Mao, Q.; Wang, C.; Yan, J. Nonradicals induced degradation of organic pollutants by peroxydisulfate (PDS) and peroxymonosulfate (PMS): Recent advances and perspective. *Sci. Total Environ.* **2021**, *765*, 142794.

(12) Dong, J.; Xu, W.; Liu, S.; Du, L.; Chen, Q.; Yang, T.; Gong, Y.; Li, M.; Tan, X.; Liu, Y. Recent advances in applications of nonradical oxidation in water treatment: Mechanisms, catalysts and environmental effects. *J. Clean. Prod.* **2021**, *321*, 128781.

(13) Miklos, D. B.; Remy, C.; Jekel, M.; Linden, K. G.; Drewes, J. E.; Hubner, U. Evaluation of advanced oxidation processes for water and wastewater treatment - A critical review. *Water Res.* **2018**, *139*, 118−131.

(14) Gao, Y. Q.; Gao, N. Y.; Deng, Y.; Yin, D. Q.; Zhang, Y. S. Degradation of florfenicol in water by UV/$Na_2S_2O_8$ process. *Environ. Sci. Pollut. Res. Int.* **2015**, *22* (11), 8693−701.

(15) Ji, Y.; Dong, C.; Kong, D.; Lu, J.; Zhou, Q. Heat-activated persulfate oxidation of atrazine: Implications for remediation of groundwater contaminated by herbicides. *Chem. Eng. J.* **2015**, *263*, 45−54.

(16) Wei, Z.; Villamena, F. A.; Weavers, L. K. Kinetics and Mechanism of Ultrasonic Activation of Persulfate: An in Situ EPR Spin Trapping Study. *Environ. Sci. Technol.* **2017**, *51* (6), 3410−3417.

(17) Matzek, L. W.; Tipton, M. J.; Farmer, A. T.; Steen, A. D.; Carter, K. E. Understanding Electrochemically Activated Persulfate and Its Application to Ciprofloxacin Abatement. *Environ. Sci. Technol.* **2018**, *52* (10), 5875−5883.

(18) Furman, O. S.; Teel, A. L.; Watts, R. J. Mechanism of base activation of persulfate. *Environ. Sci. Technol.* **2010**, *44* (16), 6423−6428.

(19) Fang, G.; Gao, J.; Dionysiou, D. D.; Liu, C.; Zhou, D. Activation of persulfate by quinones: free radical reactions and implication for the degradation of PCBs. *Environ. Sci. Technol.* **2013**, *47* (9), 4605−11.

(20) Li, J.; Jiang, J.; Zhou, Y.; Pang, S.-Y.; Gao, Y.; Jiang, C.; Ma, J.; Jin, Y.; Yang, Y.; Liu, G.; Wang, L.; Guan, C. Kinetics of Oxidation of Iodide (I^{--}) and Hypoiodous Acid (HOI) by Peroxymonosulfate (PMS) and Formation of Iodinated Products in the PMS/I^{--}/NOM System. *Environ. Sci. Technol. Lett.* **2017**, *4* (2), 76−82.

(21) Huang, W.; Xiao, S.; Zhong, H.; Yan, M.; Yang, X. Activation of persulfates by carbonaceous materials: A review. *Chem. Eng. J.* **2021**, *418*, 129297.

https://doi.org/10.1021/acs.est.3c05153
Environ. Sci. Technol. 2023, 57, 12153−12179

(22) Zhao, H.; Wang, L.; Kong, D.; Ji, Y.; Lu, J.; Yin, X.; Zhou, Q. Degradation of triclosan in a peroxymonosulfate/Br^- system: Identification of reactive species and formation of halogenated byproducts. *Chem. Eng. J.* **2020**, *384*, 123297.
(23) Tsitonaki, A.; Petri, B.; Crimi, M.; MosbÆK, H.; Siegrist, R. L.; Bjerg, P. L. In Situ chemical oxidation of contaminated soil and groundwater using persulfate: A review. *Crit. Rev. Environ. Sci. Technol.* **2010**, *40* (1), 55−91.
(24) Zhao, D.; Liao, X.; Yan, X.; Huling, S. G.; Chai, T.; Tao, H. Effect and mechanism of persulfate activated by different methods for PAHs removal in soil. *J. Hazard. Mater.* **2013**, *254*−*255*, 228−235.
(25) Ahn, Y.-Y.; Yun, E. Heterogeneous metals and metal-free carbon materials for oxidative degradation through persulfate activation: A review of heterogeneous catalytic activation of persulfate related to oxidation mechanism. *Korean J. Chem. Eng.* **2019**, *36* (11), 1767−1779.
(26) Anipsitakis, G. P.; Dionysiou, D. D. Radical generation by the interaction of transition metals with common oxidants. *Environ. Sci. Technol.* **2004**, *38* (13), 3705−3712.
(27) Yan, J.; Lei, M.; Zhu, L.; Anjum, M. N.; Zou, J.; Tang, H. Degradation of sulfamonomethoxine with Fe_3O_4 magnetic nanoparticles as heterogeneous activator of persulfate. *J. Hazard. Mater.* **2011**, *186* (2−3), 1398−404.
(28) Hu, J.; Dong, H.; Qu, J.; Qiang, Z. Enhanced degradation of iopamidol by peroxymonosulfate catalyzed by two pipe corrosion products (CuO and delta-MnO_2). *Water Res.* **2017**, *112*, 1−8.
(29) Kim, C.; Ahn, J. Y.; Kim, T. Y.; Shin, W. S.; Hwang, I. Activation of persulfate by nanosized zero-valent iron (NZVI): Mechanisms and transformation products of NZVI. *Environ. Sci. Technol.* **2018**, *52* (6), 3625−3633.
(30) Yang, Q.; Choi, H.; Dionysiou, D. D. Nanocrystalline cobalt oxide immobilized on titanium dioxide nanoparticles for the heterogeneous activation of peroxymonosulfate. *Appl. Catal., B* **2007**, *74* (1), 170−178.
(31) Ahn, Y.-Y.; Bae, H.; Kim, H.-I.; Kim, S.-H.; Kim, J.-H.; Lee, S.-G.; Lee, J. Surface-loaded metal nanoparticles for peroxymonosulfate activation: Efficiency and mechanism reconnaissance. *Appl. Catal., B* **2019**, *241*, 561−569.
(32) Li, J.; Ren, Y.; Ji, F.; Lai, B. Heterogeneous catalytic oxidation for the degradation of *p*-nitrophenol in aqueous solution by persulfate activated with $CuFe_2O_4$ magnetic nano-particles. *Chem. Eng. J.* **2017**, *324*, 63−73.
(33) McGill, R. L. The influence of an educational fact sheet on small system water supplier attitudes toward the lead and copper rule. *J. Environ. Health* **1993**, *56*, No. 11+.
(34) Ali, M. E.; Rahman, M. M.; Sarkar, S. M.; Hamid, S. B. A. Heterogeneous metal catalysts for oxidation reactions. *J. Nanomater.* **2014**, *2014*, 1−23.
(35) Oh, W.-D.; Dong, Z.; Lim, T.-T. Generation of sulfate radical through heterogeneous catalysis for organic contaminants removal: Current development, challenges and prospects. *Appl. Catal., B* **2016**, *194*, 169−201.
(36) Thines, R. K.; Mubarak, N. M.; Nizamuddin, S.; Sahu, J. N.; Abdullah, E. C.; Ganesan, P. Application potential of carbon nanomaterials in water and wastewater treatment: A review. *J. Taiwan Inst. Chem. Eng.* **2017**, *72*, 116−133.
(37) Duan, X.; Sun, H.; Wang, S. Metal-free carbocatalysis in advanced oxidation reactions. *Acc. Chem. Res.* **2018**, *51* (3), 678−687.
(38) Oyekunle, D. T.; Zhou, X.; Shahzad, A.; Chen, Z. Review on carbonaceous materials as persulfate activators: structure-performance relationship, mechanism and future perspectives on water treatment. *J. Mater. Chem. A* **2021**, *9* (13), 8012−8050.
(39) Liu, B.; Guo, W.; Wang, H.; Si, Q.; Zhao, Q.; Luo, H.; Ren, N. B-doped graphitic porous biochar with enhanced surface affinity and electron transfer for efficient peroxydisulfate activation. *Chem. Eng. J.* **2020**, *396*, 125119.
(40) Chen, X.; Oh, W.-D.; Hu, Z.-T.; Sun, Y.-M.; Webster, R. D.; Li, S.-Z.; Lim, T.-T. Enhancing sulfacetamide degradation by peroxymonosulfate activation with N-doped graphene produced through delicately-controlled nitrogen functionalization via tweaking thermal annealing processes. *Appl. Catal., B* **2018**, *225*, 243−257.
(41) Radich, E. J.; Kamat, P. V. Making graphene holey. Gold-nanoparticle-mediated hydroxyl radical attack on reduced graphene oxide. *ACS Nano* **2013**, *7* (6), 5546−5557.
(42) Avramiotis, E.; Frontistis, Z.; Manariotis, I. D.; Vakros, J.; Mantzavinos, D. Oxidation of Sulfamethoxazole by Rice Husk Biochar-Activated Persulfate. *Catalysts* **2021**, *11* (7), 850.
(43) Li, Z.; Chen, X.; Teng, X.; Lu, C. Chemiluminescence as a new indicator for monitoring hydroxylated intermediates in persulfate-based advanced oxidation processes. *J. Phys. Chem. C* **2019**, *123* (35), 21704−21712.
(44) Bai, L.; Jiang, Y.; Xia, D.; Wei, Z.; Spinney, R.; Dionysiou, D. D.; Minakata, D.; Xiao, R.; Xie, H.-B.; Chai, L. Mechanistic Understanding of Superoxide Radical-Mediated Degradation of Perfluorocarboxylic Acids. *Environ. Sci. Technol.* **2022**, *56* (1), 624−633.
(45) Bai, L.; He, L.; Fu, Y.; Chu, C.; Wei, Z.; Spinney, R.; Dionysiou, D. D.; Liang, Y.; Xiao, R. New insight to superoxide radical-mediated degradation of pentachlorophenate: Kinetic determination and theoretical calculations. *Chem. Commun.* **2022**, *58* (16), 2666−2669.
(46) Gao, B.; Zhu, S.; Gu, J.; Liu, Y.; Yi, X.; Zhou, H. Superoxide radical mediated Mn(III) formation is the key process in the activation of peroxymonosulfate (PMS) by Mn-incorporated bacterial-derived biochar. *J. Hazard. Mater.* **2022**, *431*, 128549.
(47) Qi, C.; Liu, X.; Ma, J.; Lin, C.; Li, X.; Zhang, H. Activation of peroxymonosulfate by base: Implications for the degradation of organic pollutants. *Chemosphere* **2016**, *151*, 280−8.
(48) Xiao, G.; Xu, T.; Faheem, M.; Xi, Y.; Zhou, T.; Moryani, H. T.; Bao, J.; Du, J. Evolution of singlet oxygen by activating peroxydisulfate and peroxymonosulfate: A review. *Int. J. Environ. Res. Public Health* **2021**, *18* (7), 3344.
(49) Yun, E. T.; Yoo, H. Y.; Bae, H.; Kim, H. I.; Lee, J. Exploring the role of persulfate in the activation process: Radical precursor versus electron acceptor. *Environ. Sci. Technol.* **2017**, *51* (17), 10090−10099.
(50) Sun, C.; Chen, T.; Huang, Q.; Zhan, M.; Li, X.; Yan, J. Activation of persulfate by CO_2-activated biochar for improved phenolic pollutant degradation: Performance and mechanism. *Chem. Eng. J.* **2020**, *380*, 122519.
(51) Guan, C.; Jiang, J.; Pang, S.; Ma, J.; Chen, X.; Lim, T.-T. Nonradical transformation of sulfamethoxazole by carbon nanotube activated peroxydisulfate: Kinetics, mechanism and product toxicity. *Chem. Eng. J.* **2019**, *378*, 122147.
(52) Su, H.; Wei, Y.; Qu, X.; Yu, C.; Li, Q.; Alvarez, P. J. J.; Long, M. Mechanistic inference on the reaction kinetics of phenols and anilines in carbon nanotubes-activated peroxydisulfate systems: pp-LFERs and QSARs analyses. *Chem. Eng. J.* **2020**, *385*, 123923.
(53) Bu, Y.; Li, H.; Yu, W.; Pan, Y.; Li, L.; Wang, Y.; Pu, L.; Ding, J.; Gao, G.; Pan, B. Peroxydisulfate activation and singlet oxygen generation by oxygen vacancy for degradation of contaminants. *Environ. Sci. Technol.* **2021**, *55* (3), 2110−2120.
(54) Gao, Y.; Li, T.; Zhu, Y.; Chen, Z.; Liang, J.; Zeng, Q.; Lyu, L.; Hu, C. Highly nitrogen-doped porous carbon transformed from graphitic carbon nitride for efficient metal-free catalysis. *J. Hazard. Mater.* **2020**, *393*, 121280.
(55) Cheng, X.; Guo, H.; Zhang, Y.; Wu, X.; Liu, Y. Non-photochemical production of singlet oxygen via activation of persulfate by carbon nanotubes. *Water Res.* **2017**, *113*, 80−88.
(56) Jawad, A.; Zhan, K.; Wang, H.; Shahzad, A.; Zeng, Z.; Wang, J.; Zhou, X.; Ullah, H.; Chen, Z.; Chen, Z. Tuning of persulfate activation from a free radical to a nonradical pathway through the incorporation of non-redox magnesium oxide. *Environ. Sci. Technol.* **2020**, *54* (4), 2476−2488.
(57) Li, H.; Tian, J.; Xiao, F.; Huang, R.; Gao, S.; Cui, F.; Wang, S.; Duan, X. Structure-dependent catalysis of cuprous oxides in peroxymonosulfate activation via nonradical pathway with a high oxidation capacity. *J. Hazard. Mater.* **2020**, *385*, 121518.
(58) Luo, H.; Lin, Q.; Zhang, X.; Huang, Z.; Fu, H.; Xiao, R.; Liu, S.-S. Determining the key factors of nonradical pathway in activation of

persulfate by metal-biochar nanocomposites for bisphenol A degradation. *Chem. Eng. J.* **2020**, *391*, 123555.
(59) Wang, Z.; Qiu, W.; Pang, S.-y.; Zhou, Y.; Gao, Y.; Guan, C.; Jiang, J. Further understanding the involvement of Fe(IV) in peroxydisulfate and peroxymonosulfate activation by Fe(II) for oxidative water treatment. *Chem. Eng. J.* **2019**, *371*, 842−847.
(60) Wang, Z.; Qiu, W.; Pang, S.; Gao, Y.; Zhou, Y.; Cao, Y.; Jiang, J. Relative contribution of ferryl ion species (Fe(IV)) and sulfate radical formed in nanoscale zero valent iron activated peroxydisulfate and peroxymonosulfate processes. *Water Res.* **2020**, *172*, 115504.
(61) Chen, X.; Oh, W.-D.; Lim, T.-T. Graphene- and CNTs-based carbocatalysts in persulfates activation: Material design and catalytic mechanisms. *Chem. Eng. J.* **2018**, *354*, 941−976.
(62) Chen, T.; Ma, J.; Zhang, Q.; Xie, Z.; Zeng, Y.; Li, R.; Liu, H.; Liu, Y.; Lv, W.; Liu, G. Degradation of propranolol by UV-activated persulfate oxidation: Reaction kinetics, mechanisms, reactive sites, transformation pathways and Gaussian calculation. *Sci. Total Environ.* **2019**, *690*, 878−890.
(63) Liu, T.; Aniagor, C. O.; Ejimofor, M. I.; Menkiti, M. C.; Tang, K. H. D.; Chin, B. L. F.; Chan, Y. H.; Yiin, C. L.; Cheah, K. W.; Ho Chai, Y.; Lock, S. S. M.; Yap, K. L.; Wee, M. X. J.; Yap, P.-S. Technologies for removing pharmaceuticals and personal care products (PPCPs) from aqueous solutions: Recent advances, performances, challenges and recommendations for improvements. *J. Mol. Liq.* **2023**, *374*, 121144.
(64) Yang, L.; He, L.; Xue, J.; Ma, Y.; Xie, Z.; Wu, L.; Huang, M.; Zhang, Z. Persulfate-based degradation of perfluorooctanoic acid (PFOA) and perfluorooctane sulfonate (PFOS) in aqueous solution: Review on influences, mechanisms and prospective. *J. Hazard. Mater.* **2020**, *393*, 122405.
(65) Wang, A.; Zhu, B. Z.; Huang, C. H.; Zhang, W. X.; Wang, M.; Li, X.; Ling, L.; Ma, J.; Fang, J. Generation mechanism of singlet oxygen from the interaction of peroxymonosulfate and chloride in aqueous systems. *Water Res.* **2023**, *235*, 119904.
(66) Gao, Y.; Liu, Y.-z.; Wang, W.-L.; Wu, Q.-Y. Recent advances in the single-atom catalysts for persulfate activation and pollutant oxidation: A review. *J. Clean. Prod.* **2023**, *397*, 136576.
(67) Boczkaj, G.; Fernandes, A. Wastewater treatment by means of advanced oxidation processes at basic pH conditions: A review. *Chem. Eng. J.* **2017**, *320*, 608−633.
(68) Ren, W.; Cheng, C.; Shao, P.; Luo, X.; Zhang, H.; Wang, S.; Duan, X. Origins of Electron-Transfer Regime in Persulfate-Based Nonradical Oxidation Processes. *Environ. Sci. Technol.* **2022**, *56* (1), 78−97.
(69) Wang, L.; Xiao, K.; Zhao, H. The debatable role of singlet oxygen in persulfate-based advanced oxidation processes. *Water Res.* **2023**, *235*, 119925.
(70) Luo, R.; Wang, C.; Yao, Y.; Qi, J.; Li, J. Insights into the relationship of reactive oxygen species and anions in persulfate-based advanced oxidation processes for saline organic wastewater treatment. *Environ. Sci.: Water Res. Technol.* **2022**, *8* (3), 465−483.
(71) Jing, B.; Li, J.; Nie, C.; Zhou, J.; Li, D.; Ao, Z. Flow line of density functional theory in heterogeneous persulfate-based advanced oxidation processes for pollutant degradation: A review. *Crit. Rev. Environ. Sci. Technol.* **2023**, *53* (4), 483−503.
(72) Zhang, P.; Yang, Y.; Duan, X.; Liu, Y.; Wang, S. Density Functional Theory Calculations for Insight into the Heterocatalyst Reactivity and Mechanism in Persulfate-Based Advanced Oxidation Reactions. *ACS Catal.* **2021**, *11* (17), 11129−11159.
(73) Hayat, W.; Zhang, Y.; Hussain, I.; Huang, S.; Du, X. Comparison of radical and non-radical activated persulfate systems for the degradation of imidacloprid in water. *Ecotoxicol. Environ. Saf.* **2020**, *188*, 109891.
(74) Yu, J.; Qiu, W.; Xu, H.; Lu, X.; Ma, J.; Lu, D. Highly-efficient and stable $MgCo_2O_4$ spinel for bisphenol a removal by activating peroxymonosulfate via radical and non-radical pathways. *Chem. Eng. J.* **2021**, *421*, 129498.
(75) Yu, J.; Zeng, T.; Wang, H.; Zhang, H.; Sun, Y.; Chen, L.; Song, S.; Li, L.; Shi, H. Oxygen-defective MnO_{2-x} rattle-type microspheres mediated singlet oxygen oxidation of organics by peroxymonosulfate activation. *Chem. Eng. J.* **2020**, *394*, 124458.
(76) Tan, C.; Gao, N.; Deng, Y.; Deng, J.; Zhou, S.; Li, J.; Xin, X. Radical induced degradation of acetaminophen with Fe_3O_4 magnetic nanoparticles as heterogeneous activator of peroxymonosulfate. *J. Hazard. Mater.* **2014**, *276*, 452−60.
(77) Fanaei, F.; Moussavi, G.; Srivastava, V.; Sillanpää, M. The enhanced catalytic potential of sulfur-doped MgO (S-MgO) nanoparticles in activation of peroxysulfates for advanced oxidation of acetaminophen. *Chem. Eng. J.* **2019**, *371*, 404−413.
(78) Ma, J.; Minakata, D.; O'Shea, K.; Bai, L.; Dionysiou, D. D.; Spinney, R.; Xiao, R.; Wei, Z. Determination and environmental implications of aqueous-phase rate constants in radical reactions. *Water Res.* **2021**, *190*, 116746.
(79) Wojnarovits, L.; Takacs, E. Rate constants of sulfate radical anion reactions with organic molecules: A review. *Chemosphere* **2019**, *220*, 1014−1032.
(80) Wojnárovits, L.; Tóth, T.; Takács, E. Critical evaluation of rate coefficients for hydroxyl radical reactions with antibiotics: A review. *Crit. Rev. Environ. Sci. Technol.* **2018**, *48* (6), 575−613.
(81) Wilkinson, F.; Helman, W. P.; Ross, A. B. Rate constants for the decay and reactions of the lowest electronically excited singlet state of molecular oxygen in solution. An expanded and revised compilation. *J. Phys. Chem. Ref. Data* **1995**, *24* (2), 663−677.
(82) Armstrong, D. A.; Huie, R. E.; Koppenol, W. H.; Lymar, S. V.; Merényi, G.; Neta, P.; Ruscic, B.; Stanbury, D. M.; Steenken, S.; Wardman, P. Standard electrode potentials involving radicals in aqueous solution: inorganic radicals (IUPAC Technical Report). *Pure Appl. Chem.* **2015**, *87* (11−12), 1139−1150.
(83) Yang, Y.; Jiang, J.; Lu, X.; Ma, J.; Liu, Y. Production of sulfate radical and hydroxyl radical by reaction of ozone with peroxymonosulfate: a novel advanced oxidation process. *Environ. Sci. Technol.* **2015**, *49* (12), 7330−9.
(84) Erickson, P. R.; Walpen, N.; Guerard, J. J.; Eustis, S. N.; Arey, J. S.; McNeill, K. Controlling factors in the rates of oxidation of anilines and phenols by triplet methylene blue in aqueous solution. *J. Phys. Chem. A* **2015**, *119* (13), 3233−43.
(85) Yuan, Y.; Zhao, D.; Li, J.; Wu, F.; Brigante, M.; Mailhot, G. Rapid oxidation of paracetamol by Cobalt(II) catalyzed sulfite at alkaline pH. *Catal. Today* **2018**, *313*, 155−160.
(86) Wols, B. A.; Hofman-Caris, C. H.; Harmsen, D. J.; Beerendonk, E. F. Degradation of 40 selected pharmaceuticals by UV/H_2O_2. *Water Res.* **2013**, *47* (15), 5876−88.
(87) Arnold, W. A.; Oueis, Y.; O'Connor, M.; Rinaman, J. E.; Taggart, M. G.; McCarthy, R. E.; Foster, K. A.; Latch, D. E. QSARs for phenols and phenolates: oxidation potential as a predictor of reaction rate constants with photochemically produced oxidants. *Environ. Sci. Process Impacts* **2017**, *19* (3), 324−338.
(88) Palumbo, M. C.; Garcia, N. A. On the mechanism of quenching of singlet oxygen by chlorinated phenolic pesticides. *Toxicol. Environ. Chem.* **1988**, *17* (2), 103−116.
(89) Sagadevan, A.; Hwang, K. C.; Su, M. D. Singlet oxygen-mediated selective C-H bond hydroperoxidation of ethereal hydrocarbons. *Nat. Commun.* **2017**, *8* (1), 1812.
(90) Bisutti, I.; Hilke, I.; Raessler, M. Determination of total organic carbon - an overview of current methods. *TrAC Trends Anal. Chem.* **2004**, *23* (10−11), 716−726.
(91) Liang, P.; Zhang, C.; Duan, X.; Sun, H.; Liu, S.; Tade, M. O.; Wang, S. N-Doped graphene from metal-organic frameworks for catalytic oxidation of p-hydroxylbenzoic acid: N-Functionality and mechanism. *ACS Sustain. Chem. Eng.* **2017**, *5* (3), 2693−2701.
(92) Zong, Y.; Guan, X.; Xu, J.; Feng, Y.; Mao, Y.; Xu, L.; Chu, H.; Wu, D. Unraveling the Overlooked Involvement of High-Valent Cobalt-Oxo Species Generated from the Cobalt(II)-Activated Peroxymonosulfate Process. *Environ. Sci. Technol.* **2020**, *54* (24), 16231−16239.
(93) Sharma, V. K.; Feng, M.; Dionysiou, D. D.; Zhou, H.-C.; Jinadatha, C.; Manoli, K.; Smith, M. F.; Luque, R.; Ma, X.; Huang, C.-

H. Reactive High-Valent Iron Intermediates in Enhancing Treatment of Water by Ferrate. *Environ. Sci. Technol.* **2022**, *56* (1), 30−47.
(94) Gligorovski, S.; Strekowski, R.; Barbati, S.; Vione, D. Environmental implications of hydroxyl radicals (•OH). *Chem. Rev.* **2015**, *115* (24), 13051−92.
(95) Xia, X.; Zhu, F.; Li, J.; Yang, H.; Wei, L.; Li, Q.; Jiang, J.; Zhang, G.; Zhao, Q. A review study on sulfate-radical-based advanced oxidation processes for domestic/industrial wastewater treatment: Degradation, efficiency, and mechanism. *Front. Chem.* **2020**, *8*, 592056.
(96) Criquet, J.; Leitner, N. K. Degradation of acetic acid with sulfate radical generated by persulfate ions photolysis. *Chemosphere* **2009**, *77* (2), 194−200.
(97) von Sonntag, C.; Dowideit, P.; Xingwang, F.; Mertens, R.; Xianming, P.; Schuchmann, M. N.; Schuchmann, H.-P. The fate of peroxyl radicals in aqueous solution. *Water Sci. Technol.* **1997**, *35* (4), 9−15.
(98) Singleton, D. A.; Hang, C.; Szymanski, M. J.; Meyer, M. P.; Leach, A. G.; Kuwata, K. T.; Chen, J. S.; Greer, A.; Foote, C. S.; Houk, K. N. Mechanism of ene reactions of singlet oxygen. A two-step no-intermediate mechanism. *J. Am. Chem. Soc.* **2003**, *125* (5), 1319−1328.
(99) Zeinali, N.; Oluwoye, I.; Altarawneh, M.; Dlugogorski, B. Z. The mechanism of electrophilic addition of singlet oxygen to pyrrolic ring. *Theor. Chem. Acc.* **2019**, *138* (7), 90.
(100) Jensen, F.; Greer, A.; Clennan, E. L. Reaction of Organic Sulfides with Singlet Oxygen. A Revised Mechanism. *J. Am. Chem. Soc.* **1998**, *120* (18), 4439−4449.
(101) Ishiguro, K.; Hayashi, M.; Sawaki, Y. Mechanism of Sulfone Formation in the Reaction of Sulfides and Singlet Oxygen: Intermediacy of *S*-Hydroperoxysulfonium Ylide. *J. Am. Chem. Soc.* **1996**, *118* (31), 7265−7271.
(102) Scully, F. E.; Hoigné, J. Rate constants for reactions of singlet oxygen with phenols and other compounds in water. *Chemosphere* **1987**, *16* (4), 681−694.
(103) Yu, S.; Peng, Y.; Shao, P.; Wang, Y.; He, Y.; Ren, W.; Yang, L.; Shi, H.; Luo, X. Electron-transfer-based peroxymonosulfate activation on defect-rich carbon nanotubes: Understanding the substituent effect on the selective oxidation of phenols. *J. Hazard. Mater.* **2023**, *442*, 130108.
(104) Li, N.; Ye, J.; Dai, H.; Shao, P.; Liang, L.; Kong, L.; Yan, B.; Chen, G.; Duan, X. A critical review on correlating active sites, oxidative species and degradation routes with persulfate-based antibiotics oxidation. *Water Res.* **2023**, *235*, 119926.
(105) Wang, Y.; Song, Y.; Li, N.; Liu, W.; Yan, B.; Yu, Y.; Liang, L.; Chen, G.; Hou, L.; Wang, S. Tunable active sites on biogas digestate derived biochar for sulfanilamide degradation by peroxymonosulfate activation. *J. Hazard. Mater.* **2022**, *421*, 126794.
(106) Li, J.; Li, Y.; Xiong, Z.; Yao, G.; Lai, B. The electrochemical advanced oxidation processes coupling of oxidants for organic pollutants degradation: A mini-review. *Chin. Chem. Lett.* **2019**, *30* (12), 2139−2146.
(107) Maezono, T.; Tokumura, M.; Sekine, M.; Kawase, Y. Hydroxyl radical concentration profile in photo-Fenton oxidation process: generation and consumption of hydroxyl radicals during the discoloration of azo-dye Orange II. *Chemosphere* **2011**, *82* (10), 1422−30.
(108) Buxton, G. V.; Greenstock, C. L.; Helman, W. P.; Ross, A. B. Critical Review of rate constants for reactions of hydrated electrons, hydrogen atoms and hydroxyl radicals (•OH/•O$^-$) in Aqueous Solution. *J. Phys. Chem. Ref. Data* **1988**, *17* (2), 513−886.
(109) Poskrebyshev, G. Standard enthalpies of formation of SO_x^- radicals (x = 2−5) involved in oxidation of S(IV). *Russ. J. Phys. Chem. B* **1997**, *71*, 1360−1363.
(110) Ouannes, C.; Wilson, T. Quenching of singlet oxygen by tertiary aliphatic amines. Effect of DABCO (1,4-diazabicyclo[2.2.2]-octane). *J. Am. Chem. Soc.* **1968**, *90* (23), 6527−6528.
(111) Thorning, F.; Jensen, F.; Ogilby, P. R. Modeling the effect of solvents on nonradiative singlet oxygen deactivation: Going beyond weak coupling in intermolecular electronic-to-vibrational energy transfer. *J. Phys. Chem. B* **2020**, *124* (11), 2245−2254.
(112) Partanen, S. B.; Erickson, P. R.; Latch, D. E.; Moor, K. J.; McNeill, K. Dissolved organic matter singlet oxygen quantum yields: Evaluation using time-resolved singlet oxygen phosphorescence. *Environ. Sci. Technol.* **2020**, *54* (6), 3316−3324.
(113) Chen, Z.; Yin, G. The reactivity of the active metal oxo and hydroxo intermediates and their implications in oxidations. *Chem. Soc. Rev.* **2015**, *44* (5), 1083−100.
(114) Zong, Y.; Shao, Y.; Zeng, Y.; Shao, B.; Xu, L.; Zhao, Z.; Liu, W.; Wu, D. Enhanced Oxidation of Organic Contaminants by Iron(II)-Activated Periodate: The Significance of High-Valent Iron-Oxo Species. *Environ. Sci. Technol.* **2021**, *55* (11), 7634−7642.
(115) Li, H.; Shan, C.; Pan, B. Fe(III)-Doped g-C_3N_4 Mediated Peroxymonosulfate Activation for Selective Degradation of Phenolic Compounds via High-Valent Iron-Oxo Species. *Environ. Sci. Technol.* **2018**, *52* (4), 2197−2205.
(116) Wang, Z.; Jiang, J.; Pang, S.; Zhou, Y.; Guan, C.; Gao, Y.; Li, J.; Yang, Y.; Qiu, W.; Jiang, C. Is Sulfate Radical Really Generated from Peroxydisulfate Activated by Iron(II) for Environmental Decontamination? *Environ. Sci. Technol.* **2018**, *52* (19), 11276−11284.
(117) Wang, C.; Wang, X.; Wang, H.; Zhang, L.; Wang, Y.; Dong, C. L.; Huang, Y. C.; Guo, P.; Cai, R.; Haigh, S. J.; Yang, X.; Sun, Y.; Yang, D. Low-coordinated Co-N_3 sites induce peroxymonosulfate activation for norfloxacin degradation via high-valent cobalt-oxo species and electron transfer. *J. Hazard. Mater.* **2023**, *455*, 131622.
(118) Liu, B.; Guo, W.; Wang, H.; Zheng, S.; Si, Q.; Zhao, Q.; Luo, H.; Ren, N. Peroxymonosulfate activation by cobalt(II) for degradation of organic contaminants via high-valent cobalt-oxo and radical species. *J. Hazard. Mater.* **2021**, *416*, 125679.
(119) Wu, Y.; Wang, Y.; Pan, T.; Yang, X. Oxidation of tetrabromobisphenol A (TBBPA) by peroxymonosulfate: The role of in-situ formed HOBr. *Water Res.* **2020**, *169*, 115202.
(120) Liu, T.; Zhang, D.; Yin, K.; Yang, C.; Luo, S.; Crittenden, J. C. Degradation of thiacloprid via unactivated peroxymonosulfate: The overlooked singlet oxygen oxidation. *Chem. Eng. J.* **2020**, *388*, 124264.
(121) Zhou, Y.; Gao, Y.; Pang, S.-Y.; Jiang, J.; Yang, Y.; Ma, J.; Yang, Y.; Duan, J.; Guo, Q. Oxidation of fluoroquinolone antibiotics by peroxymonosulfate without activation: Kinetics, products, and antibacterial deactivation. *Water Res.* **2018**, *145*, 210−219.
(122) Berruti, I.; Oller, I.; Polo-Lopez, M. I. Direct oxidation of peroxymonosulfate under natural solar radiation: Accelerating the simultaneous removal of organic contaminants and pathogens from water. *Chemosphere* **2021**, *279*, 130555.
(123) Yang, X.; Rosario-Ortiz, F. L.; Lei, Y.; Pan, Y.; Lei, X.; Westerhoff, P. Multiple Roles of Dissolved Organic Matter in Advanced Oxidation Processes. *Environ. Sci. Technol.* **2022**, *56* (16), 11111−11131.
(124) Carena, L.; Vione, D.; Minella, M.; Canonica, S.; Schonenberger, U. Inhibition by phenolic antioxidants of the degradation of aromatic amines and sulfadiazine by the carbonate radical (CO(3)(*-)). *Water Res.* **2022**, *209*, 117867.
(125) Munoz-Rugeles, L.; Galano, A.; Alvarez-Idaboy, J. R. The other side of the superoxide radical anion: its ability to chemically repair DNA oxidized sites. *Chem. Commun.* **2018**, *54* (97), 13710−13713.
(126) Yin, R.; Guo, W.; Wang, H.; Du, J.; Zhou, X.; Wu, Q.; Zheng, H.; Chang, J.; Ren, N. Selective degradation of sulfonamide antibiotics by peroxymonosulfate alone: Direct oxidation and nonradical mechanisms. *Chem. Eng. J.* **2018**, *334*, 2539−2546.
(127) Yang, Y.; Banerjee, G.; Brudvig, G. W.; Kim, J. H.; Pignatello, J. J. Oxidation of Organic Compounds in Water by Unactivated Peroxymonosulfate. *Environ. Sci. Technol.* **2018**, *52* (10), 5911−5919.
(128) Lado Ribeiro, A. R.; Moreira, N. F. F.; Li Puma, G.; Silva, A. M. T. Impact of water matrix on the removal of micropollutants by advanced oxidation technologies. *Chem. Eng. J.* **2019**, *363*, 155−173.
(129) Darko, B.; Jiang, J.-Q.; Kim, H.; Machala, L.; Zboril, R.; Sharma, V. K. 8—Advances Made in Understanding the Interaction of

https://doi.org/10.1021/acs.est.3c05153
Environ. Sci. Technol. 2023, 57, 12153−12179

Ferrate(VI) with Natural Organic Matter in Water. In *Water Reclamation and Sustainability*; Ahuja, S., Ed.; Elsevier: Boston, 2014; pp 183−197.
(130) Shon, H. K.; Vigneswaran, S.; Snyder, S. A. Effluent organic matter (EfOM) in wastewater: Constituents, effects, and treatment. *Crit. Rev. Environ. Sci. Technol.* **2006**, *36* (4), 327−374.
(131) Cai, M. J.; Lin, Y. P. Effects of effluent organic matter (EfOM) on the removal of emerging contaminants by ozonation. *Chemosphere* **2016**, *151*, 332−8.
(132) Lebik-Elhadi, H.; Frontistis, Z.; Ait-Amar, H.; Madjene, F.; Mantzavinos, D. Degradation of pesticide thiamethoxam by heat-activated and ultrasound-activated persulfate: Effect of key operating parameters and the water matrix. *Process Saf. Environ. Prot.* **2020**, *134*, 197−207.
(133) Li, B.; Li, L.; Lin, K.; Zhang, W.; Lu, S.; Luo, Q. Removal of 1,1,1-trichloroethane from aqueous solution by a sono-activated persulfate process. *Ultrason. Sonochem.* **2013**, *20* (3), 855−63.
(134) Fang, J.; Fu, Y.; Shang, C. The roles of reactive species in micropollutant degradation in the UV/free chlorine system. *Environ. Sci. Technol.* **2014**, *48* (3), 1859−68.
(135) Wu, Z.; Fang, J.; Xiang, Y.; Shang, C.; Li, X.; Meng, F.; Yang, X. Roles of reactive chlorine species in trimethoprim degradation in the UV/chlorine process: Kinetics and transformation pathways. *Water Res.* **2016**, *104*, 272−282.
(136) Liao, C.-H.; Kang, S.-F.; Wu, F.-A. Hydroxyl radical scavenging role of chloride and bicarbonate ions in the H_2O_2/UV process. *Chemosphere* **2001**, *44* (5), 1193−1200.
(137) Wojnarovits, L.; Toth, T.; Takacs, E. Rate constants of carbonate radical anion reactions with molecules of environmental interest in aqueous solution: A review. *Sci. Total Environ.* **2020**, *717*, 137219.
(138) Frontistis, Z. Degradation of the nonsteroidal anti-inflammatory drug piroxicam by iron activated persulfate: The role of water matrix and ultrasound synergy. *Int. J. Environ. Res. Public Health* **2018**, *15* (11), 2600.
(139) Lutze, H. V.; Bircher, S.; Rapp, I.; Kerlin, N.; Bakkour, R.; Geisler, M.; von Sonntag, C.; Schmidt, T. C. Degradation of chlorotriazine pesticides by sulfate radicals and the influence of organic matter. *Environ. Sci. Technol.* **2015**, *49* (3), 1673−1680.
(140) Zhou, L.; Sleiman, M.; Ferronato, C.; Chovelon, J.-M.; Richard, C. Reactivity of sulfate radicals with natural organic matters. *Environ. Chem. Lett.* **2017**, *15* (4), 733−737.
(141) Lian, L.; Yao, B.; Hou, S.; Fang, J.; Yan, S.; Song, W. Kinetic Study of Hydroxyl and Sulfate Radical-Mediated Oxidation of Pharmaceuticals in Wastewater Effluents. *Environ. Sci. Technol.* **2017**, *51* (5), 2954−2962.
(142) Ma, J.; Li, H.; Yang, Y.; Li, X. Influence of water matrix species on persulfate oxidation of phenol: reaction kinetics and formation of undesired degradation byproducts. *Water Sci. Technol.* **2018**, *2017* (2), 340−350.
(143) Ma, J.; Yang, Y.; Jiang, X.; Xie, Z.; Li, X.; Chen, C.; Chen, H. Impacts of inorganic anions and natural organic matter on thermally activated persulfate oxidation of BTEX in water. *Chemosphere* **2018**, *190*, 296−306.
(144) Neta, P.; Huie, R. E.; Ross, A. B. Rate constants for reactions of inorganic radicals in aqueous solution. *J. Phys. Chem. Ref. Data* **1988**, *17* (3), 1027−1284.
(145) Wojnárovits, L.; Tóth, T.; Takács, E. Rate constants of carbonate radical anion reactions with molecules of environmental interest in aqueous solution: A review. *Sci. Total Environ.* **2020**, *717*, 137219.
(146) Guan, Z.; Zuo, S.; Yang, F.; Zhang, B.; Xu, H.; Xia, D.; Huang, M.; Li, D. The p and d hybridization interaction in Fe-N-C boosts peroxymonosulfate non-radical activation. *Sep. Purif. Technol.* **2021**, *258*, 118025.
(147) Rao, L.; Yang, Y.; Chen, L.; Liu, X.; Chen, H.; Yao, Y.; Wang, W. Highly efficient removal of organic pollutants via a green catalytic oxidation system based on sodium metaborate and peroxymonosulfate. *Chemosphere* **2020**, *238*, 124687.
(148) Zeng, H.; Zhao, X.; Zhao, F.; Park, Y.; Repo, E.; Thangaraj, S. K.; Janis, J.; Sillanpaa, M. Oxidation of 2,4-dichlorophenol in saline water by unactivated peroxymonosulfate: Mechanism, kinetics and implication for in situ chemical oxidation. *Sci. Total Environ.* **2020**, *728*, 138826.
(149) Zhou, Y.; Jiang, J.; Gao, Y.; Pang, S. Y.; Ma, J.; Duan, J.; Guo, Q.; Li, J.; Yang, Y. Oxidation of steroid estrogens by peroxymonosulfate (PMS) and effect of bromide and chloride ions: Kinetics, products, and modeling. *Water Res.* **2018**, *138*, 56−66.
(150) Jiang, M.; Lu, J.; Ji, Y.; Kong, D. Bicarbonate-activated persulfate oxidation of acetaminophen. *Water Res.* **2017**, *116*, 324−331.
(151) Lou, X.; Fang, C.; Geng, Z.; Jin, Y.; Xiao, D.; Wang, Z.; Liu, J.; Guo, Y. Significantly enhanced base activation of peroxymonosulfate by polyphosphates: Kinetics and mechanism. *Chemosphere* **2017**, *173*, 529−534.
(152) Meyer, M. P. Chapter Two: New Applications of Isotope Effects in the Determination of Organic Reaction Mechanisms. In *Advances in Physical Organic Chemistry*; Williams, I. H., Williams, N. H., Eds.; Academic Press: 2012; Vol. *46*, pp 57−120.
(153) Luo, S.; Wei, Z.; Dionysiou, D. D.; Spinney, R.; Hu, W.-P.; Chai, L.; Yang, Z.; Ye, T.; Xiao, R. Mechanistic insight into reactivity of sulfate radical with aromatic contaminants through single-electron transfer pathway. *Chem. Eng. J.* **2017**, *327*, 1056−1065.
(154) Wang, Z.; Du, C.; Lei, S.; Ding, D.; Chen, R.; Yang, S.; Cai, T. Modulation of carbon induced persulfate activation by nitrogen dopants: recent advances and perspectives. *J. Mater. Chem. A* **2021**, *9* (46), 25796−25826.
(155) Hu, P.; Su, H.; Chen, Z.; Yu, C.; Li, Q.; Zhou, B.; Alvarez, P. J. J.; Long, M. Selective degradation of organic pollutants using an efficient metal-free catalyst derived from carbonized polypyrrole via peroxymonosulfate activation. *Environ. Sci. Technol.* **2017**, *51* (19), 11288−11296.
(156) Pan, L.; Shi, W.; Sen, T.; Wang, L.; Zhang, J. Visible light-driven selective organic degradation by $FeTiO_3$/persulfate system: the formation and effect of high valent Fe(IV). *Appl. Catal., B* **2021**, *280*, 119414.
(157) Zhu, S.; Li, X.; Kang, J.; Duan, X.; Wang, S. Persulfate activation on crystallographic manganese oxides: Mechanism of singlet oxygen evolution for nonradical selective degradation of aqueous contaminants. *Environ. Sci. Technol.* **2019**, *53* (1), 307−315.
(158) Lee, H.; Lee, H.-J.; Jeong, J.; Lee, J.; Park, N.-B.; Lee, C. Activation of persulfates by carbon nanotubes: Oxidation of organic compounds by nonradical mechanism. *Chem. Eng. J.* **2015**, *266*, 28−33.
(159) Al-Amri, A. H.; Elroby, S. A.; Hilal, R. H. Theoretical insight into the structure and bonding characteristics of Bisphenol-A. QTAIM and NBO analyses. *J. Thoer. Comput. Chem.* **2018**, *17* (05), 1850034.
(160) Benoit, F. Substituent effects in mass spectrometry—III: Substituent effects in the dissociation of the molecular ions of para and meta substituted benzoic acids. *Organic Mass Spectrometry* **1973**, *7* (3), 295−303.
(161) Tiam, E. R.; Bikobo, D. S. N.; Ndassa, I. M.; Nyemeck, N. M.; Zintchem, A. A. A.; Ayong, L.; Diboué, P. H. B.; Ndjakou, B. L.; Mbing, J. N.; Pegnyemb, D. E. Experimental and computational studies of an antiplasmodial derivative of allantoin; antimycobacterial essential oil from Cordia batesii WERNHAM (Boraginaceae). *BMC Chemistry* **2021**, *15* (1), 15.
(162) Guerra-Rodríguez, S.; Rodríguez, E.; Singh, D. N.; Rodríguez-Chueca, J. Assessment of sulfate radical-based advanced oxidation processes for water and wastewater treatment: A review. *Water* **2018**, *10* (12), 1828.
(163) Neta, P.; Madhavan, V.; Zemel, H.; Fessenden, R. W. Rate constants and mechanism of reaction of sulfate radical anion with aromatic compounds. *J. Am. Chem. Soc.* **1977**, *99* (1), 163−164.
(164) Ruckenstein, E.; Karpe, P. Control of metal distribution in supported catalysts by pH, ionic strength, and coimpregnation. *Langmuir* **1989**, *5* (6), 1393−1407.

(165) Yang, Y.; Zhang, P.; Hu, K.; Duan, X.; Ren, Y.; Sun, H.; Wang, S. Sustainable redox processes induced by peroxymonosulfate and metal doping on amorphous manganese dioxide for nonradical degradation of water contaminants. *Appl. Catal., B* **2021**, *286*, 119903.
(166) Liang, C. J.; Bruell, C. J.; Marley, M. C.; Sperry, K. L. Thermally Activated Persulfate Oxidation of Trichloroethylene (TCE) and 1,1,1-Trichloroethane (TCA) in Aqueous Systems and Soil Slurries. *Soil Sediment Contam.* **2003**, *12* (2), 207−228.
(167) Norzaee, S.; Taghavi, M.; Djahed, B.; Kord Mostafapour, F. Degradation of Penicillin G by heat activated persulfate in aqueous solution. *J. Environ. Manage.* **2018**, *215*, 316−323.
(168) Hussain, I.; Li, M.; Zhang, Y.; Li, Y.; Huang, S.; Du, X.; Liu, G.; Hayat, W.; Anwar, N. Insights into the mechanism of persulfate activation with nZVI/BC nanocomposite for the degradation of nonylphenol. *Chem. Eng. J.* **2017**, *311*, 163−172.
(169) Wang, C.-W.; Liang, C. Oxidative degradation of TMAH solution with UV persulfate activation. *Chem. Eng. J.* **2014**, *254*, 472−478.
(170) Wang, L.; Peng, L.; Xie, L.; Deng, P.; Deng, D. Compatibility of Surfactants and Thermally Activated Persulfate for Enhanced Subsurface Remediation. *Environ. Sci. Technol.* **2017**, *51* (12), 7055−7064.
(171) Guo, H.; Gao, N.; Yang, Y.; Zhang, Y. Kinetics and transformation pathways on oxidation of fluoroquinolones with thermally activated persulfate. *Chem. Eng. J.* **2016**, *292*, 82−91.
(172) Guerra-Rodríguez, S.; Rodríguez, E.; Singh, D. N.; Rodríguez-Chueca, J. Assessment of sulfate radical-based advanced oxidation processes for water and wastewater treatment: A review. *Water* **2018**, *10*, 1828.
(173) Hori, H.; Nagaoka, Y.; Murayama, M.; Kutsuna, S. Efficient decomposition of perfluorocarboxylic acids and alternative fluorochemical surfactants in hot water. *Environ. Sci. Technol.* **2008**, *42* (19), 7438−7443.
(174) Anipsitakis, G. P.; Dionysiou, D. D.; Gonzalez, M. A. Cobalt-mediated activation of peroxymonosulfate and sulfate radical attack on phenolic compounds. Implications of chloride ions. *Environ. Sci. Technol.* **2006**, *40* (3), 1000−1007.
(175) Mora, V. C.; Rosso, J. A.; Martire, D. O.; Gonzalez, M. C. Phenol depletion by thermally activated peroxydisulfate at 70 °C. *Chemosphere* **2011**, *84* (9), 1270−5.
(176) Zrinyi, N.; Pham, A. L.-T. Oxidation of benzoic acid by heat-activated persulfate: Effect of temperature on transformation pathway and product distribution. *Water Res.* **2017**, *120*, 43−51.
(177) Chu, W.; Hu, J.; Bond, T.; Gao, N.; Xu, B.; Yin, D. Water temperature significantly impacts the formation of iodinated haloacetamides during persulfate oxidation. *Water Res.* **2016**, *98*, 47−55.
(178) Duan, X.; Ao, Z.; Sun, H.; Indrawirawan, S.; Wang, Y.; Kang, J.; Liang, F.; Zhu, Z. H.; Wang, S. Nitrogen-doped graphene for generation and evolution of reactive radicals by metal-free catalysis. *ACS Appl. Mater. Interfaces* **2015**, *7* (7), 4169−78.
(179) Tang, L.; Liu, Y.; Wang, J.; Zeng, G.; Deng, Y.; Dong, H.; Feng, H.; Wang, J.; Peng, B. Enhanced activation process of persulfate by mesoporous carbon for degradation of aqueous organic pollutants: Electron transfer mechanism. *Appl. Catal., B* **2018**, *231*, 1−10.
(180) Duan, X.; Ao, Z.; Zhang, H.; Saunders, M.; Sun, H.; Shao, Z.; Wang, S. Nanodiamonds in sp^2 /sp^3 configuration for radical to nonradical oxidation: Core-shell layer dependence. *Appl. Catal., B* **2018**, *222*, 176−181.
(181) Du, X.; Zhou, M. Strategies to enhance catalytic performance of metal-organic frameworks in sulfate radical-based advanced oxidation processes for organic pollutants removal. *Chem. Eng. J.* **2021**, *403*, 126346.
(182) Guan, Y. H.; Ma, J.; Li, X. C.; Fang, J. Y.; Chen, L. W. Influence of pH on the formation of sulfate and hydroxyl radicals in the UV/peroxymonosulfate system. *Environ. Sci. Technol.* **2011**, *45* (21), 9308−14.
(183) Oh, W. D.; Dong, Z.; Ronn, G.; Lim, T. T. Surface-active bismuth ferrite as superior peroxymonosulfate activator for aqueous sulfamethoxazole removal: Performance, mechanism and quantification of sulfate radical. *J. Hazard. Mater.* **2017**, *325*, 71−81.
(184) An, D.; Westerhoff, P.; Zheng, M.; Wu, M.; Yang, Y.; Chiu, C. A. UV-activated persulfate oxidation and regeneration of NOM-Saturated granular activated carbon. *Water Res.* **2015**, *73*, 304−10.
(185) Feng, Y.; Song, Q.; Lv, W.; Liu, G. Degradation of ketoprofen by sulfate radical-based advanced oxidation processes: Kinetics, mechanisms, and effects of natural water matrices. *Chemosphere* **2017**, *189*, 643−651.
(186) Zhang, Y.; Tran, H. P.; Du, X.; Hussain, I.; Huang, S.; Zhou, S.; Wen, W. Efficient pyrite activating persulfate process for degradation of *p*-chloroaniline in aqueous systems: A mechanistic study. *Chem. Eng. J.* **2017**, *308*, 1112−1119.
(187) Tian, Y.; Li, Q.; Zhang, M.; Nie, Y.; Tian, X.; Yang, C.; Li, Y. pH-dependent oxidation mechanisms over FeCu doped g-C_3N_4 for ofloxacin degradation via the efficient peroxymonosulfate activation. *J. Clean. Prod.* **2021**, *315*, 128207.
(188) Furman, O. S.; Teel, A. L.; Ahmad, M.; Merker, M. C.; Watts, R. J. Effect of basicity on persulfate reactivity. *J. Environ. Eng.* **2011**, *137* (4), 241−247.
(189) Liang, C.; Wang, Z. S.; Bruell, C. J. Influence of pH on persulfate oxidation of TCE at ambient temperatures. *Chemosphere* **2007**, *66* (1), 106−13.
(190) Ma, J.; Li, H.; Chi, L.; Chen, H.; Chen, C. Changes in activation energy and kinetics of heat-activated persulfate oxidation of phenol in response to changes in pH and temperature. *Chemosphere* **2017**, *189*, 86−93.
(191) Fan, Y.; Ji, Y.; Kong, D.; Lu, J.; Zhou, Q. Kinetic and mechanistic investigations of the degradation of sulfamethazine in heat-activated persulfate oxidation process. *J. Hazard. Mater.* **2015**, *300*, 39−47.
(192) Wen, D.; Li, W.; Lv, J.; Qiang, Z.; Li, M. Methylene blue degradation by the VUV/UV/persulfate process: Effect of pH on the roles of photolysis and oxidation. *J. Hazard. Mater.* **2020**, *391*, 121855.
(193) Olmez-Hanci, T.; Arslan-Alaton, I.; Genc, B. Bisphenol A treatment by the hot persulfate process: oxidation products and acute toxicity. *J. Hazard. Mater.* **2013**, *263*, 283−290.
(194) Carre-Burritt, A. E.; Van Hoomissen, D. J.; Vyas, S. Role of pH in the transformation of perfluoroalkyl carboxylic acids by activated persulfate: Implications from the determination of absolute electron-transfer rates and chemical computations. *Environ. Sci. Technol.* **2021**, *55* (13), 8928−8936.
(195) Qiu, H.-B.; Guo, P.-C.; Yuan, L.; Sheng, G.-P. Different non-radical oxidation processes of persulfate and peroxymonosulfate activation by nitrogen-doped mesoporous carbon. *Chin. Chem. Lett.* **2020**, *31* (10), 2614−2618.
(196) Jiang, N.; Xu, H.; Wang, L.; Jiang, J.; Zhang, T. Nonradical oxidation of pollutants with single-atom-Fe(III)-activated persulfate: Fe(V) being the possible intermediate oxidant. *Environ. Sci. Technol.* **2020**, *54* (21), 14057−14065.
(197) Liu, B.; Li, Y.; Wu, Y.; Xing, S. Enhanced degradation of ofloxacin by persulfate activation with Mn doped CuO: Synergetic effect between adsorption and non-radical activation. *Chem. Eng. J.* **2021**, *417*, 127972.
(198) Yin, R.; Guo, W.; Wang, H.; Du, J.; Wu, Q.; Chang, J.-S.; Ren, N. Singlet oxygen-dominated peroxydisulfate activation by sludge-derived biochar for sulfamethoxazole degradation through a non-radical oxidation pathway: Performance and mechanism. *Chem. Eng. J.* **2019**, *357*, 589−599.
(199) Gao, Y.-q.; Gao, N.-y.; Chu, W.-h.; Zhang, Y.-f.; Zhang, J.; Yin, D.-q. UV-activated persulfate oxidation of sulfamethoxypyridazine: Kinetics, degradation pathways and impact on DBP formation during subsequent chlorination. *Chem. Eng. J.* **2019**, *370*, 706−715.
(200) Liu, J.; Peng, C.; Shi, X. Preparation, characterization, and applications of Fe-based catalysts in advanced oxidation processes for organics removal: A review. *Environ. Pollut.* **2022**, *293*, 118565.

(201) Lefebvre, O.; Moletta, R. Treatment of organic pollution in industrial saline wastewater: a literature review. *Water Res.* **2006**, *40* (20), 3671−82.
(202) Grebel, J. E.; Pignatello, J. J.; Mitch, W. A. Effect of halide ions and carbonates on organic contaminant degradation by hydroxyl radical-based advanced oxidation processes in saline waters. *Environ. Sci. Technol.* **2010**, *44* (17), 6822−6828.
(203) Zhang, T.; Chen, Y.; Wang, Y.; Le Roux, J.; Yang, Y.; Croue, J. P. Efficient peroxydisulfate activation process not relying on sulfate radical generation for water pollutant degradation. *Environ. Sci. Technol.* **2014**, *48* (10), 5868−75.
(204) Liu, K.; Lu, J.; Ji, Y. Formation of brominated disinfection by-products and bromate in cobalt catalyzed peroxymonosulfate oxidation of phenol. *Water Res.* **2015**, *84*, 1−7.
(205) Xu, X.; Xiao, R.; Dionysiou, D. D.; Spinney, R.; Fu, T.; Li, Q.; Wang, Z.; Wang, D.; Wei, Z. Kinetics and mechanisms of the formation of chlorinated and oxygenated polycyclic aromatic hydrocarbons during chlorination. *Chem. Eng. J.* **2018**, *351*, 248−257.
(206) Liu, Q.; Xu, X.; Fu, J.; Du, Y.; Lin, L.; Bai, L.; Wang, D. Role of hypobromous acid in the transformation of polycyclic aromatic hydrocarbons during chlorination. *Water Res.* **2021**, *207*, 117787.
(207) Köppel, C.; Tenczer, J. Scope and limitations of a general unknown screening by gas chromatography—mass spectrometry in acute poisoning. *J. Am. Soc. Mass Spectrom.* **1995**, *6* (11), 995−1003.
(208) Fernando, S.; Jobst, K. J.; Taguchi, V. Y.; Helm, P. A.; Reiner, E. J.; McCarry, B. E. Identification of the halogenated compounds resulting from the 1997 Plastimet Inc. fire in Hamilton, Ontario, using comprehensive two-dimensional gas chromatography and (ultra)high resolution mass spectrometry. *Environ. Sci. Technol.* **2014**, *48* (18), 10656−63.
(209) He, L.; Bai, L.; Dionysiou, D. D.; Wei, Z.; Spinney, R.; Chu, C.; Lin, Z.; Xiao, R. Applications of computational chemistry, artificial intelligence, and machine learning in aquatic chemistry research. *Chem. Eng. J.* **2021**, *426*, 131810.
(210) Dong, F.; Li, C.; Ma, X.; Lin, Q.; He, G.; Chu, S. Degradation of estriol by chlorination in a pilot-scale water distribution system: Kinetics, pathway and DFT studies. *Chem. Eng. J.* **2020**, *383*, 123187.
(211) Zhou, Y.; Jiang, J.; Gao, Y.; Pang, S.-Y.; Ma, J.; Duan, J.; Guo, Q.; Li, J.; Yang, Y. Oxidation of steroid estrogens by peroxymonosulfate (PMS) and effect of bromide and chloride ions: Kinetics, products, and modeling. *Water Res.* **2018**, *138*, 56−66.
(212) Bolton, J. R.; Bircher, K. G.; Tumas, W.; Tolman, C. A. Figures-of-merit for the technical development and application of advanced oxidation technologies for both electric- and solar-driven systems (IUPAC Technical Report). *Pure Appl. Chem.* **2001**, *73* (4), 627−637.
(213) Bolton, J. R.; Bircher, K. G.; Tumas, W.; Tolman, C. A. Figures-of-Merit for the technical development and application of advanced oxidation processes. *J. Adv. Oxid. Technol.* **1996**, *1* (1), 13−17.
(214) Bolton, J. R.; Valladares, J. E.; Zanin, J. P.; Cooper, W. J.; Nickelsen, M. G.; Kajdi, D. C.; Waite; Kurucz, C. N. Figures-of-Merit for advanced oxidation technologies: A comparison of homogeneous UV/H_2O_2, heterogeneous UV/TiO_2 and electron beam processes. *J. Adv. Oxid. Technol.* **1998**, *3* (2), 174−181.
(215) Rosenfeldt, E. J.; Linden, K. G.; Canonica, S.; von Gunten, U. Comparison of the efficiency of ·OH radical formation during ozonation and the advanced oxidation processes O_3/H_2O_2 and UV/H_2O_2. *Water Res.* **2006**, *40* (20), 3695−704.
(216) Alaton, I. A.; Balcioglu, I. A.; Bahnemann, D. W. Advanced oxidation of a reactive dyebath effluent: comparison of O_3, H_2O_2/UV-C and TiO_2/UV-A processes. *Water Res.* **2002**, *36* (5), 1143−1154.
(217) Sun, P.; Tyree, C.; Huang, C. H. Inactivation of Escherichia coli, Bacteriophage MS2, and Bacillus Spores under UV/H_2O_2 and UV/peroxydisulfate advanced disinfection conditions. *Environ. Sci. Technol.* **2016**, *50* (8), 4448−58.
(218) Lee, Y. M.; Lee, G.; Zoh, K. D. Benzophenone-3 degradation via UV/H_2O_2 and UV/persulfate reactions. *J. Hazard. Mater.* **2021**, *403*, 123591.
(219) Li, D.; Feng, Z.; Zhou, B.; Chen, H.; Yuan, R. Impact of water matrices on oxidation effects and mechanisms of pharmaceuticals by ultraviolet-based advanced oxidation technologies: A review. *Sci. Total Environ.* **2022**, *844*, 157162.
(220) Huang, H.; Guo, T.; Wang, K.; Li, Y.; Zhang, G. Efficient activation of persulfate by a magnetic recyclable rape straw biochar catalyst for the degradation of tetracycline hydrochloride in water. *Sci. Total Environ.* **2021**, *758*, 143957.
(221) Lin, X.; Ma, Y.; Wan, J.; Wang, Y.; Li, Y. Efficient degradation of Orange G with persulfate activated by recyclable $FeMoO_4$. *Chemosphere* **2019**, *214*, 642−650.
(222) Ren, W.; Xiong, L.; Yuan, X.; Yu, Z.; Zhang, H.; Duan, X.; Wang, S. Activation of peroxydisulfate on carbon nanotubes: Electron-transfer mechanism. *Environ. Sci. Technol.* **2019**, *53* (24), 14595−14603.
(223) Cheng, X.; Guo, H.; Zhang, Y.; Korshin, G. V.; Yang, B. Insights into the mechanism of nonradical reactions of persulfate activated by carbon nanotubes: Activation performance and structure-function relationship. *Water Res.* **2019**, *157*, 406−414.
(224) Lin, C.-C.; Wu, M.-S. Degradation of ciprofloxacin by UV/$S_2O_8^{2-}$ process in a large photoreactor. *J. Photochem. Photobiol. A: Chem.* **2014**, *285*, 1−6.
(225) Guan, C.; Jiang, J.; Pang, S.; Luo, C.; Ma, J.; Zhou, Y.; Yang, Y. Oxidation Kinetics of Bromophenols by Nonradical Activation of Peroxydisulfate in the Presence of Carbon Nanotube and Formation of Brominated Polymeric Products. *Environ. Sci. Technol.* **2017**, *51* (18), 10718−10728.
(226) Zhang, Y. J.; Huang, G. X.; Winter, L. R.; Chen, J. J.; Tian, L.; Mei, S. C.; Zhang, Z.; Chen, F.; Guo, Z. Y.; Ji, R.; You, Y. Z.; Li, W. W.; Liu, X. W.; Yu, H. Q.; Elimelech, M. Simultaneous nanocatalytic surface activation of pollutants and oxidants for highly efficient water decontamination. *Nat. Commun.* **2022**, *13* (1), 3005.
(227) Martijn, A. J. Impact of the water matrix on the effect and the side effect of MP UV/H_2O_2 treatment for the removal of organic micropollutants in drinking water production. PhD thesis, Wageningen University, Wageningen, NL, 2015.
(228) Kang, J.; Duan, X.; Wang, C.; Sun, H.; Tan, X.; Tade, M. O.; Wang, S. Nitrogen-doped bamboo-like carbon nanotubes with Ni encapsulation for persulfate activation to remove emerging contaminants with excellent catalytic stability. *Chem. Eng. J.* **2018**, *332*, 398−408.
(229) Ren, W.; Xiong, L.; Nie, G.; Zhang, H.; Duan, X.; Wang, S. Insights into the Electron-Transfer Regime of Peroxydisulfate Activation on Carbon Nanotubes: The Role of Oxygen Functional Groups. *Environ. Sci. Technol.* **2020**, *54* (2), 1267−1275.
(230) Huie, R. E.; Clifton, C. L. Rate constants for hydrogen abstraction reactions of the sulfate radical, SO_4^{-}. Alkanes and ethers. *Int. J. Chem. Kinet.* **1989**, *21* (8), 611−619.
(231) Clifton, C. L.; Huie, R. E. Rate constants for hydrogen abstraction reactions of the sulfate radical, SO_4^{-}. Alcohols. *Int. J. Chem. Kinet.* **1989**, *21* (8), 677−687.
(232) Luo, C.; Jiang, J.; Ma, J.; Pang, S.; Liu, Y.; Song, Y.; Guan, C.; Li, J.; Jin, Y.; Wu, D. Oxidation of the odorous compound 2,4,6-trichloroanisole by UV activated persulfate: Kinetics, products, and pathways. *Water Res.* **2016**, *96*, 12−21.
(233) Tang, W. Z.; Huang, C. P. Effect of chlorine content of chlorinated phenols on their oxidation kinetics by Fenton's reagent. *Chemosphere* **1996**, *33* (8), 1621−1635.
(234) Ziajka, J.; Rudzinski, K. J. Autoxidation of S^{IV} inhibited by chlorophenols reacting with sulfate radicals. *Environ. Chem.* **2007**, *4* (5), 355−363.
(235) Kochany, J.; Bolton, J. R. Mechanism of photodegradation of aqueous organic pollutants. 2. Measurement of the primary rate constants for reaction of hydroxyl radicals with benzene and some halobenzenes using an EPR spin-trapping method following the photolysis of hydrogen peroxide. *Environ. Sci. Technol.* **1992**, *26* (2), 262−265.
(236) Gao, L.; Guo, Y.; Zhan, J.; Yu, G.; Wang, Y. Assessment of the validity of the quenching method for evaluating the role of reactive

species in pollutant abatement during the persulfate-based process. *Water Res.* **2022**, *221*, 118730.
(237) Rudziński, K. J.; Szmigielski, R. Aqueous reactions of sulfate radical-anions with nitrophenols in atmospheric context. *Atmosphere* **2019**, *10*, 795.
(238) Liu, Y.; Wang, D.; Sun, B.; Zhu, X. Aqueous 4-nitrophenol decomposition and hydrogen peroxide formation induced by contact glow discharge electrolysis. *J. Hazard. Mater.* **2010**, *181* (1−3), 1010−5.
(239) Sharma, S. B.; Mudaliar, M.; Rao, B. S. M.; Mohan, H.; Mittal, J. P. Radiation chemical oxidation of benzaldehyde, acetophenone, and benzophenone. *J. Phys. Chem. A* **1997**, *101* (45), 8402−8408.
(240) Willson, R. L.; Greenstock, C. L.; Adams, G. E.; Wageman, R.; Dorfman, L. M. The standardization of hydroxyl radical rate data from radiation chemistry. *International Journal for Radiation Physics and Chemistry* **1971**, *3* (3), 211−220.
(241) Darmanyan, A. P.; Vidoczy, T.; Irinii, G.; Gal, D. Influence of medium on lifetime and reactivity of $^1O_2$ with 1,3-diphenylisobenzofuran, and the role of $^1O_2$ in liquid-phase oxidation of ethylbenzene. *Russ. Chem. Bull.* **1983**, *32* (12), 2423−2429.
(242) Xiao, R.; Ye, T.; Wei, Z.; Luo, S.; Yang, Z.; Spinney, R. Quantitative structure-activity relationship (QSAR) for the oxidation of trace organic contaminants by sulfate radical. *Environ. Sci. Technol.* **2015**, *49* (22), 13394−13402.
(243) Mandal, S. Reaction rate constants of hydroxyl radicals with micropollutants and their significance in advanced oxidation processes. *J. Adv. Oxid. Technol.* **2018**, *21* (1), 178−195.
(244) O'Neill, P.; Steenken, S.; Schulte-Frohlinde, D. Formation of radical cations of methoxylated benzenes by reaction with hydroxyl radicals, Tl^{2+}, Ag^{2+}, and SO_4·- in aqueous solution. Optical and conductometric pulse radiolysis and in situ radiolysis electron spin resonance study. *J. Phys. Chem.* **1975**, *79* (25), 2773−2779.
(245) Corey, E. J.; Khan, A. U.; Deok-Chan, H. Heavy atom quenching of the singlet delta dioxygen molecule ($^1\Delta_g$ O_2). *Tetrahedron Lett.* **1990**, *31* (10), 1389−1392.
(246) Land, E. J.; Porter, G. Extinction coefficients of triplet-triplet transitions. *Proc. R. Soc. A: Math. Phys. Eng. Sci.* **1968**, *305* (1483), 457−471.
(247) Stevens, B.; Marsh, K. L. Photoperoxidation of unsaturated organic molecules. 24. Mixed solvent quenching of molecular oxygen(1.DELTA.g) phosphorescence. *J. Phys. Chem.* **1982**, *86* (23), 4473−4476.
(248) Peller, J. R.; Mezyk, S. P.; Cooper, W. J. Bisphenol A reactions with hydroxyl radicals: diverse pathways determined between deionized water and tertiary treated wastewater solutions. *Res. Chem. Intermed.* **2009**, *35* (1), 21−34.
(249) Merga, G.; Aravindakumar, C. T.; Rao, B. S. M.; Mohan, H. R.; Mittal, J. P. Pulse radiolysis study of the reactions of $SO_4^{\cdot-}$ with some substituted benzenes in aqueous solution. *J. Chem. Soc., Faraday trans.* **1994**, *90*, 597−604.
(250) Ashton, L.; Buxton, G. V.; Stuart, C. R. Temperature dependence of the rate of reaction of OH with some aromatic compounds in aqueous solution. Evidence for the formation of a π-complex intermediate? *J. Chem. Soc., Faraday Trans.* **1995**, *91* (11), 1631−1633.
(251) Padmaja, S.; Alfassi, Z. B.; Neta, P.; Huie, R. E. Rate constants for reactions of $SO_4^{\cdot-}$ radicals in acetonitrile. *Int. J. Chem. Kinet.* **1993**, *25* (3), 193−198.
(252) Mahdi Ahmed, M.; Barbati, S.; Doumenq, P.; Chiron, S. Sulfate radical anion oxidation of diclofenac and sulfamethoxazole for water decontamination. *Chem. Eng. J.* **2012**, *197*, 440−447.
(253) Huber, M. M.; Canonica, S.; Park, G.-Y.; von Gunten, U. Oxidation of pharmaceuticals during ozonation and advanced oxidation processes. *Environ. Sci. Technol.* **2003**, *37* (5), 1016−1024.
(254) Deister, U.; Warneck, P. Photooxidation of sulfite (SO_3^{2-}) in aqueous solution. *J. Phys. Chem.* **1990**, *94* (5), 2191−2198.
(255) Park, H.-R.; Getoff, N. Radiolysis of aqueous ethanol in the presence of CO. *Zeitschrift für Naturforschung A* **1992**, *47* (9), 985−991.
(256) Mohan, H.; Mittal, J. P. Direct evidence for H+-catalysed dehydration of fluorohydroxycyclohexadienyl radical: a pulse radiolysis study. *J. Chem. Soc., Faraday Trans.* **1995**, *91* (14), 2121−2126.
(257) He, X.; Mezyk, S. P.; Michael, I.; Fatta-Kassinos, D.; Dionysiou, D. D. Degradation kinetics and mechanism of beta-lactam antibiotics by the activation of H_2O_2 and $Na_2S_2O_8$ under UV-254nm irradiation. *J. Hazard. Mater.* **2014**, *279*, 375−83.
(258) Shah, N. S.; Khan, J. A.; Sayed, M.; Khan, Z. U. H.; Rizwan, A. D.; Muhammad, N.; Boczkaj, G.; Murtaza, B.; Imran, M.; Khan, H. M.; Zaman, G. Solar light driven degradation of norfloxacin using as-synthesized Bi^{3+} and Fe^{2+} co-doped ZnO with the addition of HSO_5^-: Toxicities and degradation pathways investigation. *Chem. Eng. J.* **2018**, *351*, 841−855.
(259) Zhang, P.; Yao, S.; Li, H.; Song, X.; Liu, Y.; Wang, W. Pulse radiolysis study on several fluoroquinolones. *Radiat. Phys. Chem.* **2011**, *80* (4), 548−553.
(260) Ziajka, J.; Pasiuk-Bronikowska, W. Rate constants for atmospheric trace organics scavenging SO_4^- in the Fe-catalysed autoxidation of S(IV). *Atmos. Environ.* **2005**, *39* (8), 1431−1438.
(261) Zemel, H. Electron Spin Resonance and Pulse Radiolysis Studies of the Mechanism and Kinetics of SO_4^- Reactions with Aromatic Compounds in Aqueous Solution. PhD thesis, Carnegie Mellon University, United States, 1977.
(262) Zhang, R.; Sun, P.; Boyer, T. H.; Zhao, L.; Huang, C. H. Degradation of pharmaceuticals and metabolite in synthetic human urine by UV, UV/H_2O_2, and UV/PDS. *Environ. Sci. Technol.* **2015**, *49* (5), 3056−66.
(263) Huie, R. E.; Clifton, C. L.; Kafafi, S. A. Rate constants for hydrogen abstraction reactions of the sulfate radical, SO_4^-: experimental and theoretical results for cyclic ethers. *J. Phys. Chem.* **1991**, *95* (23), 9336−9340.
(264) Eibenberger, J. Pulse radiolytic investigations concerning the formation and the oxidation of organic radicals in aqueous solutions. PhD thesis, University of Vienna, Austria, 1980.
(265) Hug, G. L. *Optical Spectra of Nonmetallic Inorganic Transient Species in Aqueous Solution*; National Standard Reference Data System, 1981.
(266) Li, S. H.; Guo, J. J.; Li, R.; Wang, F.; Li, X. Y. Theoretical prediction of rate constants for hydrogen abstraction by OH, H, O, CH_3, and HO_2 radicals from toluene. *J. Phys. Chem. A* **2016**, *120* (20), 3424−32.
(267) Kishimoto, N. State of the art of UV/Chlorine advanced oxidation processes: Their mechanism, byproducts formation, process variation, and applications. *J. Water Environ. Technol.* **2019**, *17*, 302−335.
(268) Lei, Y.; Lei, X.; Yu, Y.; Li, K.; Li, Z.; Cheng, S.; Ouyang, G.; Yang, X. Rate constants and mechanisms for reactions of bromine radicals with trace organic contaminants. *Environ. Sci. Technol.* **2021**, *55* (15), 10502−10513.
(269) Shafirovich, V.; Dourandin, A.; Huang, W.; Geacintov, N. E. The carbonate radical is a site-selective oxidizing agent of guanine in double-stranded oligonucleotides*. *J. Biol. Chem.* **2001**, *276* (27), 24621−24626.
(270) Czapski, G.; Lymar, S. V.; Schwarz, H. A. Acidity of the Carbonate Radical. *J. Phys. Chem. A* **1999**, *103* (18), 3447−3450.
(271) Barrios, B.; Mohrhardt, B.; Doskey, P. V.; Minakata, D. Mechanistic insight into the reactivities of aqueous-phase singlet oxygen with organic compounds. *Environ. Sci. Technol.* **2021**, *55* (12), 8054−8067.
(272) Ashby, M. T. Chapter 8: Hypothiocyanite. In *Advances in Inorganic Chemistry*; Eldik, R. v.; Ivanović-Burmazović, I., Eds.; Academic Press: 2012; Vol. *64*, pp 263−303.
(273) Ennis, C.; Birks, J. Rateconstants for the reactions OH + HOCl → H_2O + ClO and H + HOCl → Products. *J. Phys. Chem.* **1988**, *92*, 1119−1126.
(274) Harris, D. C. *Exploring Chemical Analysis*; Macmillan: 2012.
(275) Burkholder, J. B. Ultraviolet absorption spectrum of HOCl. *J. Geophys. Res. Atmos.* **1993**, *98* (D2), 2963−2974.

https://doi.org/10.1021/acs.est.3c05153
Environ. Sci. Technol. 2023, 57, 12153−12179

(276) Denis, P. A. Thermochemistry of the hypobromous and hypochlorous acids, HOBr and HOCl. *j. phys. Chem. A* **2006**, *110* (17), 5887−5892.
(277) He, X.; de la Cruz, A. A.; Dionysiou, D. D. Destruction of cyanobacterial toxin cylindrospermopsin by hydroxyl radicals and sulfate radicals using UV-254nm activation of hydrogen peroxide, persulfate and peroxymonosulfate. *J. Photochem. Photobiol. A: Chem.* **2013**, *251*, 160−166.
(278) Antoniou, M. G.; Boraei, I.; Solakidou, M.; Deligiannakis, Y.; Abhishek, M.; Lawton, L. A.; Edwards, C. Enhancing photocatalytic degradation of the cyanotoxin microcystin-LR with the addition of sulfate-radical generating oxidants. *J. Hazard. Mater.* **2018**, *360*, 461−470.
(279) Pirsaheb, M.; Hossaini, H.; Janjani, H. Reclamation of hospital secondary treatment effluent by sulfate radicals based-advanced oxidation processes (SR-AOPs) for removal of antibiotics. *Microchem. J.* **2020**, *153*, 104430.
(280) Yadav, M. S. P.; Neghi, N.; Kumar, M.; Varghese, G. K. Photocatalytic-oxidation and photo-persulfate-oxidation of sulfadiazine in a laboratory-scale reactor: Analysis of catalyst support, oxidant dosage, removal-rate and degradation pathway. *J. Environ. Manage.* **2018**, *222*, 164−173.
(281) Xiao, Y.; Zhang, L.; Zhang, W.; Lim, K.-Y.; Webster, R. D.; Lim, T.-T. Comparative evaluation of iodoacids removal by UV/persulfate and UV/H_2O_2 processes. *Water Res.* **2016**, *102*, 629−639.
(282) Nasseri, S.; Mahvi, A. H.; Seyedsalehi, M.; Yaghmaeian, K.; Nabizadeh, R.; Alimohammadi, M.; Safari, G. H. Degradation kinetics of tetracycline in aqueous solutions using peroxydisulfate activated by ultrasound irradiation: Effect of radical scavenger and water matrix. *J. Mol. Liq.* **2017**, *241*, 704−714.
(283) Rehman, F.; Sayed, M.; Khan, J. A.; Shah, N. S.; Khan, H. M.; Dionysiou, D. D. Oxidative removal of brilliant green by UV/$S_2O_8^{2-}$, UV/HSO_5^- and UV/H_2O_2 processes in aqueous media: A comparative study. *J. Hazard. Mater.* **2018**, *357*, 506−514.
(284) Tan, C.; Fu, D.; Gao, N.; Qin, Q.; Xu, Y.; Xiang, H. Kinetic degradation of chloramphenicol in water by UV/persulfate system. *J. Photochem. Photobiol. A: Chem.* **2017**, *332*, 406−412.
(285) Dhaka, S.; Kumar, R.; Lee, S.-h.; Kurade, M. B.; Jeon, B.-H. Degradation of ethyl paraben in aqueous medium using advanced oxidation processes: Efficiency evaluation of UV-C supported oxidants. *J. Clean. Prod.* **2018**, *180*, 505−513.
(286) Lu, X.; Shao, Y.; Gao, N.; Chen, J.; Deng, H.; Chu, W.; An, N.; Peng, F. Investigation of clofibric acid removal by UV/persulfate and UV/chlorine processes: Kinetics and formation of disinfection byproducts during subsequent chlor(am)ination. *Chem. Eng. J.* **2018**, *331*, 364−371.
(287) Khan, J. A.; He, X.; Shah, N. S.; Khan, H. M.; Hapeshi, E.; Fatta-Kassinos, D.; Dionysiou, D. D. Kinetic and mechanism investigation on the photochemical degradation of atrazine with activated H_2O_2, $S_2O_8^{2-}$ and HSO_5^-. *Chem. Eng. J.* **2014**, *252*, 393−403.
(288) Ding, H.; Hu, J. Degradation of ibuprofen by UVA-LED/TiO_2/persulfate process: Kinetics, mechanism, water matrix effects, intermediates and energy consumption. *Chem. Eng. J.* **2020**, *397*, 125462.
(289) Wang, F.; Wang, W.; Yuan, S.; Wang, W.; Hu, Z.-H. Comparison of UV/H_2O_2 and UV/PS processes for the degradation of thiamphenicol in aqueous solution. *J. Photochem. Photobiol. A: Chem.* **2017**, *348*, 79−88.
(290) Lee, Y.; Lee, S.; Cui, M.; Ren, Y.; Park, B.; Ma, J.; Han, Z.; Khim, J. Activation of peroxodisulfate and peroxymonosulfate by ultrasound with different frequencies: Impact on ibuprofen removal efficient, cost estimation and energy analysis. *Chem. Eng. J.* **2021**, *413*, 127487.
(291) Bhandari, P. S.; Makwana, B. P.; Gogate, P. R. Microwave and ultrasound assisted dual oxidant based degradation of sodium dodecyl sulfate: Efficacy of irradiation approaches and oxidants. *J. Water Process Eng.* **2020**, *36*, 101316.
(292) Dionisio, D.; Motheo, A. J.; Sáez, C.; Cañizares, P.; Rodrigo, M. A. Effects of ultrasound irradiation on the electrochemical treatment of wastes containing micelles. *Appl. Catal., B* **2019**, *248*, 108−114.
(293) Neghi, N.; Krishnan, N. R.; Kumar, M. Analysis of metronidazole removal and micro-toxicity in photolytic systems: Effects of persulfate dosage, anions and reactor operation-mode. *J. Environ. Chem. Eng.* **2018**, *6* (1), 754−761.
(294) Roy, K.; Moholkar, V. S. Mechanistic analysis of carbamazepine degradation in hybrid advanced oxidation process of hydrodynamic cavitation/UV/persulfate in the presence of ZnO/$ZnFe_2O_4$. *Sep. Purif. Technol.* **2021**, *270*, 118764.
(295) Ghavi, A.; Bagherian, G.; Rezaei-Vahidian, H. Degradation of paraquat herbicide using hybrid AOP process: statistical optimization, kinetic study, and estimation of electrical energy consumption. *Environ. Sci. Eur.* **2021**, *33* (1), 117.
(296) Liu, L.; Yang, C.; Tan, W.; Wang, Y. Degradation of acid red 73 by activated persulfate in a heat/Fe_3O_4@AC system with ultrasound intensification. *ACS Omega* **2020**, *5* (23), 13739−13750.
(297) Al Hakim, S.; Baalbaki, A.; Tantawi, O.; Ghauch, A. Chemically and thermally activated persulfate for theophylline degradation and application to pharmaceutical factory effluent. *RSC Adv.* **2019**, *9* (57), 33472−33485.
(298) Liu, J.; Zhong, S.; Song, Y.; Wang, B.; Zhang, F. Degradation of tetracycline hydrochloride by electro-activated persulfate oxidation. *J. Electroanal. Chem.* **2018**, *809*, 74−79.
(299) Hasani, K.; Moradi, M.; Mokhtari, S. A.; sadeghi, H.; Dargahi, A.; Vosoughi, M. Degradation of basic violet 16 dye by electro-activated persulfate process from aqueous solutions and toxicity assessment using microorganisms: determination of by-products, reaction kinetic and optimization using Box-Behnken design. *Int. J. Chem. React. Eng.* **2021**, *19* (3), 261−275.
(300) Alkhuraiji, T. S.; Boukari, S. O. B.; Leitner, N. K. V. Gallic acid degradation by electron beam irradiation under various conditions. *Environ. Sci. Pollut. Res.* **2019**, *26* (7), 6939−6947.
(301) Criquet, J.; Karpel Vel Leitner, N. Electron beam irradiation of aqueous solution of persulfate ions. *Chem. Eng. J.* **2011**, *169* (1), 258−262.
(302) Boukari, S. O. B.; Pellizzari, F.; Karpel Vel Leitner, N. Influence of persulfate ions on the removal of phenol in aqueous solution using electron beam irradiation. *J. Hazard. Mater.* **2011**, *185* (2), 844−851.
(303) Li, W.; Wu, Y.; Gao, Y.; Xing, S. Mechanism of persulfate activation with CuO for removing cephalexin and ofloxacin in water. *Res. Chem. Intermed.* **2019**, *45* (11), 5549−5558.
(304) Ding, Y.; Zhu, L.; Wang, N.; Tang, H. Sulfate radicals induced degradation of tetrabromobisphenol A with nanoscaled magnetic $CuFe_2O_4$ as a heterogeneous catalyst of peroxymonosulfate. *Appl. Catal., B* **2013**, *129*, 153−162.
(305) Li, G.; Zhong, Z.; Yang, C.; He, Q.; Peng, G. Degradation of Acid Orange 7 by peroxymonosulfate activated by cupric oxide. *J. Water Supply: Res. Technol. - AQUA* **2019**, *68* (1), 29−38.
(306) Jaafarzadeh, N.; Ghanbari, F.; Ahmadi, M. Catalytic degradation of 2,4-dichlorophenoxyacetic acid (2,4-D) by nano-Fe_2O_3 activated peroxymonosulfate: Influential factors and mechanism determination. *Chemosphere* **2017**, *169*, 568−576.
(307) Yang, S.; Yang, X.; Shao, X.; Niu, R.; Wang, L. Activated carbon catalyzed persulfate oxidation of Azo dye acid orange 7 at ambient temperature. *J. Hazard. Mater.* **2011**, *186* (1), 659−66.
(308) Yun, E.-T.; Lee, J. H.; Kim, J.; Park, H.-D.; Lee, J. Identifying the nonradical mechanism in the peroxymonosulfate activation process: Singlet oxygenation versus mediated electron transfer. *Environ. Sci. Technol.* **2018**, *52* (12), 7032−7042.
(309) Shao, P.; Yu, S.; Duan, X.; Yang, L.; Shi, H.; Ding, L.; Tian, J.; Yang, L.; Luo, X.; Wang, S. Potential difference driving electron transfer via defective carbon nanotubes toward selective oxidation of organic micropollutants. *Environ. Sci. Technol.* **2020**, *54* (13), 8464−8472.

(310) Cheng, X.; Guo, H.; Li, W.; Yang, B.; Wang, J.; Zhang, Y.; Du, E. Metal-free carbocatalysis for persulfate activation toward nonradical oxidation: Enhanced singlet oxygen generation based on active sites and electronic property. *Chem. Eng. J.* **2020**, *396*, 125107.
(311) Wang, S.; Xu, L.; Wang, J. Nitrogen-doped graphene as peroxymonosulfate activator and electron transfer mediator for the enhanced degradation of sulfamethoxazole. *Chem. Eng. J.* **2019**, *375*, 122041.
(312) Gao, Y.; Chen, Z.; Zhu, Y.; Li, T.; Hu, C. New Insights into the generation of singlet oxygen in the metal-free peroxymonosulfate activation process: Important role of electron-deficient carbon atoms. *Environ. Sci. Technol.* **2020**, *54* (2), 1232−1241.
(313) Wang, S.; Gao, S.; Tian, J.; Wang, Q.; Wang, T.; Hao, X.; Cui, F. A stable and easily prepared copper oxide catalyst for degradation of organic pollutants by peroxymonosulfate activation. *J. Hazard. Mater.* **2020**, *387*, 121995.
(314) Gao, Y.; Zhu, Y.; Lyu, L.; Zeng, Q.; Xing, X.; Hu, C. Electronic structure modulation of graphitic carbon nitride by oxygen doping for enhanced catalytic degradation of organic pollutants through peroxymonosulfate activation. *Environ. Sci. Technol.* **2018**, *52* (24), 14371−14380.
(315) Henderson, N. *The Discovery of Organic Free Radicals by Moses Gomberg: A National Historic Chemical Landmark, University of Michigan, Ann. Arbor, Michigan, June 25, 2000*; American Chemical Society: 2000.
(316) Dogliotti, L.; Hayon, E. Flash photolysis of peroxydisulfate ions in aqueous solutions. The sulfate and ozonide radical anions. *J. Phys. Chem.* **1967**, *71* (8), 2511−2516.
(317) Glaze, W. H.; Kang, J.-W. Advanced oxidation processes for treating groundwater contaminated with TCE and PCE: Laboratory studies. *Journal AWWA* **1988**, *80* (5), 57−63.
(318) Wang, Y.; Hong, C.-s. Effect of hydrogen peroxide, periodate and persulfate on photocatalysis of 2-chlorobiphenyl in aqueous TiO_2 suspensions. *Water Res.* **1999**, *33* (9), 2031−2036.
(319) Huang, K.-C.; Couttenye, R. A.; Hoag, G. E. Kinetics of heat-assisted persulfate oxidation of methyl tert-butyl ether (MTBE). *Chemosphere* **2002**, *49* (4), 413−420.
(320) Anipsitakis, G. P.; Dionysiou, D. D. Degradation of organic contaminants in water with sulfate radicals generated by the conjunction of peroxymonosulfate with cobalt. *Environ. Sci. Technol.* **2003**, *37* (20), 4790−4797.
(321) Behrman, E. J. The Persulfate Oxidation of Phenols and Arylamines (The Elbs and the Boyland-Sims Oxidations). *Organic Reactions* **1988**, 421−511.
(322) Yang, Q.; Choi, H.; Chen, Y.; Dionysiou, D. D. Heterogeneous activation of peroxymonosulfate by supported cobalt catalysts for the degradation of 2,4-dichlorophenol in water: The effect of support, cobalt precursor, and UV radiation. *Appl. Catal., B* **2008**, *77* (3), 300−307.
(323) Fang, G.; Gao, J.; Dionysiou, D. D.; Liu, C.; Zhou, D. Activation of persulfate by quinones: Free radical reactions and implication for the degradation of PCBs. *Environ. Sci. Technol.* **2013**, *47* (9), 4605−4611.

NOTE ADDED AFTER ASAP PUBLICATION

Due to a production error, this paper was published ASAP on August 3, 2023, with errors in Tables 1, 3, and 6. The corrected version was reposted on August 8, 2023.

https://doi.org/10.1021/acs.est.3c05153
Environ. Sci. Technol. 2023, 57, 12153−12179